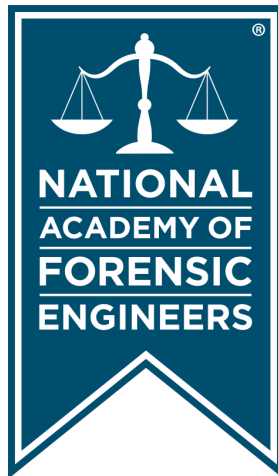


Journal of the
National
Academy OF
Forensic
Engineers[®]



<http://www.nafe.org>

ISSN: 2379-3252

DOI: 10.51501/jotnafe.v40i1

Vol. 40 No. 1 June 2023

National Academy of Forensic Engineers®

Journal Staff

Editor-in-Chief:

Bart Kemper, PE, DFE, F.ASME, F.NSPE

Managing Editor:

Ellen Parson

Technical Review Process

The Technical Review Committee Chair chooses the reviewers for each Journal manuscript from amongst the members and affiliates of the NAFE according to their competence and the subject of the paper, and then arbitrates (as necessary) during the review process. External reviewers may also be utilized when necessary. This confidential process concludes with the acceptance of the finished paper for publication or its rejection/withdrawal. The name(s) of authors are included with their published works. However, unpublished drafts together with the names and comments of reviewers are entirely confidential during the review process and are excised upon publication of the finished paper.

National Academy of Forensic Engineers®

Board of Directors

President

Joseph Leane, PE, DFE
Fellow

President-Elect

Steven Pietropaolo, PE, DFE
Senior Member

Senior Vice President

Michael Aitken, PE, DFE
Senior Member

Vice President

Tonja Koob Marking, PhD, PE, DFE
Senior Member

Treasurer

Bruce Wiers, PE, DFE
Senior Member

Secretary

James Drebelbis, AIA, PE, DFE
Fellow

Past Presidents

Samuel Sudler, PE, DFE
Senior Member

Liberty Janson, PE, DFE
Senior Member

James Petersen, PE, DFE
Fellow

Directors at Large

Daniel Couture, PEng, DFE
Senior Member

Robert Peruzzi, PhD, PE, DFE
Member

Executive Director

Monika Schulz, CAE

Journal of the National Academy of Forensic Engineers®

Editorial Board

Editor-in-Chief

Bart Kemper, PE, DFE, F.ASME, F.NSPE
Fellow

Associate Editor

Robert Peruzzi, PhD, PE, DFE
Member

Managing Editor

Ellen Parson
Affiliate

Associate Editor

Steven Pietropaolo, PE, DFE
Senior Member

Senior Associate Editor

James Green, PE, DFE
Fellow, Life Member

Associate Editor

Michael Plick, PE, DFE
Fellow

Associate Editor

Zohaib Alvi, PE
Associate

Associate Editor

Paul Stephens, PE, DFE
Fellow

Associate Editor

Rebecca Bowman, PE, Esq.
Member

Associate Editor

Paul Swanson, PE, DFE
Life Member

Associate Editor

David Icove, PhD, PE, DFE
Fellow

OJS Technical Editor

Mitchell Maifeld, PE, DFE
Member

Associate Editor

Mark McFarland, PE, DFE
Member

Submitting Proposed Papers to NAFE for Consideration

Please visit the Journal's author page at <http://journal.nafe.org/ojs/index.php/nafe/information/authors> for submission details.

We are looking for NAFE members who are interested in giving presentations on technical topics that will further the advancement and understanding of forensic engineering at one of the academy's biannual meetings and then developing those presentations into written manuscripts/papers, which will go through a single-blind peer review process before publication. Only papers presented at a NAFE regular technical seminar and that have received oral critique at the seminar will be accepted for review and publication. We recommend that you review the [About the Journal](#) page for the journal's section policies as well as the [Author Guidelines](#) listed on the Submissions page. Authors need to register with the journal prior to submitting, or (if already registered) they can simply log in and begin the process. The first step is for potential authors to submit a 150-word maximum abstract for consideration at an upcoming conference into the online journal management system.

Copies of the Journal

The Journal of the National Academy of Forensic Engineers® contains papers that have been accepted by NAFE. Members and Affiliates receive a PDF download of the Journal as part of their annual dues. All Journal papers may be individually downloaded from the [NAFE website](#). There is no charge to NAFE Members & Affiliates. A limited supply of Volume 33 and earlier hardcopy Journals (black & white) are available. The costs are as follows: \$15.00 for NAFE Members and Affiliates; \$30.00 for members of the NSPE not included in NAFE membership; \$45.00 for all others. Requests should be sent to NAFE Headquarters, 1420 King St., Alexandria, VA 22314-2794.

Comments by Readers

Comments by readers are invited, and, if deemed appropriate, will be published. Send to: Ellen Parson, Journal Managing Editor, 3780 SW Boulder Dr, Lee's Summit, MO 64082. Comments can also be sent via email to journal@nafe.org.

Material published in this Journal, including all interpretations and conclusions contained in papers, articles, and presentations, are those of the specific author or authors and do not necessarily represent the view of the National Academy of Forensic Engineers® (NAFE) or its members.

© 2023 National Academy of Forensic Engineers® (NAFE). ISSN: 2379-3252

Table of Contents

| | |
|---|----|
| § Forensic Analysis of a CNC Lathe Window Guard Failure | 1 |
| <i>By Stephen Batzer, PhD, PE, DFE (NAFE 677F)</i> | |
| ∪ Methodology and Tools for Forensic Engineering | |
| Analysis of Electrical Shocks | 11 |
| <i>By Chris Korinek, PE, DFE (NAFE 716S)</i> | |
| § Forensic Examination of Post-Fire Damaged Electrical Conductors by Using X-Ray Radiographs | 27 |
| <i>By Mark J. Svare, PhD, PE, DFE (NAFE 851M) and Niamh Nic Daeid, PhD</i> | |
| ‡ Forensic Examination of Post-Fire Damaged Electrical Conductors by Quantitative Measurement | 41 |
| <i>By Mark J. Svare, PhD, PE, DFE (NAFE 851M), Neal W. Hanke, PE (NAFE 1219A), and Niamh Nic Daeid, PhD</i> | |
| ‡ Application of Matchmoving for Forensic Video Analysis with Recorded Event Data | 57 |
| <i>By Richard M. Ziernicki, PhD, PE, DFE (NAFE 308F) and Ricky Nguyen, PE, DFE (NAFE 1223M)</i> | |
| ‡ Nondestructive Forensic Investigation of a Scissor Lift Fatality | 67 |
| <i>By Michael Stichter, PhD, PE, DFE (NAFE 1162M), Zachary Ball, PhD, PE, and Wade Lanning, PhD</i> | |
| φ Forensic Analysis of Roof Deterioration Due to Condensation | 79 |
| <i>By James Drebelbis, PE, DFE (NAFE 938S)</i> | |

φ Paper presented at the NAFE seminar held in January 2017 in New Orleans.

∪ Paper presented at the NAFE seminar held virtually in January 2021.

§ Paper presented at the NAFE seminar held in July 2022 in Toronto.

‡ Paper presented at the NAFE seminar held in January 2023 in San Antonio.

Forensic Analysis of a CNC Lathe Window Guard Failure

By Stephen A. Batzer, PhD, PE, DFE (NAFE 677F)

Abstract

An analysis of an industrial lathe accident is presented in this paper. During operation, the rotating chuck lost its grip upon the cylindrical workpiece. The detached workpiece impacted the inside of the lathe cabinet, rebounded, struck the composite viewing window, and penetrated it. While observing the machining process through the window, the machinist was struck in the chest by the workpiece. He fell backward, suffering a severe traumatic brain injury when the back of his head impacted the concrete floor. The forensic analysis incorporated an event reconstruction to include an estimate of the ejection angle, velocity, and kinetic energy of the workpiece, the impact energy capacity of the window, and a failure analysis of the window and its frame. A kinetic energy analysis was performed by destructive testing of door/window replicas and high-speed videography. Impact testing of exemplar workpieces against alternative design highly impact-resistant windows was also performed.

Keywords

Lathe, machine guarding, window failure, forensic engineering, hazard analysis

Introduction

This accident occurred at a small family-owned machining job shop. To improve the shop's efficiency, the owner/lead machinist had purchased a new computer numerically controlled (CNC) lathe. The machine was equipped with a steel cabinet that captured chips and fluid during operation and discharged these waste products using a mechanical conveyor that emptied into an adjacent container. The cabinet was equipped with a sliding sheet metal door that featured a viewing window to allow observation of the process. This door and window acted as a guard. A representative of the retailer had delivered the machine, set it up, and trained the purchaser on-site in safe and efficient usage practices over the course of nearly two days just prior to the incident.

The machine measured 12 feet (ft) in length, 5 ft in width, and could turn materials up to 23.6 inches (in.) in length. During the initial job of the first day of production use, a heavy workpiece exited the CNC lathe through the window guard, impacting and severely injuring the machinist. The reason for the detachment of the cylindrical workpiece from the chuck jaws was not in dispute. The hydraulic jaws were only lightly engaged against the outer convex axial periphery of the steel workpiece — with the three jaws each engaging less than 10% of the workpiece

length. The center of the 28.2 lbm (12.8 kilograms) 6-in. (15.2 millimeter) diameter steel cylinder had been rough drilled, and a boring bar was engaging the distal end of the cantilevered workpiece to machine this inner hole to its final dimension.

Given the light fixation, the boring tool cut was overly aggressive, and, during turning, the secured end of the steel cylinder opposite the boring bar was pried out of the chuck jaws. Contact impressions strongly suggested that the workpiece interacted with one or more of the chuck jaws upon detachment, which increased the magnitude of the workpiece's translational kinetic energy.

The only surviving exterior photograph of the door and window immediately post-accident is a low-resolution black and white scan (**Figure 1**). The construction of the window was a composite using two different materials. The inner pane nearest the workpiece was made of tempered common window glass (silica-soda-lime), which provided scratch resistance to the metal chips and was inert to the cutting fluid. This inner pane was separated from the outer pane by a modest air gap. The outer pane on the machinist side was made of a kinetic energy absorbing polymer; this outer pane provided the substantive impact protection. **Figure 1** shows the polymer exterior window panel

bowed outward with a hinge-like crease in the center, and the workpiece chuck is visible at the lower center of the window. The angled red arrow in **Figure 1** is included to show that the surviving polymer window pane is slightly bigger in width and height as compared to the overlapping viewing aperture. The vertical green arrow of **Figure 1** shows the position of the workpiece chuck. The horizontal blue arrow of **Figure 1** indicates where the workpiece grazed the inner steel door window frame and dented the sheet metal. A higher quality color image of the damaged door and window assembly is shown in **Figure 2** with the door detached from the lathe enclosure. This photograph shows the door's interior side. The horizontal blue arrow shows the witness mark of the workpiece against the now-bent inner window frame, which corresponds to the arrow shown in **Figure 1**. The cylindrical workpiece grazed and damaged the steel window periphery as it struck the window substantially off window center.

Accident Details and Initial Analysis

The lathe was powered by a 18.6 kilowatt (kW) 25-hp motor, which could drive the spindle to a maximum 3,500 rpm. The spindle was rated to hold a 62-kg (137-lb) workpiece. The three jaw chuck, which held the workpiece, was of 254 mm (10-in.) diameter and designed to safely grip a 230 mm (9-in.) diameter workpiece. The chuck was rated to 4,600 rpm. Jaws that were constructed from annealed steel were installed on the chuck at the time of the incident. A stop was machined into the jaws and documented the modest depth of workpiece fixation — ~10 mm (0.40 in.) of the overall ~90 mm (3.5-in.) length. The chuck rotated counter-clockwise when viewed from the direction of the chuck face back toward the spindle and motor.

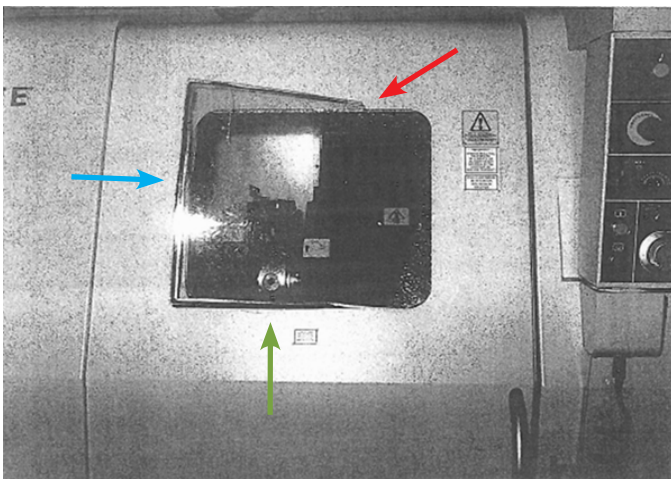


Figure 1

Exterior photograph of the mounted lathe door with the outward-side polymer window pane bent and folded outward.



Figure 2

Interior side photograph of the detached door guard showing the interior-side tempered glass fragments of the shattered inner window pane and the witness mark damage against the steel frame.

The relevant portion of the door guard consisted of two offset steel panels that framed the observation window — each sheet being 2.3 mm (0.090 in.) thick. The layered window assembly consisted of a 5.0-mm tempered glass inboard surface for abrasion and chemical resistance, then a 5.5-mm air gap, and finally a 4.5-mm polycarbonate outboard panel used for impact energy absorption. The total window thickness was 15 mm (0.59 in.). The unmounted pane measured 532 mm x 452 mm (20.9 in. x 17.8 in.). The daylight opening was reduced by 15 mm per edge through frame overlap (equal to the composite thickness). The opening also featured modestly radiused corners (see **Figures 2** and **3**). The modest edge overlap of the steel frame to the composite window suggests why the polycarbonate pane was pulled out of its frame and plastically deformed rather than being fractured and directly penetrated.

The incident occurred during the first week of unsupervised operation. The workpiece was a steel cylinder 15.2 centimeters (cm) or 6.0 in. in diameter, approximately 8.9 cm (3.5 in.) in length, with an axially drilled through hole 2.26 cm (0.891 in.) in diameter. This hole was being finish bored to its final dimension with a 0.25 mm/rev (0.010-in./rev) feed rate. The only witness to the accident was the machinist/owner who had programmed the lathe and loaded the workpiece. Due to his traumatic injuries, he was permanently incapable of being queried regarding details of the incident.

The machine code was downloaded, and the spindle speed was indicated to be at 1,945 rpm plus an additional 20% manual override (totaling 2,234 rpm). As the workpiece left the chuck, it is believed to have interacted with the rotating jaws — somewhat like an automated baseball pitching machine — as the workpiece had no linear

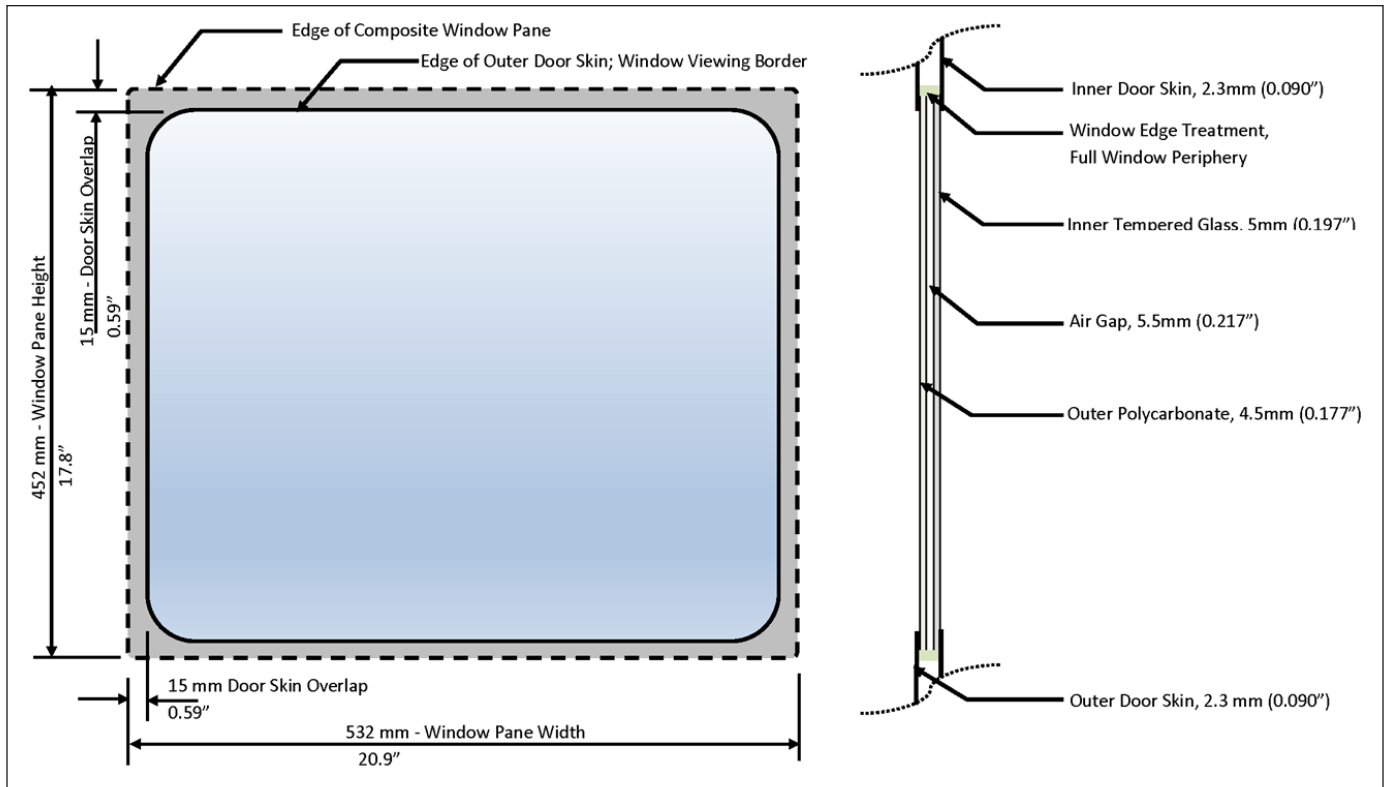


Figure 3
Diagram of the subject composite guard window.

velocity at the time of detachment. This added translational kinetic energy to the workpiece, which struck the interior of the glass in the plane at an angle $\sim 30^\circ$ off-perpendicular — making its flight more or less parallel to the shop floor. See the geometry of the window and door in **Figure 1** (in which the chuck is visible at the lower center of the window).

After fracture of the tempered glass inner pane and displacement of the outer polycarbonate pane, the energetic workpiece struck the operator in the chest and was redirected to the ceiling some 3.5 meters (m) — ~ 10 ft — above the point of the operator’s chest. The workpiece superficially damaged a perforated metal ceiling panel and then fell back to the concrete floor. The operator fell and struck the back of his head against this same concrete floor, which caused substantially more severe injuries than did the workpiece impact to his chest (**Figure 4**).

It is not believed that the rotational kinetic energy consequentially increased the severity of the impact to the observation window and, hence, the operator. All energy calculations are per *Vector Mechanics for Engineers*¹.

- Angular velocity, $\omega = 2,234 \text{ rpm} \cdot 2\pi/60 = 234 \text{ rad/s}$.

- Unbored cylinder mass, $M_o = \pi \cdot (0.5 \cdot 15.2 \text{ cm})^2 \cdot 8.9 \text{ cm} \cdot 0.0079 \text{ kg/cm}^3 = 12.8 \text{ kg} (28.2 \text{ lbm})$

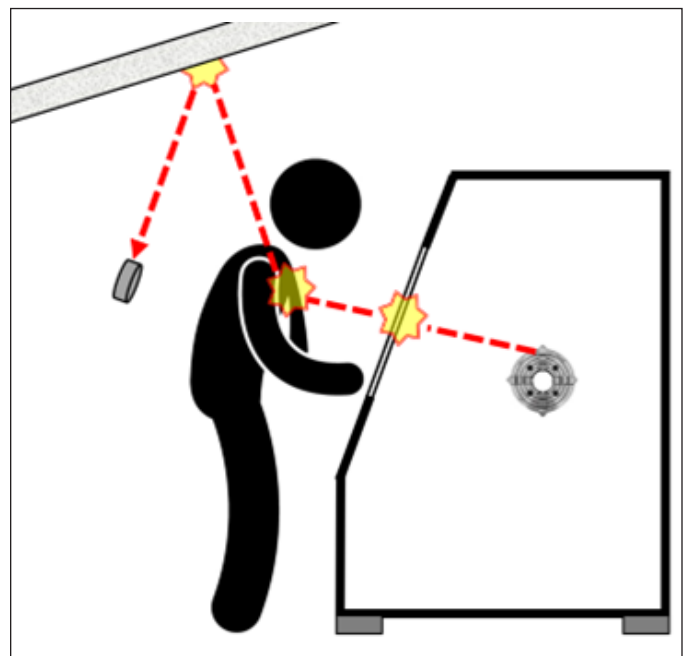


Figure 4
Schematic of the cylindrical workpiece path showing three separate impacts (not to scale).

- Lost through-hole mass, $M_1 = -\pi*(0.5*2.26 \text{ cm})^2*8.9 \text{ cm}*0.0079 \text{ kg/cm}^3 = -0.28 \text{ kg}$ (-0.62 lbm)
- Rotational moment of inertia of workpiece = $I = \frac{1}{2}(M_o R_o^2 - M_1 R_1^2) = \frac{1}{2}[12.8 \text{ kg}*(0.076 \text{ m})^2 - 0.28 \text{ kg}*(0.013 \text{ m})^2] = 0.037 \text{ kg}\cdot\text{m}^2$ (0.88 lbf-ft)
- Rotational Kinetic Energy = $0.5*I*\omega^2 = 0.5*0.037 \text{ kg}\cdot\text{m}^2 * (234 \text{ rad/s})^2 = 1,013 \text{ J}$ (747 ft-lbf)
- Initial translational velocity at loss of fixation = 0
- Maximum Calculated Translational Kinetic Energy = $0.5*mv^2 = 0.5*(12.8 \text{ kg} - 0.28 \text{ kg})*(0.127 \text{ m} * 234 \text{ rad/s})^2 = 5,530 \text{ J}$ (4,080 ft-lb)

As is shown, the calculated maximum translational kinetic energy of the detached workpiece from chuck jaw interaction was a multiple more than five times the calculated rotational kinetic energy. The amount of energy absorbed by the window and surrounding door was unknown.

Based upon the post-accident evidence, representatives of the machine tool manufacturer estimated that the accident workpiece impacted the window with 3,062 to 5,580 joules (J) — 2,260 to 4,118 ft-lbs — of translational kinetic energy. This was a multiple of the amount of energy absorption capacity of the window guard that they had previously calculated prior to selling the lathe — 1,450 J (1,064 ft-lb). This estimated window energy capacity assumed that a relatively low mass chuck jaw had detached and struck the window both centered and perpendicular.

Two mechanical engineers made independent estimates of the kinetic energy of the workpiece but only post-ejection. These estimates took into account the energy absorbed at impact to the machinist, travel to the workshop ceiling, and then damage to the ceiling. These two estimates — 440 J and 613 J (325 ft-lb and 450 ft-lb) — would be in addition to the energy absorbed by the window guard and door at impact. These engineers made no independent calculations regarding the impact kinetic energy absorption of the window based upon its construction, mostly in light of the offset nature of the strike that detached the window.

It was decided to estimate the workpiece to window impact energy based upon destructive testing accurately replicating the workpiece size and impact point, and then

adding the estimate of the kinetic energy after exit from the window guard to estimate the overall impact kinetic energy of the workpiece against the inner window pane and frame.

Initial Destructive Testing

A number of test door guards matching the relevant construction details of the accident door were fabricated in order to economically facilitate a series of impact tests. These construction details included the sheet metal thickness, window aperture dimensions and corner radii, tempered glass and polycarbonate thickness and area, and fasteners. The test doors were given a gray powder coat paint application for a visual match.

A series of impacts of workpieces at varying velocity was coupled with post-test analysis to estimate the subject window's generic impact resistance to the accident workpiece and trajectory at the documented impact location. After impact analysis was complete, "reasonable alternative design" door guards, featuring windows having greater impact resistance, were also tested to proof test the proposition that a more impact-resistant window guard would have adequately retained the accident workpiece and prevented the catastrophic injury.

Testing was conducted at a major contract research laboratory in a rural setting that had a large pneumatic launching device. This machine was principally used to launch euthanized chickens at prototype aircraft windshields for impact-resistance validation. The launcher consisted of a breech loading smooth bore rectangular barrel that was attached to a large air reservoir separated from the barrel by a quick-opening valve. Rectangular sabots (thrust transmitting projectile carriers) were constructed from glued up layers of expanded polystyrene to provide a seal between the workpieces and the barrel.

One difference between the testing and the accident was that no consequential rotation was imparted to the workpieces. A second difference was that solid workpieces were used without drilled through holes, making them ~2% heavier than the accident workpieces. Considering that the solid test workpieces were only modestly heavier — and also that the bored hole did not interact with the window during the accident — the geometric differences were not considered to be consequential. Each cylindrical steel workpiece was marked on the face nearest the digital image recording equipment with an "X" to indicate the workpiece center. Launches were recorded using a high-speed video camera oriented perpendicular to the

projectile path and centered on the impact point. Since this testing featured 12.8 kg workpieces being launched at an initial velocity of ~30 m/s, all personnel were situated at a remote location during launch.

Two photographs of Test 1, with the first exemplar workpiece leaving the pneumatic launcher, are shown in **Figure 5**. The steel cylinder is moving in free flight from left to right horizontally and is called out with a red arrow in the top photograph. The test door is mounted on a test stand such that the projectile will only modestly impact the right edge of the window frame, accurately simulating the accident. The test door is inclined such that the relative angle of impact, ~28° from perpendicular, is identical to that documented with the accident lathe. The “X” inscribed on the right side of the projectile for frame-by-frame distance determination is also visible in the top photograph. The rectangular detail at left (blue arrow) is a “stripper,” which is a barrel end trap that captures the polystyrene sabot after it and the projectile have exited in tandem from the rectangular barrel’s muzzle. The four white vertical lines on the ruler centered above the stripper (four green arrows)

act as a length reference to facilitate workpiece positional analysis, frame by frame, post-test. These white reference lines are 1 ft (0.30 m) apart. The background behind the test stand and the mounted door also contains a reference dimension grid with 1-ft square offsets.

A plywood sheet was located behind the impacted test door assembly (shown at the right side of each photograph of **Figure 5** with the grain of the wood visible). This wood provided a somewhat neutral visual background for post-test photographs. A photograph of the first tested door post-impact is shown in **Figure 6**. Notice the impact damage at the right side of the steel window frame. The projectile shattered the near side tempered glass and then punctured the far side polycarbonate. In each of the four initial tests, the tempered glass and polycarbonate fractured. In none of the four initial tests did the polycarbonate window flex and peripherally detach as did the polymer window in the subject incident, which may have been a consequence of the orientation of the test projectile being different than that of the unknown impact inclination angle of the incident workpiece. Results of the first four tests conducted

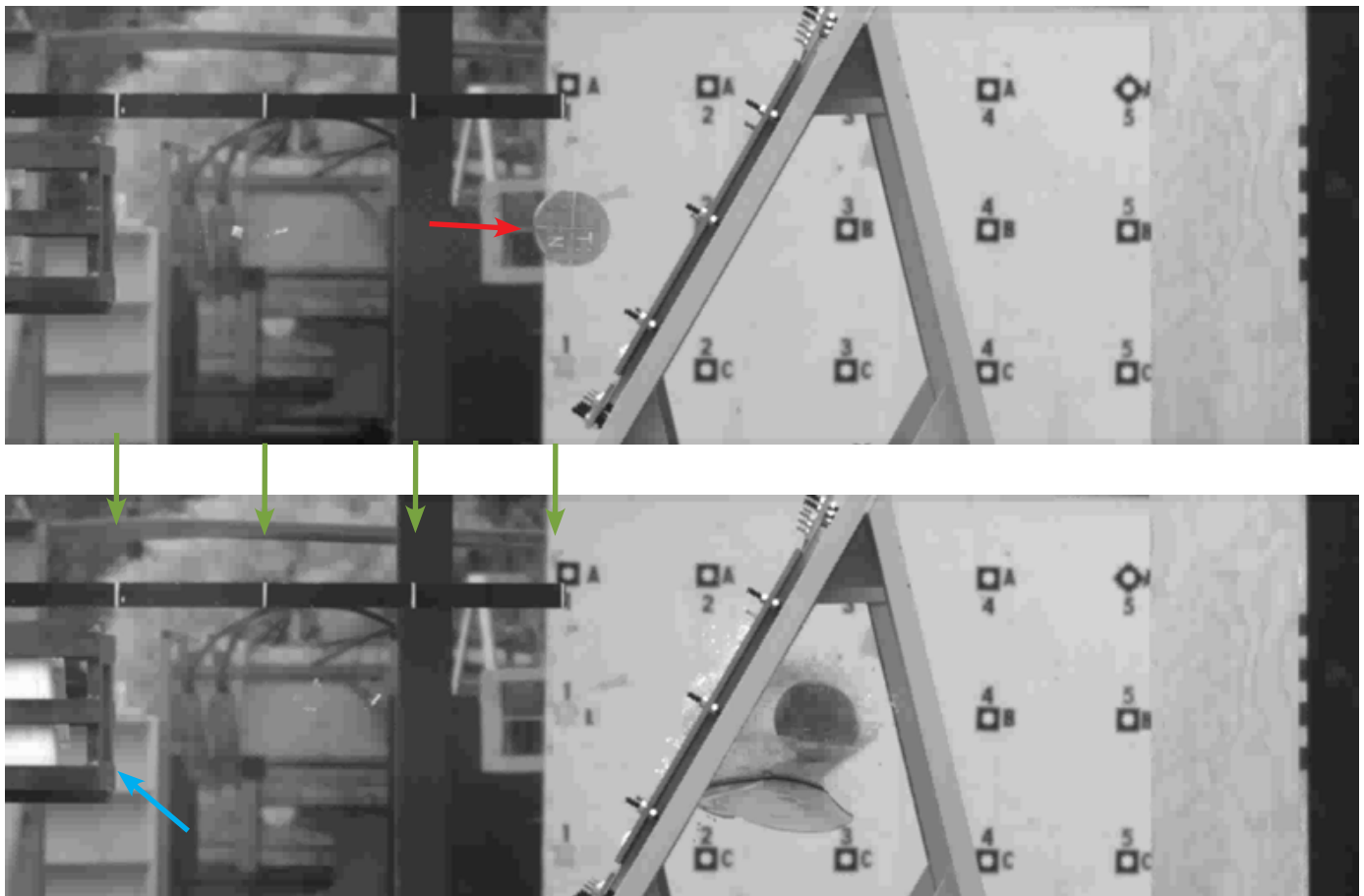


Figure 5

Test 1 — the projectile between the launcher and the inclined test door (top); post window penetration (bottom).

are summarized in **Figure 7**.

The data from impact Tests 1 – 4 are plotted in **Figure 8**, which also gives a least-squares curve fit of the data determined by the Excel software. The equation in the inset gives the calculated linear relationship between the workpiece impact kinetic energy and the workpiece exit kinetic energy. As the data set is small (limited to four empirical

data points), no R² goodness of fit value has been provided.

Using the developed equation $KE_{EXIT} = 0.600 * KE_{IMPACT} - 146$ J and the estimated range of workpiece post-guard penetration kinetic energy (440 J to 613 J), the estimates for workpiece impact kinetic energy are 977 to 1,265 J. This range of estimated workpiece impact severity is significantly less than the estimates of the machine tool manufacturer’s engineers: 3,062 to 5,580 J. Further, the testing-based estimate of window guard energy capacity using the most severe of the two impact estimates (1,265 J) gives an estimated window energy absorption of 652 J. This is also less than the analysis of the manufacturer’s designers, which was a 1,450 J capacity, albeit using a different impact scenario. Any estimated window guard energy capacity developed by this destructive testing necessarily overstates the capacity of the transparent window panes alone compared to impacts against both the window and the steel frame.

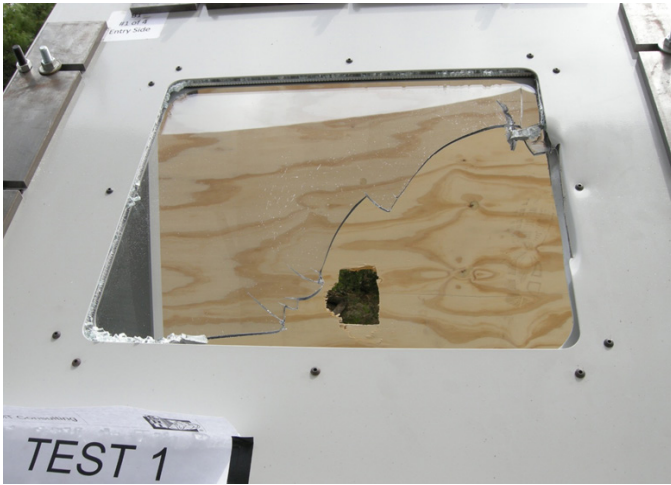


Figure 6

Test 1 — photograph of the door from the inclined impact side, post-test, showing impact damage similar to that shown in **Figure 2**.

Relevant Viewing Portal Construction Standards

As this door was sold within the domestic market, U.S. laws and regulations were applicable. However, no federal governmental safety regulation existed at the time of sale for energy absorption of the window/door combination. Two American National Standards Institute (ANSI)

| Test | Mass kg / lbs | V-Impact m/s / ft/s | V-Exit m/s / ft/s | KE-Impact J / ft-lbs | KE-Exit J / ft-lbs | Absorbed KE J / ft-lbs |
|------|------------------|------------------------|----------------------|-------------------------|-----------------------|---------------------------|
| T1 | 12.8 / 28.2 | 29.8 / 97.8 | 22.6 / 74.2 | 5686 / 4194 | 3270 / 2412 | 2416 / 1782 |
| T2 | 12.8 / 28.1 | 21.3 / 69.9 | 15.7 / 51.5 | 2901 / 2140 | 1576 / 1162 | 1325 / 978 |
| T3 | 12.8 / 28.1 | 15.8 / 51.8 | 12.0 / 39.2 | 1596 / 1177 | 921 / 679 | 675 / 498 |
| T4 | 12.8 / 28.1 | 15.0 / 49.1 | 9.9 / 32.6 | 1442 / 1064 | 628 / 463 | 814 / 601 |

Figure 7
Initial impact testing.

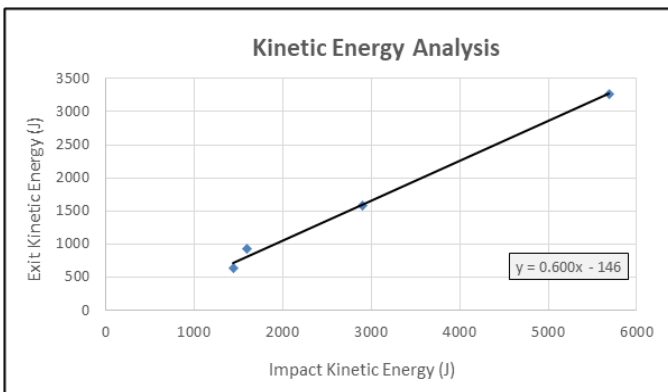


Figure 8

Tests 1 – 4 plotted along with a linear curve-fit relationship.

standards were applicable, though not governing. The first, ANSI B11.19-2003, “Performance Criteria for Safeguarding,”²² states under Paragraph 7.1 Design and Construction:

- 7.1.1. Material used in the construction of guards shall be of such design and strength as to protect individuals from identified hazards.

A second standard, ANSI B11.22-2002, “Safety Requirements for Turning Centers and Automatic, Numerically Controlled Turning Machines,”²³ contains the following text relative to the subject CNC lathe guard:

- 6.23 Ejected Parts or Fluids

Persons shall be protected against ejected parts by shields of sufficient strength (including means of fixing to the machine/floor) to contain these parts... These could include things such as broken tools, work material, machine parts and coolant.

- 6.24 Viewing Windows

When safety guards are equipped with viewing windows, which are also intended to contain ejected parts, consideration shall be given to the selection of materials and the method of their installation.

While these two ANSI standards were informative, they were but aspirational in that neither detailed a protocol for the validation of the minimum level of impact resistance.

The subject CNC lathe was also sold in western Europe. In this market, specific regulatory requirements existed for impact energy resistance of viewing windows. Specifically, regulation EN 12415, "Safety Of Machine Tools - Small Numerically Controlled Turning Machines And Turning Centres," 2001 edition⁴, was applicable. *Note: The EN 12415 standard has since been withdrawn and replaced by the ISO 23125:2010 standard, "Machine Tools-Safety-Turning Machines"⁵. This ISO standard had not been written at the time of the lathe's manufacture (2006) or the accident (2007). Further, the initial 2010 edition has been superseded by the 2015 revision⁶. The energy requirements are very nearly identical between the ISO standard and the EN standard upon which it was based.*

Table B.2 of EN 12415 is entitled, "Resistance Classes of Windows." For the subject lathe, the diameter of the chuck exceeded 250 mm by 4 mm, making it a "C" class machine. The peripheral speed developed at the rated 3,500 rpm was 46.5 m/s; this placed it in the C2 class as the peripheral velocity exceeded 40 m/s. A window guard for this machine size was required to resist a 2.5 kg impactor at 63 m/s, an impact of 4,960 J (3,658 ft-lbs). The relevant table from the EN 12415 standard is reprinted in **Figure 9**. The tests are conducted using a cylindrical hardened steel projectile with a pyramidal leading endform that has been truncated, giving it a square and flat impact surface. In **Figure 9**, the dimension "a" represents the side length of the square.

Note that the table giving resistance classes for the various windows for machine tools is unchanged except for the borderline between B and C class guard windows between the EN 12415 standard and the ISO 23125 standard of 2010, which replaced it. The ISO standard expanded the B class window category "from 130 up to 250 mm" turning diameter maximum to "from 130 mm up to <260 mm." The subject workpiece chuck, being 10 in. in diameter, would require a C2-class window under the EN standard, but only a B2-class window under the superseding ISO standard.

A 2.5 kg impactor is substantially lighter than was the 12.8 kg accident workpiece. However, the case-specific destructive initial destructive testing strongly suggested that the window pane sold in the unregulated American market would not be able to withstand the required 4,960 J impact of a 2.5 kg impactor as the window was defeated by three impacts of lesser energy — the least of

| Turning Diameter (mm) | | Circumferential Velocity | Projectile Size $\phi \times a$ | Projectile Mass | Impact Velocity | Impact Energy | Resistance Class |
|-----------------------|-------|--------------------------|---------------------------------|-----------------|-----------------|----------------------|------------------|
| From | Up To | v (m/s) | (mm x mm) | (kg) | v (ms/s) | (J) | |
| | 130 | 25 40 63 | 30 x 19 | 0.625 | 32 50 80 | 320 781 2000 | A1 A2 A3 |
| 130 | 250 | 40 50 63 | 40 x 25 | 1.25 | 50 63 80 | 1562 2480 4000 | B1 B2 B3 |
| 250 | | 40 50 63 | 50 x 30 | 2.5 | 50 63 80 | 3124 4960 8000 | C1 C2 C3 |

Figure 9

Impact resistance classes per European Standard EN 12415 as of 2006⁴.

which was 1,442 J. Note also that in each of the initial tests, some portion of the impact energy was absorbed by the window frame, rather than the tempered glass and polycarbonate panes alone.

The unregulated American market lathe window used a 4.5-mm-thick polycarbonate window pane for energy absorption. The regulated European market lathe window used a 12-mm-thick polycarbonate window pane for energy absorption. The EN 12415 standard, along with the superseding ISO 23125 standard, provided a table of polycarbonate window thicknesses for which 6 mm is the listed minimum (**Figure 10**). Note that for the C2 class window, 10 mm of polycarbonate was minimal, while for the B2 class window, 8 mm sufficed.

The development of the EN 12415 and the successor ISO 23125 standards were based upon the seminal work of Mewes and Trapp⁷ who used a pneumatic gun similar to that used in the current study to launch a standard projectile at a number of different guard materials, including polycarbonate, several sheet steel alloys, and the aluminum alloy AlMg3. Inspection of **Figure 10** shows that both kinetic energy and projectile mass are relevant to polycarbonate window penetration performance; a projectile of greater mass and — hence greater cross sectional area — requires more kinetic energy to penetrate a given polycarbonate window. For example, a 6-mm polycarbonate window will pass the B1 requirement as it can absorb a 1562 J impact by a 1.25 kg standard projectile, but that same window cannot absorb a lesser 781 J impact by a 0.625 kg standard projectile. Similar comparisons can be made for the 8-mm polycarbonate window (B2 at 2480 J = Pass; A3 at 2000 J = Fail) and the 10 mm polycarbonate window (C2 at 4960 J Pass; B3 at 4000 J = Fail).

The previous work by Mewes cannot be used to directly analyze the subject accident and window capacity, as no 4.5 mm polycarbonate window is listed, and the accident workpiece at 12.8 kg was somewhat more than five times as massive as the largest standard projectile used by Mewes. Further, these validation tests did not have the impactor graze the window frame.

The substantial increase in absorbed kinetic energy of the test windows in this study, as a result of increased projectile velocity (tests T4 → T1), strongly suggests that the window frame was a significant absorber of impact energy. This is supported by earlier work of Mewes⁸, which showed the relative insensitivity of polycarbonate energy absorption to impact velocity. This can be attributed to the brittle nature of polycarbonate, which, while energy absorbing, does not deform in a similar fashion to low carbon steel for which the balance of the door/window guard was manufactured. Thus, the substantial increase in window guard energy absorption with increasing workpiece impact velocity can be attributed to the steel construction of the window frame rather than the polycarbonate glazing that was penetrated. One further relevant observation is that when Mewes conducted his testing, he used a 25-mm (1-in.) frame to viewing panel overlap, rather than the 15-mm (0.6-in.) overlap design of the accident lathe window.

Alternative Design Validation Testing

Two additional tests were performed to validate alternative design windows given two different workpiece impact scenarios. Test 5 used a 12-mm polycarbonate window replicating the construction of the window that was sold on the European market. The frame engagement of this test window was also extended from 15 mm to 25 mm to diminish the probability of a peripheral

| Impact Resistance Classes of Machine Tool Safety Windows Energy Capacity Requirements (J) | | | | | | | | | |
|--|-----------|-----------|------------|------------|------------|------------|------------|------------|------------|
| PC Thickness (mm) | A1 320 | A2 781 | A3 2000 | B1 1562 | B2 2480 | B3 4000 | C1 3124 | C2 4960 | C3 8000 |
| 6 | • | - | - | • | - | - | - | - | - |
| 8 | • | • | - | • | • | - | • | - | - |
| 10 | • | • | • | • | • | - | • | • | - |
| 12 | • | • | • | • | • | • | • | • | - |
| 15 | • | • | • | • | • | • | • | • | • |
| 19 | • | • | • | • | • | • | • | • | • |

• Passes requirements of the applicable impact class

- Insufficient to satisfy requirement of the applicable impact class

Figure 10
Impact resistance classes per European Standard EN 12415 as of 2006⁴.

pullout. Test 5 was conducted to determine if this window design would have adequately retained the workpiece in the subject accident. The workpiece was launched at a velocity of 15.0 m/s (49.1 ft/s) to achieve an impact kinetic energy of 1,439 J (1,061 ft-lb), more than 10% greater than the larger of the two estimates of impact kinetic energy provided by the plaintiff's engineers (1,265 J = 933 ft-lb). At impact, the tempered glass shattered, but the polycarbonate window held — and the workpiece was retained.

Test 6 was of a hypothetical “maximum protection” window designed to see if a redesigned window could retain the subject workpiece given an impact energy in excess of the highest impact energy estimated for the

subject accident by any party. This alternative design used thicker steel for the exterior door panel and a lattice work of steel across the viewing pane. Lattice work subdivides the daylight opening of the window into a grid and is called “muntin bars” in glazier jargon. In this case, the muntin bars were intended to absorb impact energy in tandem with the polycarbonate window. The Test 6 workpiece (weighing 12.8 kg) was launched at a velocity of 30.7 m/s (49.1 fps), which developed over four times the kinetic energy estimated for the subject accident. The test was successful in that the door and window were heavily damaged, but the workpiece was retained.

Photographs of Tests 5 and 6 are presented in **Figures 11 and 12**. In **Figure 11**, the workpiece is highlighted with



Figure 11

Test 5 – European market CNC lathe window using 12-mm polycarbonate pane.



Figure 12

Test 6 – “Maximum Protection” CNC lathe window using muntin bars at exterior surface.

| Test | Mass kg / lbs | V-Impact m/s / ft/s | V-Exit | KE-Impact J / ft-lbs | KE-Exit | Comments |
|------|------------------|------------------------|--------|-------------------------|---------|--|
| T5 | 12.8 / 28.1 | 15.0 / 49.1 | 0 | 1439 / 1061 | 0 | 12 mm polycarbonate |
| T6 | 12.8 / 28.2 | 30.7 / 100.6 | 0 | 6033 / 4450 | 0 | 12 mm polycarbonate + 4.2 mm steel construction + window muntin bars |

Figure 13
Validation impact testing.

a green arrow showing rebound. In this test (and this test only), the workpiece missed the frame edge and interacted only with the window proper, ensuring that no energy was dissipated by frame deformation. The test details of Tests 5 and 6 are recorded in **Figure 13**.

Results and Conclusions

It has frequently been observed in mechanical design that adequate component strength is necessary but otherwise uninteresting. That is, a factor of safety in excess of a consensus standard and justifiably adequate level does not provide any incremental safety benefit, and “more strong than strong enough” is not any more beneficial than is “strong enough” in a practical sense.

For the analyzed accident, inadequate window guard strength was incorporated into the studied U.S. domestic market CNC lathe, and this inadequate window strength was a cause of the injury incurred by the operator. Had the stronger European market window utilizing 12-mm-thick polycarbonate been used instead of the weaker domestic market 4.5-mm polycarbonate window, then the accident would still have caused the door/window guard assembly to be severely damaged and in need of replacement. However, that is likely all that would have happened — no operator injury would have been incurred.

Acknowledgements

Special thanks to engineer Fritz Kucklick for his collaboration and insights.

References

1. Ferdinand Pierre Beer and E. Russell Johnston, *Vector Mechanics for Engineers*. McGraw-Hill Science, Engineering & Mathematics, 1977.
2. Performance Criteria for Safeguarding, ANSI B11.19-2003, 2003.
3. Safety Requirements for Turning Centers and Automatic, Numerically Controlled Turning Machines, ANSI B11.22-2002, 2002.
4. Safety Of Machine Tools - Small Numerically Controlled Turning Machines And Turning Centres, BS EN 12415:2001, 2001.
5. Machine tools - Safety - Turning machines, ISO 23125:2010, 2010.
6. Machine tools - Safety - Turning machines, ISO 23125:2015, 2015.
7. D. Mewes and R.-P. Trapp, “Impact Resistance of Materials for Guards on Cutting Machine Tools—Requirements in Future European Safety Standards,” *International Journal of Occupational Safety and Ergonomics*, vol. 6, no. 4, pp. 507–520, Jan. 2000.
8. D. Mewes, O. Mewes, S. Augustin, P. Herbst, “Festigkeit von Werkstoffen bei Aufprallbeanspruchungen: Einfluss von Projektilwerkstoff, -festigkeit und -form,” *Materials Testing*, 51(4):227-233, April 2009.

Methodology and Tools for Forensic Engineering Analysis of Electrical Shocks

By Chris Korinek, PE, DFE (NAFE 716S)

Abstract

Forensic engineering analyses (FEA) of electrical shock incidents are challenging because many factors need to be considered to understand how and why the incident happened. The goal is to determine how and why the victim's body became part of an electrical circuit that caused the shock injury. To do this, the engineer needs to determine, if possible, all of the connected portions that combined to make the complete circuit at the time of the shock, including the energized and non-energized conductors. Then, failures (defects) of components and violations from standards by parties involved with manufacturing, installing, inspecting, operating, and servicing the electrical circuits/systems involved need to be determined and their relation to the cause (failure-modes) evaluated¹. There will often be multiple circuits in the vicinity of the shock victim, some of which are pertinent to the shock and others that are not. These circuits need to be analyzed and non-pertinent circuits ruled out. When the pertinent circuit is determined, all the conductive elements and connections that form the (often three-dimensional) circuit should be identified. This includes service conductors, branch conductors, cords, portable devices, victims with their specific circumstances and conditions, their clothes, any moisture, tools, vehicles, and nearby materials, such as soil and vegetation. This paper outlines the scientific methodology and tools, logical decision analyses, and procedures for performing a shock analysis and provides specific examples based on actual investigations.

Keywords

Electrical shock injury, leakage current, resistance and impedance, insulation, stray voltage, electrophysiology, grounded conductor, grounding conductor, electrolyte, ground fault circuit interrupter

Background and Terms

This paper will focus on the forensic engineering investigations of electrical injuries involving an individual becoming part of an electrical circuit versus injuries due to flash, fire, or lightning. In the United States, there are approximately 1,000 deaths per year as a result of electrical injuries. Of these, approximately 400 are due to high-voltage electrical injuries, while lightning causes 50 to 300. There are also at least 30,000 shock incidents per year that are non-fatal. Each year, approximately 5% of all burn unit admissions in the United States occur as a result of electrical injuries. Approximately 20% of all electrical injuries occur in children. The incidence is highest in toddlers and adolescents. In adults, these injuries occur mostly in occupational settings and are the fourth-leading cause of workplace-related traumatic death, whereas, in children, electrical injuries occur most often at home². This paper will focus on the electrical causes — not the pathology,

diagnosis, therapy, or sequelae (except for a brief introduction to a diagnostic method that relates to how current flows in human tissue and informs the reader on one mechanism of shock injury). The general term “shock” is used in place of “electrocution,” since shock injuries may or may not be fatal — the common implication is that an electrocution is a fatal shock injury.

Using the scientific method, a forensic analyst should strive to complete the following steps³:

1. Gather data on all the parties and circuits that need to be analyzed, including actions taken by parties, photographs, interviews, measurements, pertinent standards in effect that impact electrical safety, history of the circuits, documentation on their installation, any alterations, and injuries sustained. Gather this information as early in the

investigation as possible because memories fade. The results from the data-gathering step will impact how scene and lab examination protocols are planned and performed.

2. Rule-in or rule-out circuits regarding causality, based upon scientific hypothesis testing.
3. Determine how and why any stray electrical current occurred and the path of the stray current that caused the electrical shock. Often multiple failures occur to cause the electrical hazard to be present. All of these necessary failures should be identified and their relation to the shock hazard discussed.
4. Evaluate if the results are consistent with the victim's condition and activities before and at the time of the accident.
5. Determine what human actions may have violated one or more standards that were causative to the electrical shock. An example of a party not meeting a standard is an electrician not installing a grounding and bonding conductor for a pool pump that is explicitly required in the installation manual and the electrical code requirements per the local inspector.

The following basic terms, which are often referred to without the adjective “electrical”⁴, are important as they have precise meanings and are consistent with the terms of art used in the electrical codes, standards, and trades.

Electrical charge: An excess or deficiency of electrons in a body⁵. Charged particles can be electrons (sub-atomic) or ions (atomic)⁶. Charge has units of Coulombs.

Conductors and insulators: Conductors permit the passage of charge through them; insulators do not⁶. The passage or lack of passage of charge is not perfect in the sense of 100 or zero percent passage. All materials allow some (large to minute amounts of) passage of charge — this will be discussed further in the section on resistance and impedance. Many conductors are metallic wires, but uninsulated metal enclosures that can pass charge in an abnormal situation after an insulation breakdown occurs are also important conductors in a system that guards against shock injury.

Voltage: A measure of the electrical potential difference

between two points⁷. Voltage has units of volts (V).

Electrical current: The current in a conductor is measured in amperes (A) and is a measure of the rate of motion of charge carriers in the conductor. Current is important in that it is related to conductor heating and determines the required size of the conductor, whereas voltage determines the insulation required for the conductor. The continuous current rating (ampacity) for a conductor depends on the temperature rise permitted for the conductor and its insulation because heat in a conductor is related to the square of the current in the conductor⁷. Direct current (DC) is a flow of charge in one direction only from a constant voltage source. Alternating current (AC) is charge flowing in alternating directions due to a voltage source that alternates from positive to negative voltage at a frequency of typically 50 or 60 cycles per second or hertz (Hz).

Electric circuit: An interconnection of electrical elements linked together in a closed path so that an electric current may flow continuously⁸.

Electrical resistance and impedance: The resistance of a given circuit, measured in ohms (symbol Ω), is used to determine the current in a circuit for a given voltage difference across elements of the circuit⁷. Impedance consists of resistive, capacitive, and inductive components⁸. Appliance electrical insulation resistance is typically millions of ohms (Meg Ω) and only allows minimal leakage current. For example, only 1.2 micro-amp (0.0000012A) flows through 100 M Ω (100,000,000 Ω) resistance when exposed to a voltage of 120V. Load resistances typically have much lower resistance, and the human body has a range of resistance of approximately 500 to many 1,000s of ohms, depending on the voltage, frequency, path of the current, time, and the condition or presence of the skin⁹. Tissues (such as blood, muscles, and nerves), moisture, and earth can also be conductors in a circuit path — and have their different impedances affect the flow of current^{4,9,10}.

Ground: The earth⁴. The earth is presumed to be at a potential of zero volts when it is not conducting current.

Grounded (or grounding): Connected (or connecting) to ground or a conductive body that extends the ground connection⁴.

Grounded conductor: A system or circuit conductor (designed to carry current under normal operating conditions) that is intentionally grounded⁴. An example is a

neutral conductor that can be at a potential greater than zero volts due to a voltage gradient while it carries current.

Grounding electrode (GE): A conducting object through which a direct connection to earth is established⁴. Common grounding electrodes include copper ground rods, metal water pipes, or building steel.

Grounding electrode conductor (GEC): A conductor used to connect the system grounded conductor or the equipment to a grounding electrode or to a point on the grounding electrode system⁴.

Equipment grounding conductor (EGC): A conductive path(s) that is part of an effective ground-fault current path and connects normally non-current-carrying metal parts of equipment together and to the system grounded conductor or to the grounding electrode conductor or both⁴.

Bonded (or bonding): Connected (or connecting) to establish electrical continuity or conductivity⁴.

Main bonding jumper (MJB): The connection between the grounded circuit conductor and the equipment grounding conductor or the supply-side bonding jumper (or both) at the service⁴.

Ungrounded: Not connected to ground or to a conductive body that extends the ground connection⁴. An example of an ungrounded conductor is one that is at full voltage for use in a device, such as 120VAC, 240VAC, 480VAC, and is often called a “hot” or “energized” conductor.

Ground fault: An unintentional, electrically conductive connection between an ungrounded conductor of an electrical circuit and the normally non-current-carrying conductors, metallic enclosures, metallic raceways, metallic equipment, or earth⁴.

Load: The device designed to use electrical energy to perform a desired purpose.

Stray voltage and stray (or leakage) current: Terms that will be used interchangeably and refer to undesired electrical potential and current flow that can cause a shock.

Figure 1 illustrates a ground fault in a load fed from a source transformer through a service circuit breaker¹¹. Numbers, letters, and arrows were added to the IAEI diagram by this author. Normally, current flows to the load

through the insulated energized conductors (“hot” and red arrows), flows through the load, and then flows safely back to the service/source through insulated grounded conductors (neutrals for 120VAC).

A correctly installed system keeps connections G1 and G2 as close to zero volts as possible as these are connected directly to earth ground. If there are separate EGC and grounded/neutral lugs, the main bonding jumper (MJB) connects the service EGC lug to the grounded/neutral lugs in the service panel to keep them at zero potential (G2). Problematically, a ground fault is shown where fault current flows, as shown by the purple arrows and lines, through the EGC, which is the conduit between the load and service enclosures, including bonding connections (A). Once this fault current reaches the area of the bonded service lug (G2), it can return to the source grounded connection at (G1) through three paths simultaneously:

1. Through the grounded conductor (neutral wire), as shown with the thick blue arrows (reference #1).
2. Through the bonded enclosures and conduit through bonding B connections, as shown with the thick green arrows (reference #2).
3. Through the earth ground loop as shown with the thick orange arrows (reference #3).

Normally, most fault current should flow through paths #1 and #2 as path #3 has the relatively high-impedance earth as part of the conductive path. The result of fault current flow through #1 and #2 is normally a short-duration

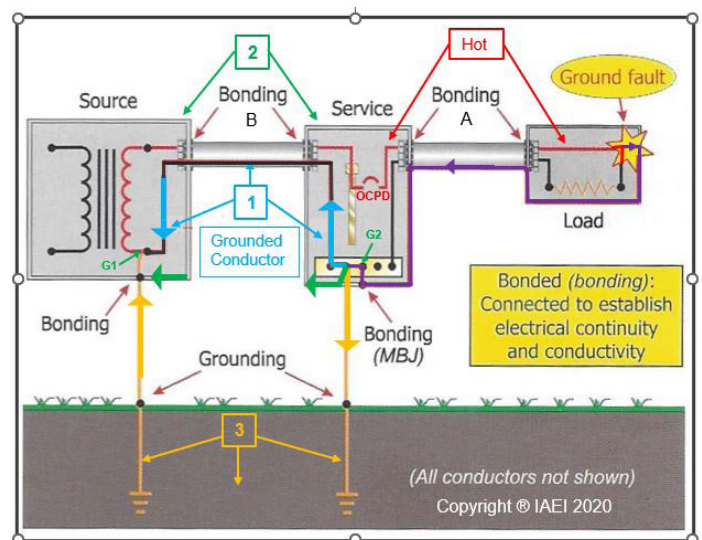


Figure 1
A ground fault and the resulting current paths¹¹.

overcurrent that trips an overcurrent device (OCPD), such as a fuse or circuit breaker so that no permanent damage occurs to the conductors or insulation systems — and the shock injury hazard is very short in duration. However, in a situation where there is no EGC between the service and the load and/or no bonding connections (A), the load enclosure may remain at 120VAC or a voltage substantially higher than a safe level. The load may or may not still be operating. The dangerous situation is further depicted as the shock hazard in **Figure 2**.

People Protection

The following devices and systems help protect users from shock hazards^{4,12}:

- A proper grounding network (made from the grounding and bonding components discussed above) forms a reservoir of zero potential materials. This is designed to allow stray current to be passively diverted away from vulnerable persons and cause active devices to operate and further decrease the probability of a shock injury.
- An OCPD is an active device that deenergizes a circuit after it senses overcurrent, commonly at or more than 120% of the current rating of the device. Refer to the trip curve for a particular OCPD as the trip time varies with the percentage of overcurrent. The OCPD can protect the wiring from overheating as well as persons from becoming part of the circuit if the circuit is de-energized prior to a person contacting the damaged device.

- A ground-fault circuit interrupter (GFCI or GFI) is an active device that measures the imbalance (leakage current) between the grounded and ungrounded conductors and will trip off if this imbalance reaches a nominal level of 5 milliamps (mA) or 0.005A.
- An arc-fault circuit interrupter (AFCI) or a residual current device (RCD) works in a similar way as a GFCI, but these devices trip at a nominal imbalance level of 30 mA (0.030 A) due to an abnormal current waveform.
- A double-insulated device has two independent insulation systems and no accessible grounded metal to become energized.
- A low-voltage device is one that operates at or less than 30VAC.

Normally, when electrical insulation is new and functioning well, its impedance can be thought of as infinitely high; however, it always has a finite quantity of impedance. When the insulation becomes degraded, its impedance can decrease to levels that may cause an electrical hazard.

Degradation due to surface contamination, moisture absorption, charring, dimensional and internal changes, and biological alterations may occur and cause the impedance to be reduced. Note the resistance drawn between the ungrounded and the EGC in **Figure 3**. This causes undesired current to flow. New plastic insulation for a 120VAC appliance cord may start out at an impedance of 100 MegΩ and only allow leakage current to ground of 1.2 microamps (0.0012 mA). If this impedance drops to 24 kilohms (24 kΩ), the leakage current increases to 5 mA, which is the

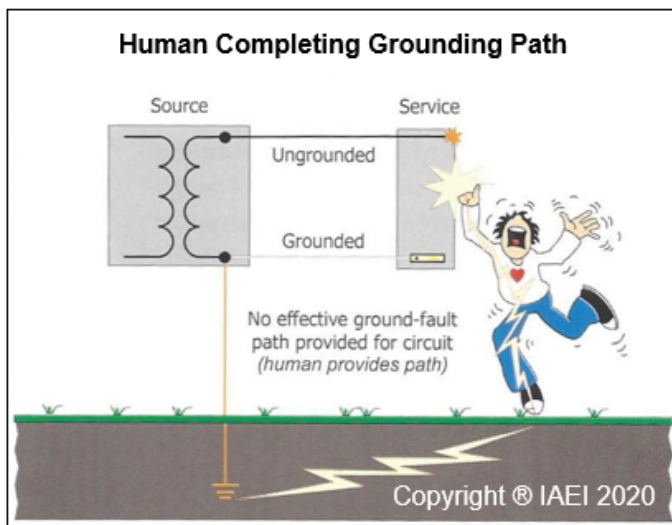


Figure 2
Shock through person in contact with an enclosure¹¹.

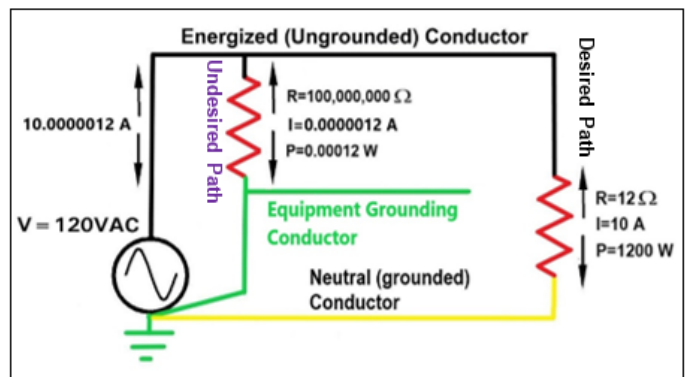


Figure 3
Schematic of current flowing through a desired path (black and yellow conductors) and an undesired path (green conductors).

leakage current level that should trip a GFCI. If there is no GFCI and the impedance drops to zero ohms, a person contacting the energized conductor will be the only impedance holding back the current from flowing. If a person contacts this energized conductor with no insulation, it is possible that the person may only add 500 to 1,000 Ω of impedance to this circuit, respectively, and the leakage current could reach 240 to 120 mA, which is above the level that can be fatal. The leakage current can normally be analyzed independently from the desired electrical current load (10A in this example) as seen in **Figure 3**.

If the conductor insulation inside an enclosure fails, the conductor contacts an accessible metal surface, and energizes the metal surface, the current path to ground can be through a person during a shock event, as shown in **Figure 2**¹¹.

How Electricity Affects the Human Body

Figure 4 shows how the body responds to increasing AC current⁷. The data shows the non-injurious perception at 1.0 mA through serious cardiac arrhythmia at 60 mA and other more serious conditions as the current increases. There are some differences between the effects on males versus females. Based upon this data, the trip levels for GFCIs were set at 5 mA, above the perception threshold and below the let-go currents (both considered safe levels).

The results of studies by Charles Dalziel in **Figure 5** show the different effects of electricity on the human body (men and women) for DC and AC⁹. It was found that, on average, the human body can tolerate DC current at a higher level than AC current, and males can tolerate higher currents than females.

Figure 6 shows valuable relationships between imbalance trip current versus shock duration for a typical GFCI, electrocution threshold, let-go thresholds for adults,

Table 3.3 Thresholds for effects of commercial electrical power

| Response | Threshold current* |
|---|--------------------|
| Perception | 1.0 mA (M) |
| | 0.5 mA (F) |
| Let-go | 16 mA (M) |
| | 11 mA (F) |
| Cardiac Arrhythmia | 60 mA |
| Ventricular fibrillation | 100 mA |
| Disruption of skeletal muscle membranes | 1500 mA [20] |

Notes:
 * Assumes current path in the upper extremity.
 (M) Males, (F) Females

Figure 4

Thresholds for effects of commercial electrical power.

and body resistances for 120VAC shock scenarios¹³. Highlights of red, yellow, and blue were added by this author for clarification and perspective. The black curves show the approximate GFCI performances for zero load and an imbalance with a load of 15A. There are also data points shown. Note that the vertical axis represents shock current, and the horizontal axis shows shock duration or trip time in log scales. From the graph, note the following:

- GFCIs have short trip times at high-current imbalances and longer trip times at low-current imbalances, but all are generally well under 0.1 second.
- All GFCIs trips shown are at an imbalance current of 4 mA and above. Below 3 mA, the GFCI will not trip.
- The yellow region represents the region where a GFCI will trip to safely deenergize a circuit.
- The maximum current of 240 mA level corresponds to a minimum body resistance of 500 Ω at 120VAC; other current levels are shown for the corresponding body resistances.
- The red line shows the locus of points for electrocution for adults, which corresponds to severe injury or death.
- The region where a GFCI will trip is outside the threshold for electrocution for adults.
- The blue line represents the let-go threshold for men, which can be inside the trip region; however, the trip time for this let-go phenomena will be less than 0.1 seconds.

| Effect | Direct Current (mA) | | 60-HZ Current (mA rms) | |
|---|---------------------|-------|------------------------|-------|
| | Men | Women | Men | Women |
| No sensation on hand | 1 | 0.6 | 0.4 | 0.3 |
| Slight tingling. Perception threshold | 5.2 | 3.5 | 1.1 | 0.7 |
| Shock — not painful and muscular control not lost | 9 | 6 | 1.8 | 1.2 |
| Painful shock — painful but muscular control not lost | 62 | 41 | 9 | 6 |
| Painful shock — let-go threshold | 76 | 51 | 16.0 | 10.5 |
| Painful and severe shock — muscular contractions, breathing difficult | 90 | 60 | 23 | 15 |

* From Dalziel, IEEE Trans. Bio. Med. Eng. 1956. 5:44-62.

Figure 5

Thresholds for effects of DC and AC for men and women.

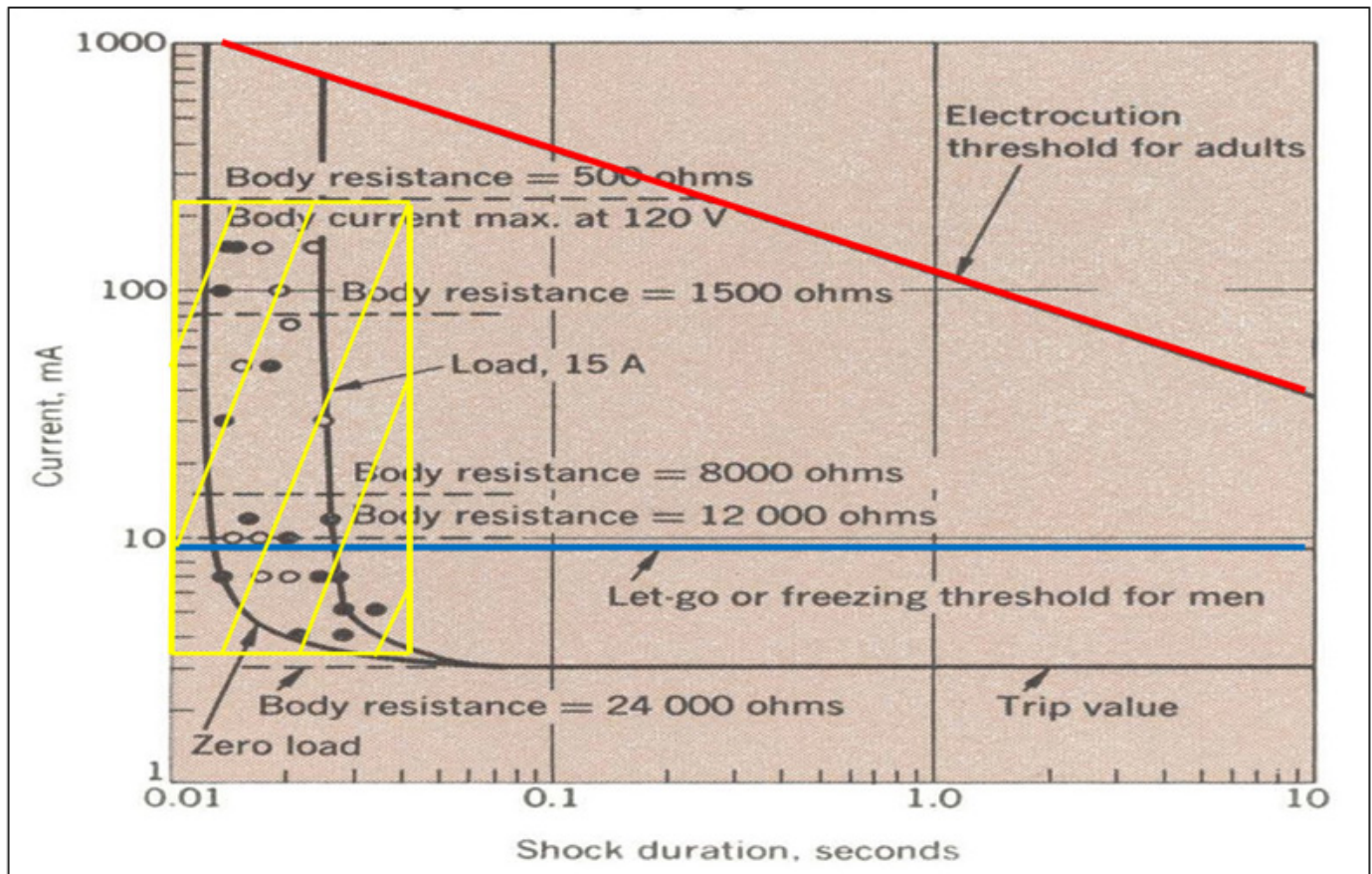


Figure 6

Imbalance trip current vs. shock duration for a typical GFCI, electrocution threshold, let-go thresholds for adults¹³. Colored lines were added by the author.

While it is interesting to know the effect of current on the human body, the exact value of the current at the time of the shock may not be known. There may be methods available to approximate the current for some shock scenarios, one of which will be discussed later in this paper. What is often more readily available is the voltage for the ungrounded conductors that often can stay constant for a given current draw. If the shock current exceeds the available current, the voltage may drop — this may need to be factored into the analysis. For all further discussions in this paper, it is assumed that the voltage stays constant during a shock incident¹³.

Conditions for obtaining experimental data for human exposure to voltage included intact skin, wet hands and feet, low current densities, and maximum current while still allowing the test subject to let go. In addition, Dalziel reported that the lowest fatal shock voltage known was at 46V. Some examples of standards that refer to safe voltages are Underwriters Laboratory (UL) 1310 (Class II Power units) that mentions 30VAC and 60VDC as safe and UL 1838, “Low Voltage Landscape Lighting Systems,” which refers to 15VAC and 30VDC as safe.

Factors in the severity of a shock include:

- 1) Current available
- 2) Voltage source
 - a) Amplitude (at start of and during shock)
 - b) Waveform (AC or DC)
 - c) Frequency of voltage source
- 3) Impedance/resistance
 - a) Skin impedance/resistance
 - i) Intact or open
 - ii) Surface area of contact
 - iii) Function of voltage (the higher the voltage, the lower the impedance)
 - b) Body structures impedance/resistance
 - c) Path of current through the body and whether this path includes the heart
 - d) Remainder of current path outside the body
- 4) Current exposure time

When current flows through a metal conductor and then to the human body, the mode of conduction often changes

from electronic (the flow of electrons) to ionic (the flow of ions). At the metal to skin contact point, the current flow undergoes an electrochemical reaction from electronic to ionic current flow that can generate rapid heating. The reaction rate is dependent on the voltage drop at this contact and can generate toxic chemical byproducts. All current flow through liquids is ionic in nature. By itself, saline solution has only resistive impedance; however, other tissues can have resistive and capacitive impedances that influence the magnitude and path of current flow through the tissues. **Figure 7** illustrates these concepts⁷.

Three main injury mechanisms for shocks include:

1. Arcing due to a dielectric breakdown in the current path — consists of ionized current flow through superheated air, which is highly conductive. Often, a bright flash of light is observed. There are approximately 300V required for a minimum gap to initiate the arc. After the arc is established, the arc continues with lower voltage across the gap. A metal to skin contact at 10 kilovolts (kV) can vaporize skin at 1,000°C and cause 10 to 20 A to flow through the body⁷.
2. Pure resistive or Joule heating — proportional to the square of the voltage for a given impedance⁷.
3. Electroporation due to cell membranes rupturing — the cells break open like soap bubbles with a pin. If the cell membranes rupture, the cells then most likely die. The cells function as capacitors

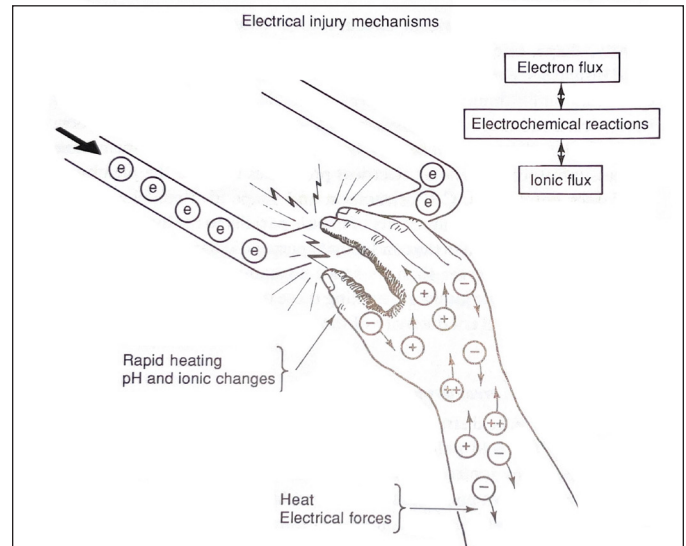


Figure 7

Effects of electrochemical conversion at the body surface during an electrical shock.

with their impedance being an inverse function with frequency⁷.

Electrical Impedance Spectroscopy

A diagnosis method called electrical impedance spectroscopy (EIS) evaluates the viability of burn tissue by measuring the capacitive impedance of tissue cells. It also gives insights as to how current flows in tissues due to resistive and capacitive (reactive) impedances. Measurements of the real and reactive impedances are made during a frequency sweep to determine if the cells have been ruptured.

Figure 8 shows a healthy tissue impedance plot (red

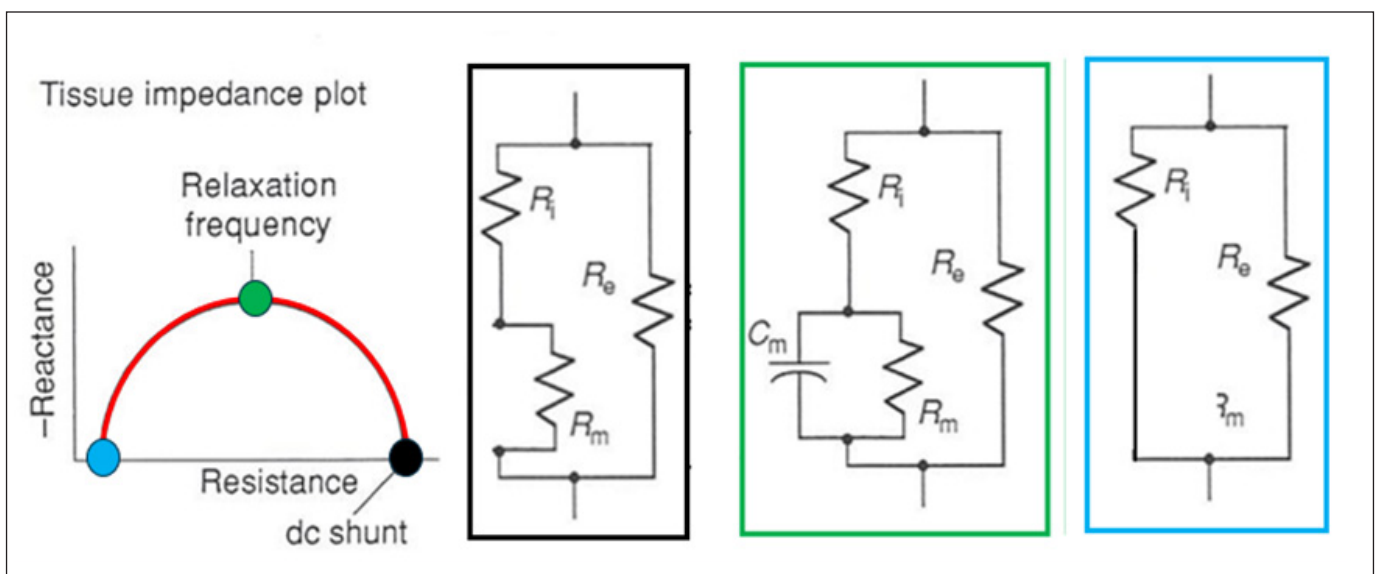


Figure 8

Healthy tissue impedance EIS plot.

curve) and its equivalent circuits in the colored boxes⁷. Lee's diagram was rearranged by this author for clarification and illustration of the frequency sweep concept, and colored highlights were added. As the frequency of the voltage changes from zero Hz (black) to the relaxation frequency (green) and then to a maximum frequency (blue), the plot would follow a circular curve, indicating if the cell walls were intact and acting like capacitors. From this diagram, it is seen that cells can conduct more current at higher frequencies because the impedances are lower at higher frequencies.

Figure 9 shows four plots, ranging from healthy (largest plot), partially damaged, and severely damaged, tissue (smallest plot)⁷. Colored dots and a dotted line were added to illustrate the change of the relaxation frequency impedances in healthy and damaged tissue. The resistive and reactive impedances for the zero, relaxation, and maximum frequencies all decrease with increasing tissue damage. Lee was able to correlate the quantities of these impedances to the probabilities of tissue necrosis toward the goal of identifying and removing this damage during the minimum number of surgical procedures. From this diagram, it is seen how damaged tissue can carry more current than healthy tissue as the impedance is lowered when the tissue is damaged.

Methods and Tools

Effective methods and tools for analyzing shock incidents include the following:

- Keep safety first to make sure another shock injury does not occur. Utilize safety methods, such as lockout/tagout (LOTO), to deenergize circuits and wear appropriate personal protective

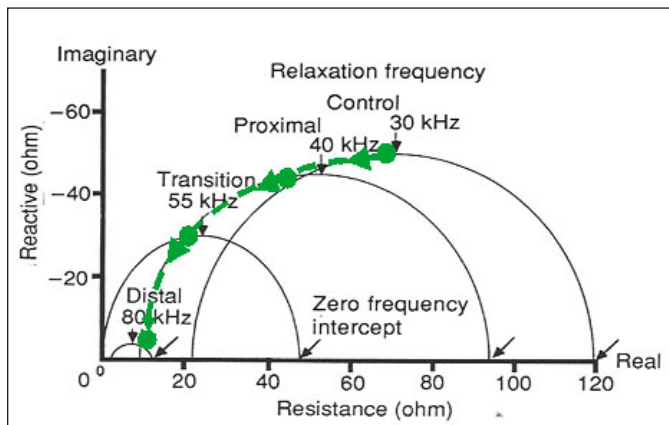


Figure 9
Comparison of healthy to damaged tissue impedance frequency plots for an EIS evaluation.

equipment (PPE) during analysis^{14,15}.

- Perform as much non-destructive data taking and analysis while the circuit is deenergized.
- Take additional precautions when energizing equipment that may be shorted to ground without tripping a protective device, and announce these precautions to all in the area. Be aware that energizing circuits may be destructive in nature.
- Use the appropriate meter in the appropriate manner for checking electrical parameters, and be aware of the limitations of the measurement devices. Read and understand the operation manuals for all meters and equipment used. In one case, an electrician attempted to measure ground continuity by obtaining a zero-voltage measurement between two exposed metal surfaces. If there was a continuous ground, there would be no voltage between the two exposed metal surfaces; however, just because there is no voltage does not mean that there is continuity. The electrician concluded that there was ground continuity, but this turned out to be erroneous. This error contributed to the potential for a future shock injury. In this case, a resistance measurement would have been the correct method to measure ground continuity.
- Measure insulation resistance when appropriate. A 12VDC powered multimeter can measure low resistances well but may not measure a more realistic resistance when the device is powered. Using a megger at 500 or 1,000VDC to non-destructively check the resistance of a device may be a more realistic value of the insulation resistance at the full operating voltage. Refer to the UL standard for the device hipot testing requirement and the operation manual for the megger used¹⁶.
- The analyst may use safety devices such as a GFCI, AFCI, or RCD during measurements while full voltage is applied to a circuit under evaluation to both assist in evaluating the level of leakage current present and to protect the persons performing the tests.

Different Shock Scenarios

Shock current paths and the impedances involved can vary between incidents requiring all possible paths to be evaluated individually. Certain shock paths are simpler

with fewer impedances in series with the victim's body (i.e., if a victim's two wet hands had grasped two metallic surfaces involved with the current path). In this case, the voltage between the metal surfaces can be measured. In parallel with the voltage reading, the current through a known impedance can be measured. This may inform the investigator as to the possible current through the victim, if the impedance is similar to the victim's impedance and if all other impedances in the circuit have remained constant since the shock incident. If the victim's hands were wet or their skin impedance were compromised, an impedance of $1,000 \Omega$ may be in the range of the impedance of the victim's body. This current reading would then also take into account other (often hidden) impedances in the complete path in series with the victim. It also helps determine if the total impedance present was low enough to allow a dangerous current to flow through the victim's body, given the available voltage source. An example of a more complex path with additional impedances may be a person swimming in a pool and not touching any metal surfaces. Current flows through the pool water, and an electric field exists. Early testing by Dalziel with dogs was done with this shock path to determine when the dogs would exhibit loss of muscle control¹³.

To simulate the type of shock path with a person having body parts immersed in water but not touching any metal, a simple lab test was performed. This test setup is shown in **Figure 10**. Various 120VAC voltage sources were placed into a plastic pan with a grounded copper pipe on the other side of the pan, approximately 14 inches (in.) apart. The voltage source and pipe were covered with tap water. Wires

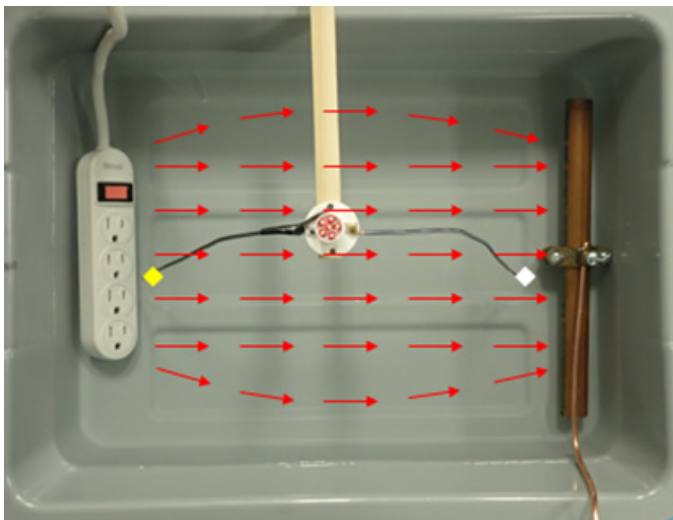


Figure 10

Test arrangement to measure voltage drop in water due to an electric field.

were placed into the water with the bare ends being 11 in. apart as shown by the yellow and white squares.

Voltage readings were taken between the ends of the wires. Red arrows were drawn onto this test setup figure to indicate an instantaneous electric field from an alternating current voltage source to a grounded metal object. The yellow diamond is an inch and a half from the power strip. The white diamond is an inch and a half from the grounded copper tube. Current measurements were not made, but it is expected that additional electrolytes in the water, such as salt, would decrease the overall impedance of the circuit and increase the current flow through the 1.5 in. of water on either of the two gaps between the ends of the wires and the metallic conductors as shown by the white arrows. The gap on the left is seen between the yellow square and the ungrounded conductors inside the RPT, and the gap on the right is seen between the white square and the grounding clamp.

The following devices were placed into the water for testing in the same position:

- A relocatable power tap (RPT) or power strip with plastic enclosure or case with EGC. This allows for three current paths: ungrounded conductor to EGC, ungrounded conductor to grounded conductor, and ungrounded conductor to grounded copper pipe.
- An RPT with a metal case with EGC. This allows for four current paths: ungrounded conductor to EGC on inside of RPT, ungrounded conductor to EGC on exterior of RPT, ungrounded conductor to grounded conductor, and ungrounded conductor to grounded copper pipe.
- A double-insulated hair dryer with a plastic case and no EGC. This allows for two current paths: ungrounded conductor to grounded conductor, and ungrounded conductor to grounded copper pipe.
- An RPT with a metal case with no internal EGC (to simulate it being plugged into a cheater plug with no ground connection to the receptacle). This allows for three current paths: ungrounded conductor to EGC, ungrounded conductor to grounded, and ungrounded conductor to grounded copper pipe.
- An RPT with a plastic case (with EGC) and

cord plugged into the RPT with only the bare un-grounded wire exposed. This allows for three current paths, ungrounded conductor to EGC, ungrounded conductor to grounded conductor, and ungrounded conductor to grounded copper pipe.

- A RPT with a metal case with no internal EGC and the metal case energized. This allows for only one current path, the ungrounded conductor to the grounded copper pipe.

The first three devices (1, 2, and 3) with no defects were placed into the water. These voltage drop readings in the water are shown as the blue bars on the graph in **Figure 11**. The red line in this graph is at 30VAC, which is the AC voltage generally deemed safe. The other three devices with defects (4, 5, and 6) were placed into the water; these voltage drop readings in the water can be seen as the red bars on the graph.

This test illustrates that, especially for defective devices and applications, a dangerous shock at a dangerous voltage is possible even if a person is not touching one or more metal surfaces. Many of the results in this chart (red-colored bars) are near and above the maximum safe level of voltages discussed earlier. A takeaway from this test is that there is a greater chance of a dangerous shock if certain defects are present. This is especially true for those that allow an energized conductor to be closer to a person

than when the defect is not present and if there is a lack of an EGC. A proper EGC can act to collect stray current because it is often near the energized conductors. If the EGC encloses the energized conductor or it is between a person and the energized conductor — even more personal protection is afforded to a person outside the enclosure.

Standards

A standard is defined as “a model accepted as correct by custom, consent, or authority or a criterion for measuring acceptability, quality, or accuracy”¹. Some common standards for various parties involved (including electricians, forensic engineers, and other experts) are used to judge the actions of the party involved prior to, during, and/or after an electrical shock incident. The pertinent standard is the document that was in effect at the time of the party’s involvement, including, but not limited to:

- Manuals, labels, and instructions provided by the manufacturer and used by installers, inspectors, operators, servicers, etc.
- Written company policies for various companies involved, such as utilities, manufacturers, etc.
- Construction and performance standards such as the NEC and International Electrical, Mechanical, and Building Codes (IEC, IMC, IBC), written by standard bodies and used by architects, designers, installers, inspectors, etc.

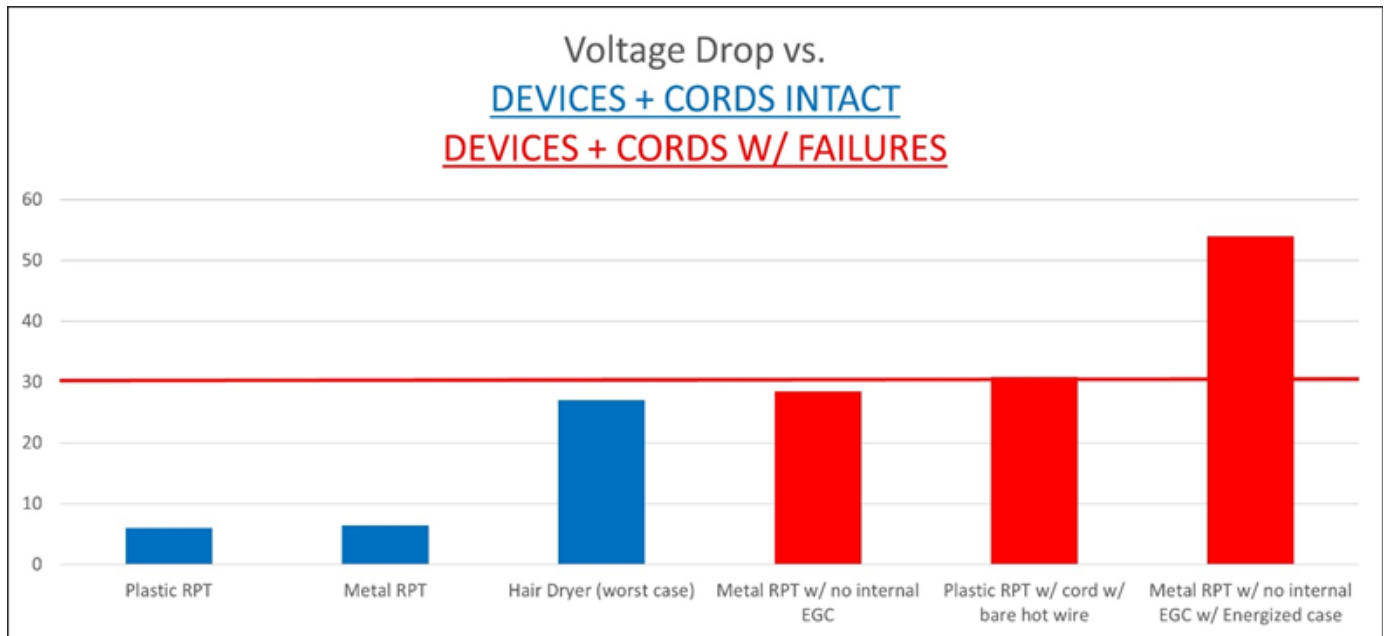


Figure 11
Voltage measurements in water due to an electrical field.

- National Electric Safety Code (NEC), written by the Institute of Electrical and Electronics Engineers (IEEE) for utilities and subcontractors to design, construct, inspect, and service electrical distribution and transmission equipment.
- National Fire Protection Association (NFPA) 70E, Standard for Electrical Safety in the Workplace used by safety and maintenance personnel, manufacturers, installers, inspectors, servicers, etc.
- Independent testing agencies such as UL, Canadian Standards Association (CSA), and Intertek (ETL), for manufacturers, installers, inspectors, etc.
- Standards-writing bodies such as American National Standards Institute (ANSI), American Society of Materials (ASM), for manufacturers, installers, inspectors, etc.
- Decisions by local authorities having jurisdiction (AHJs).
- Federal, state, and local codes that draw upon other standards with alterations as decided upon by federal, state, and local legislators and AHJs.
- Associations for specific industries for designers, manufacturers, installers, inspectors, servicers, etc. One example is the Association for the Advancement of Medical Instrumentation (AAMI) medical device standards.
- Trade association training programs and texts for trades workers, such as electricians.
- Textbooks for a particular discipline for use in applying basic principles to solving specific problems.

One pertinent example is for determining whether an electrical device was properly grounded and bonded during installation. The installation manual may give specific instructions on how to ground and bond the device. If not, the question of whether installation meets “Code” can be determined by consulting the local AHJ to determine if they have adopted the same version of the NEC (possibly with alterations) as the state or if they have different alterations of a local variety. Again, the standard to be used in

judging the installation is what was in effect at the time of installation.

Case Study

The author’s firm along with another firm were hired to investigate a tragic incident on behalf of the estate of a man who was a guest at a residential pool party who was fatally electrocuted while jumping a fence after exiting the pool to get a ball. The homeowner’s insurance carrier also hired a forensic engineer. The death certificate stated the cause of death was anoxic encephalopathy due to cardiac arrest due to ventricular fibrillation due to electrocution. In other words, electrocution caused his heart to go into an abnormal rhythm, which led to cardiac arrest and then to brain death due to lack of oxygen.

The layout of the pool is shown in **Figure 12** (a Google Earth image from before the incident). The electrical system for the pool is fed by the circuits in the pool house, and there is a chain link fence that surrounds the pool and deck. Electrical circuits in the immediate vicinity of the pool include in-pool lights, a string of lights hung on the fence that was powered from an extension cord, a light pole approximately 23 in. west of the chain link fence, and a receptacle on the southern corner of the fence.

The initial basic facts given prior to the scene visit were as follows. The man exited the pool to retrieve a ball and was in the process of climbing over a metal fence when he stopped moving and lost consciousness. The fence had always been next to the pool — since no one ever received



Figure 12
Pool layout.

a shock from the fence, it was mentioned by a member of the investigation group that it may be difficult or impossible to determine how this fence became energized. In the initial discussion, the author made a special point to not form presumptions, but to search for the source of the unwanted voltage and the ground path back to the source and let the scientific method determine the conclusions.

The police department had done interviews of the pool party attendees; these interviews yielded valuable details as to what happened as the man exited the pool and attempted to get over the fence. They also included the details that when he became stuck with one leg on either side of the fence, slid down the side of the fence, one person said his hands were stuck grabbing the fence, and another said he grabbed onto the light pole and received a shock from the pole. There was a short video of the pool party taken before the shock incident that showed the string lights operating. There were no thunderstorms in the area on the day of the incident.

There was an initial non-destructive scene exam, and the premises was surveyed as to the electrical system in the home and the visible items in the vicinity of the pool. The author found many potential electrical problems with the pool electrical systems, such as a lack of GFCIs, lack of grounding, multiple corroded conduits and exposed wires, rodent damage, etc. However, it was unknown which were causal to the injury.

The author found a hole in the lawn where there were individual visibly exposed wires (with colored insulation) as 7 in. of the underground conduit had disintegrated due to corrosion as seen in the white ellipse in **Figure 13**. Plus, there were many unanswered questions about the detailed actions of the man and other site anomalies, which caused the team to only do a non-destructive brief broad survey of the electrical characteristics over a large physical area.

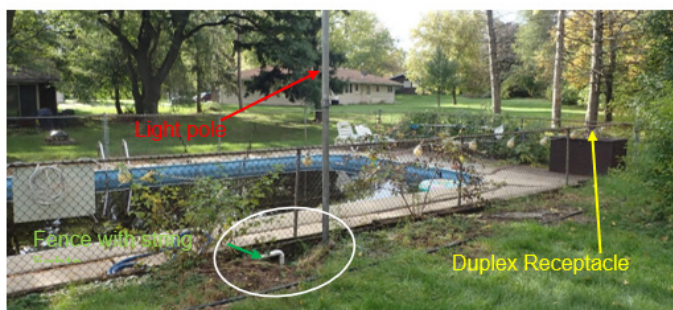


Figure 13

Pool layout and hole in lawn (see white ellipse).

There were many circuits and structures underground that could have been involved with the shock scenario. Since the forensic engineers were not allowed to energize any circuits at the pool, they could not detect stray voltage or current.

Figure 14 shows the state of the electrical pool controls inside the pool house that had a doorway, but no door. Damage found included corroded enclosures, corroded and disintegrated conduits (one is shown inside the yellow rectangles), multiple cords, and rodent damage. The individual visibly exposed wires (with colored insulation) in the yellow rectangle in **Figure 14** were similar to the wires that were visible in the hole in the lawn in the white ellipse in **Figure 13**.

Since one of the team's major investigation goals for the second scene exam was to determine what conductive materials were contacted by any of the extremities or body part — and to then determine the voltages of each of these body contact points — the author was interested in any recent electrical work, repairs, or problems, the motions of the man, the reasons for these motions, and what witnesses observed during these motions, what devices were energized and/or operating at the time of the shock, and why there was a hole in the lawn. Another goal was to discover pertinent information by examination of above-ground circuits and structures with a minimum excavation of any underground circuits and structures, such as feeders, lights, or grounding and bonding conductors.

After some discussion, it was thought by some that the team should use discretion and not ask questions early in the investigation because certain people could become

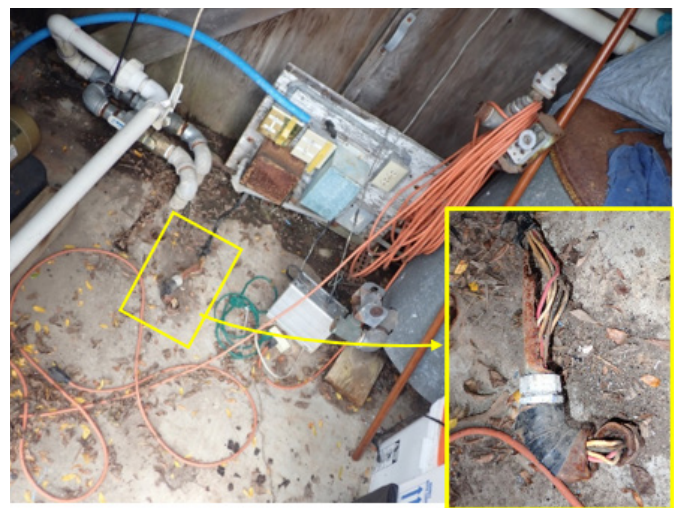


Figure 14

Pool house electrical controls.

upset, and there might not be answers forthcoming. Nonetheless, a list of 25 questions was drawn up and submitted to the homeowners. To the forensic engineering team's surprise, answers to most of the questions were forthcoming. The author learned the history of the home, that there were no recent changes or previous problems or shocks, that all lights were turned on and operating, the receptacle was not used, the man had climbed the fence near the light pole, the reason for the hole in the lawn, and that the city inspector turned off circuit breakers in the basement after the incident.

The homeowners were aware that there had been a pool pipe leak that had eroded the ground and caused the hole in the lawn. The leak had been recently repaired, and the hole in the lawn not been filled in. This information greatly allowed the author to focus the investigation on the area of the fence and light pole, even though other circuits were documented and tested as well. Prior to the second scene exam, the author also asked for permission to excavate, as little as necessary. After some initial pushback, the team was given approval to excavate with discretion.

During the second scene exam, the team was able to energize the pool circuits and measure a stray voltage of 102VAC from the light pole to the fence. To characterize the remaining circuit, a resistor of impedance of 1,000 Ω (in the ballpark of a wet body experiencing an electric shock) was wired in series with a multimeter to measure the current through the resistance. A current of 102 mA flowed through the 1,000- Ω resistor connected to the light pole and fence, indicating that the total impedance of the

circuit was only 1,000 Ω , and the impedance of the underground portions of the circuit was negligible. No other electrical anomalies were found in the general area of the fence and light pole. After the measurements were taken, the local area was minimally excavated, underground circuits documented, the light pole cut down, and the wires internal to the light pole were examined.

Figure 15 illustrates two photos that show a portion of the internal wiring for the light pole that had splices with electrical tape for insulation. It was found that a bare copper wire had worn through the tape (as seen in the yellow circles), and the copper wire was able to touch the inside of the light pole to energize the metallic light pole with 102VAC.

After the voltage between and current through the light pole and the fence was measured, the power to the light pole was turned off, and a test was performed to determine if an EGC was present, would the circuit breaker trip or the fault clear. A #12 AWG copper wire was affixed to the light pole and the grounding electrode conductor at the pool house. When the power was reapplied to the light pole, a brief current of 11.4A AC was recorded. The circuit breaker did not trip, but the fault cleared itself; the light pole was found to be not energized after this test. The author's conclusions included:

1. The causes of the electrocution in this incident were both of the following conditions occurring simultaneously:
 - a. A failure in the electrical system of the light



Figure 15

Internal wiring for the light pole with a bare copper wire protruding through a worn hole in electrical tape.

- pole circuits such that stray voltage and current occur, resulting in the light pole becoming energized. This failure was a lack of insulation on the electrical conductors such that an energized copper wire came into contact with the inside of the metallic light pole, allowing stray voltage and current to enter the light pole.
- b. A failure in the electrical system of the light pole circuits caused the energized light pole to persist and not be terminated immediately. This failure was the absence of an intact and continuous underground conduit, acting as an EGC, which would have allowed the fault current to flow and cause the circuit breaker to trip or the fault to open, thereby deenergizing the light pole.
2. The electrocution occurred when portions of the victim's wet body simultaneously touched the energized light pole and the chain link fence. When this occurred, a closed circuit was formed such that the energized light pole caused electrical current to flow through his body to ground — this electrical current caused the electrocution. Based on the information available, one hand touched the light pole, and one hand, his torso, and legs touched the chain link fence.
 3. The abnormalities and damage to the light pole conduit and wire in the hole in the lawn and the conduit in the pool house, detailed in this report, were conditions of disrepair and lack of maintenance of the pool electrical system that were visible to the homeowner.
 4. The abnormalities and damage posed hazards to persons in the yard in the vicinity of the pool house and west edge of the pool:
 - a. Physical protection of the individual wires had been lost due to the missing metallic conduit in the pool house and in the hole in the ground on the west edge of the pool. Any damage to the individual wire insulation would have allowed voltage and current leakage into materials or persons in the vicinity of these wires.
 - b. The path for stray voltage and current to return to the grounding network, which performs a critical safety function, had been lost due to the conduit being missing, disintegrated, or corroded.
 5. The lack of a conduit and the exposed wires in the hole in the ground near the light pole and fence existed prior to the electrocution, had been caused by a leak of pool water, and should have been repaired by a licensed electrician to the NEC in effect at the time.
 6. If repairs and maintenance had been performed by a licensed electrician and the circuit brought up to the NEC, an EGC would have been installed. A proper intact and continuous EGC could have been accomplished by a properly installed metallic conduit, a ground wire, or both.
 7. This electrocution would not have occurred if there had been a proper and continuous EGC for the pool light. Having proper EGCs would have caused the circuit breaker to trip or a fault to open if a ground fault to an exposed metal surface in the vicinity of the pool had occurred (such as at the light pole). This was borne out by the test that was run when an EGC was installed, and the light pole energized with the result being that the fault cleared itself without the circuit breaker tripping. Not having an EGC meant that the circuit breaker would not trip, or the ground fault would not be opened, leaving an extremely dangerous condition to persist.
 8. The conditions of disrepair and lack of maintenance inside the pool house, lack of GFCIs for the pool pump, pool receptacle, and string lights and the use of the string lights too close to the pool should have been noticed and repaired as they were safety hazards that could have been a cause of an injury.
 9. The danger of electrocution from the short circuit inside the light pole would have been eliminated by a proper intact and continuous EGC for the light pole. The discontinuity in the conduit (light pole EGC) was visible to the homeowner.
 10. On the date of loss, the local township and the state statutes required the light pole to be grounded per [redacted], following NEC 2017 and all editions of NEC from 1947 to 2017. The State statutes required all repairs to the light pole to have proper grounding to the State Electrical Code in effect at the time of the repair.
 11. The measured current of 102 mA AC through the 1,000-Ω resistor indicates that the total impedance

in the remaining portions of the completed circuit, necessary for current to flow, were negligible. The electrocution is consistent with a current at or near 102 mA AC.

12. It is the author’s opinion that the electrocution would have been prevented had the electrical system and structures around the pool been properly maintained and repaired.

For clarity’s sake, **Figure 16** shows two diagrams of the pertinent pool circuit components. The left-hand diagram shows the circuits as they should have existed under prevailing codes and standards such that a short circuit to the light pole could be carried to ground by continuously connected conduits as EGCs. The right-hand diagram shows the pool circuits as they were in the incident where the conduits were not continuous, eliminating this as a current path and creating the causal hazard.

The case was settled at mediation.

Overview

To summarize:

1. Keep safety first.
2. Strive to determine the truth as to what occurred and why regarding the incident.
3. Be proactive as to what is needed for a thorough investigation, not only reactive to information already available.

4. Perform non-destructive testing first; then consider destructive testing after notification of all interested parties.
5. Analyze applying the scientific principles and engineering methodologies.
 - a. Develop incident scenarios based upon the supplied data/information, reports, photos, examinations, statements, depositions.
 - b. Limit the forensic engineering analysis to the expertise of the engineer.
 - c. Gather data (detailed and thorough as often alterations have been made to make the scene safer).
 - d. Analyze data (evaluate data with respect to protection schemes present and defeated, patterns, circuits, time lines, consistency of injuries to shock possibilities, etc.).
 - e. Synthesize all possible hypotheses and the corresponding postulates.
 - f. Verify and validate (V&V) the hypotheses to determine the scenario and cause(s) of the incident.
 - g. Select the final (highest probability) hypothesis.
6. Develop conclusions as to whether certain standards were or were not met by the parties involved.

Conclusions

The scientific method can be used to identify the (often three-dimensional) complete circuit of current flow

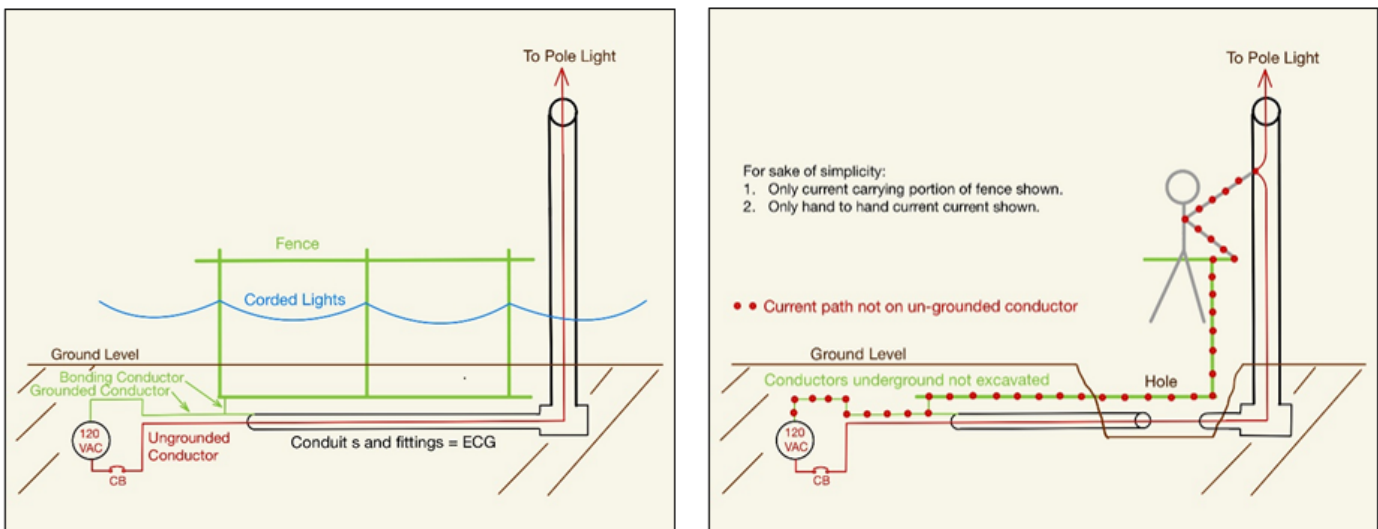


Figure 16
Two diagrams — reasonably safe circuits on the left; hazardous circuits on the right.

through the body of a shock victim. This paper lays out the fundamentals of shock analyses addressing the basics and vernacular of electrical faults, the effects of electricity on the human body, and the various ways electrical energy flows and causes tissue damage. Furthermore, it discusses the need to identify the pertinent standards (material to the cause of the shock incident) that were in effect and not met by specific parties.

This forensic engineering analysis can be challenging as equipment is often altered after the incident, conditions (e.g., the presence of moisture) may have changed since the incident, witnesses may be injured, killed, or have psychological trauma, memories fade quickly, and there are often other multiple circuits in the general or immediate area of the shock incident that need to be ruled out. Purposeful and proactive planning should be done as early as possible with the investigation team to gather the maximum amount of data as early as possible that can inform how the examinations are carried out. To maximize efficiencies, protocols can be written, distributed, and discussed amongst all interested parties to accomplish the goals of the investigation utilizing the site and lab resources and time available.

References

1. E. i. C. Brian Garner, Dictionary, Black's Law, St. Paul, MN: Thompson West, 1999.
2. M. R. Zemaitis, L. A. Foris, R. A. Lopez and M. R. Huecker, "Electrical Injuries," StatPearls Publishing LLC., 26 August 2021. [Online]. Available: <https://www.ncbi.nlm.nih.gov/books/NBK448087/#:~:text=In%20the%20United%20States%2C%20there,year%20that%20are%20non%2Dfatal>. [Accessed 22 April 2022].
3. P. Laura Liptai, "Forensic Engineering and the Scientific Method," Journal of the National Academy of Forensic Engineers, vol. XXVI, no. June 2009, p. 10, 2009.
4. NFPA, National Electric Code, NFPA 70, Quincy, MA: National Fire Protection Association (NFPA), 2020.
5. G. & C. Merriam Co., Webster's New Collegiate Dictionary, Springfield, MA USA: G. & C. Merriam Co., 1975.
6. F. W. a. Z. M. W. Sears, University Physics, Fourth Edition, Reading, MA, USA: Addison-Wesley Publishing Co., Inc., 1970.
7. R. C. Lee, Electrical Trauma, The Pathophysiology, Manifestations and Clinical Management, Cambridge UK: Cambridge University Press, 1992.
8. R. D. a. J. Svoboda, Introduction to Electric Circuits, New York, NY USA: John Wiley & Sons, Inc., 4th Edition.
9. L. A. Geddes, Handbook of Electrical Hazards and Accidents, CRC Press, Inc., 1995.
10. International Electrotechnical Committee (IEC), "Effects of Current on Human Beings and Livestock IEC TS 60479-1," International Electrotechnical Committee (IEC), Geneva Switzerland, 2005.
11. International Association of Electrical Inspectors, Soares Book on Grounding and Bonding 14E, 2020 NEC, Richardson, TX: International Association of Electrical Inspectors, 2020.
12. J. G. Webster, Medical Instrumentation, New York, NY: John Wiley and Sons, Inc., 1998.
13. C. F. , "Electrical Shock Hazard," IEEE, vol. 9, no. 2, p. 9, 1972.
14. OSHA (. Administration, "Control of Hazardous Energy (Lockout/Tagout) 29 CFR 1910.147," United States Department of Labor, [Online]. Available: <https://www.osha.gov/laws-regs/regulations/standardnumber/1910/1910.147>. [Accessed 22 April 2022].
15. OSHA, "Personal Protective Equipment CFR 1910.132," United States Department of Labor, [Online]. Available: <https://www.osha.gov/laws-regs/regulations/standardnumber/1910/1910.132>. [Accessed 22 April 2022].
16. D. Norman, "Does High Voltage Testing Damage A Motor?," Baker Instruments, [Online]. Available: <https://megger.widen.net/s/dmtw8nhqwd>. [Accessed 22 April 2022].

Forensic Examination of Post-Fire Damaged Electrical Conductors by Using X-Ray Radiographs

By Mark J. Svare, PhD, PE, DFE (NAFE 851M) and Niamh Nic Daeid, PhD

Abstract

Structural fires globally have a catastrophic impact on loss of life, property damage, and socioeconomic factors. Forensic scientists, engineers, and/or fire investigators — often working together as fire investigation practitioners — are commonly tasked with determining both the area of fire origin and its cause. During the course of a fire investigation, a fire investigation practitioner may implement an origin determination methodology termed “arc mapping” or an “arc survey.” The correct application of an arc survey as a fire origin determination method is dependent on the fire investigation practitioner’s ability to distinguish and characterize features observed on post-fire damage electrical wiring and equipment. Experiments were conducted to generate a dataset of post-fire damaged electrical conductor artifacts. Generated artifacts were visually examined, compared, and characterized by X-ray examination. The research results produced a validated, novel, non-destructive methodology for utilizing X-ray imagery to reliably distinguish and characterize electrical conductor damage features for forensic investigations.

Keywords

Arc mapping, arc survey, arc, artifact, bead, conductors, electrical, fire, fire investigation, forensic engineering, science, origin and cause investigation, microstructure, porosity, X-ray, radiograph, computed tomography, NDT

Introduction and Background

Structural fires globally have a catastrophic impact on loss of life, personal injury, property damage, and socioeconomic factors (**Figure 1**). Forensic scientists, forensic engineers, and fire investigators (fire investigation practitioners), often working together as a team, are commonly tasked with determining both the area of fire origin and its cause. The National Fire Protection Association (NFPA) 921, “Guide for Fire and Explosion Investigations,” 2021 edition¹ is currently recognized as an industry guide for fire and explosion investigations.

According to NFPA 921, the cause of a fire is identified after the fire origin has been determined by utilizing data collected from one or more of the recognized origin determination methods. During the course of a fire investigation, fire investigation practitioners may implement an electrical origin determination methodology called “arc mapping,” which is a term defined by NFPA 921 as “Identifying and documenting a fire pattern derived from the identification of arc sites used to aid in determining the area of fire origin or spread”¹. The proper application of arc mapping — or

more recently called an “arc survey” — requires the qualified fire investigation practitioner to conduct an electrical system survey, identify features of electrical fault damage, and evaluate the derived electrical data.



Figure 1
Structure fire.

Currently, the fire investigation practitioner utilizes subjective observations to attempt to identify features of damage observed on electrical conductors and conducting surfaces. X-ray imagery, a non-destructive testing (NDT) method, has been reliably utilized within manufacturing and medical industries for more than a century. X-ray imagery utilized in fire investigations can assist the fire investigation practitioner in characterizing features of post-fire damaged electrical wiring and equipment, thereby further assisting the fire investigation practitioner to more reliably analyze post-fire damaged artifacts and provide further underpinning evidence supporting an electrical system-based origin determination methodology.

Fire Investigation and Arc Mapping (Arc Survey)

Examination of post-fire damage to electrical wiring and equipment within buildings provides fire investigation practitioners with data that can assist in both fire origin and cause determination. NFPA 921 describes the origin of a fire as one of the most important hypotheses that a fire investigation practitioner develops and tests during the investigation¹. It further outlines the means of coordinating data gathered from one or more of the three recognized origin determination methods: witness information, fire patterns, and fire dynamics¹. The data collected during the fire origin determination phase of the investigation becomes the foundation of the fire investigation, which leads to understanding a fire, its sequence of events, origin determination, hypothesis development and testing, and determination of the cause of the fire. Noting the location of arc sites at the fire scene was first introduced to the fire investigation community within NFPA 921, 2001 edition². Subsequently, the terms “arc surveys” and “arc mapping” were added within later editions of NFPA 921 — 2004 and 2008, respectively^{3,4}.

Safety Note:

Electricity can be a dangerous occupational hazard. Forensic investigation practitioners may work in areas where this hazard exists. Prior to work, determine site-specific or foreseeable safety hazards, understand your employer’s health and safety program, and review safety documents related to workplace hazards. National Fire Protection Association’s NFPA 70E, “Standard for Electrical Safety in the Workplace,” which addresses safety-related work practices, can help reduce the risk of electrically related workplace injuries¹¹.

Electrical Arcing: Cause or Victim

An effort to reliably develop a methodology to distinguish between arcing events that cause a fire versus arcing events that are a victim of a fire actually began in the 1970s. Numerous researchers conducted experiments attempting to develop methodologies to distinguish the differences between causal and victim arc damage observed on post-fire damaged electrical conductors. However, some researchers concluded that they could not find much promise with any of the methods that were proposed for distinguishing between “cause” and “victim” beads — and that reliable distinctions between “cause” and “victim” beads were yet to be discovered⁵. Therefore, it is commonly accepted within the forensic investigation community that a reliable methodology has yet to be developed to distinguish the difference between causal arc sites (fire starting) and victim (fire attacked) arc sites.

Up until the 1980s, fire investigators had attempted to answer a “cause” question before answering the critical “origin” question. A reversal of this frame of thinking was (and still is) required. Once this mindset changed, then the effectiveness of an electrically based fire investigative methodology like arc mapping (otherwise known as an arc survey) for origin determination became the focus.

Electrical Arcing and Fire Investigation

The first electrical arcing research was conducted by Davy in 1812⁶. Electrical arcing research continued through the 20th century, in part, by Ayrton, Lee, Matthews, and Gammon⁷⁻¹⁰. This resulted in the development of electrical safety standards such as IEEE 1584, “Guide for Performing Arc-Flash Hazard Calculations,” and NFPA 70E, “Standard for Electrical Safety in the Workplace”¹¹. However, electrical research related to evaluating the electrical system for fire origin determinations was not theorized until the 1950s¹² and later examined in the 1980s by Delplace & Vos¹³ and Rothschild¹⁴.

Several pioneers are recognized for empirical research, testing, and the development of training programs for utilizing the electrical system for origin determinations¹⁵⁻¹⁷. The reliability of arc mapping methodology was subsequently reviewed by both Babrauskas and Icove^{18,19}. Each had questioned the application and reliability of fire investigators to perform the arc mapping methodology. McPherson also forensically examined, applied, and analyzed a systematic approach to investigating residential (domestic) fire scenes by utilizing the arc mapping (arc survey) or arc fault circuit analysis methodologies²⁰.

Reliability of any methodology as an origin determination method is dependent on the skill, knowledge, education, training, and experience of the person applying it. To successfully undertake any electrical fault analysis, one must be qualified and competent in the areas of electrical safety and electrical systems that are under investigation (residential, commercial, industrial, agricultural, and transportation vehicles). Additionally, one must be able to perform a systematic and scientific approach to accurately analyze data related to damage observed on electrical wiring and equipment. These damage sites are generally identified in the form of arc melting (arc melt site), fire melting (fire melt site), alloy melting (alloying site), and mechanical damage (mechanical damage site).

Electrical Investigations

Fundamentally, the electrical investigation begins with an electrical survey, which can be defined as a systematic approach of examining, documenting, and analyzing the electrical distribution system, wiring, and equipment. Electrical fault evaluations, in their fundamental form, consist of identifying how electrical circuits were installed and protected at the scene as well. Subsequently, this method involves identifying boundaries of faulted and non-faulted electrical circuits/equipment and analyzing the electrical system/electrical faults to determine or define a spatial relationship, sequence of events, and/or conduct hypothesis testing.

Power electrical engineers have been reliably evaluating and performing electrical transmission and distribution fault evaluations for more than a century²¹. Today, skilled and trained power electrical engineers and electricians perform short-circuit evaluations and analysis based on accepted electrical industry methods²²⁻²⁴.

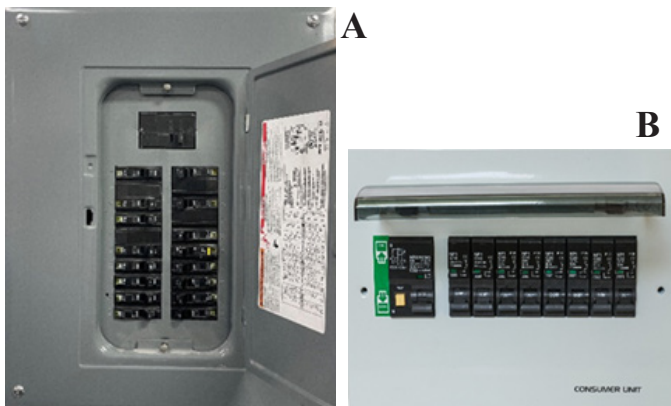


Figure 2

(A) North American electrical panel and (B) UK electrical consumer unit.

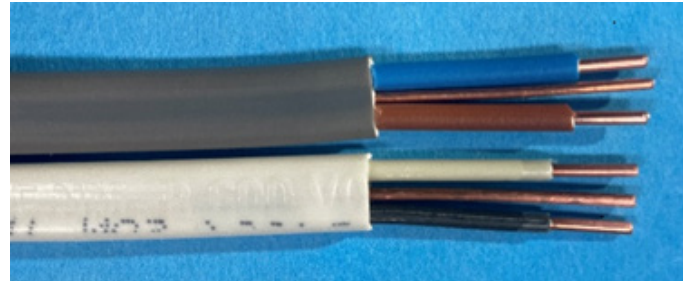


Figure 3

Non-metallic electrical cabling (UK and North America).

Examples of electrical equipment examined during an electrical survey and arcing fault evaluation may include (in part): electrical service equipment, electrical distribution panels (**Figure 2**), overcurrent protective devices, electrical feeders, branch circuits, appliances, luminaires, wiring, cables (**Figure 3**), and cords.

Therefore, the identification of electrical damage (or lack thereof) generated from a fire can lead the fire investigation practitioner to determine a bounded area(s). Independent of the constantly changing or time unstable generation of fire patterns, the area of fire origin defined by physical electrical evidence is time stable. The electrical system, an unbiased witness to the fire, responds to the event. For example, heat and flames of a fire impinging on an electrically energized 120VAC, electrical code compliant electrical circuit will respond and provide physical evidence for the fire investigation practitioner to discover and evaluate — thereby, generating a timeline or sequence of events(s) data, based on the electrical system response. It is paramount that the fire investigation practitioner is able to systematically and reliably distinguish characteristic features observed on post-fire electrical conductor damage.

Post-Fire Electrical Conductor Damage Characteristics

Arc Melt Site

When the heat of the fire is sufficient to compromise the electrical insulation of an electrically energized (with sufficient available fault current) non-metallic cable, a fault or short circuit (arcing melting event) often occurs between the energized and/or earth (grounded or grounding) conductors. The arc melt site features are formed from an electrical arcing event and subjectively identified by localized electrical arcing damage, generally identified on electrical conductors and equipment in the form of beads and/or notches (**Figure 4**).

They may exhibit, in part, a smooth surface appearance, distinct lines of demarcation, internal uniform

porosity between the different surface textures as well as obliteration of manufactured tool markings within the damage site. Conductor manufactured tool markings should be observed outside the damage site. However, they can be obscured by post-event oxidation and/or damage. In his research, Carey classified nine different categories of electrical arc melt site damage^{17,25}. Furthermore, arc melt sites are generated by electricity — not by fire.

Fire Melt Site

Fire melt site features will generally form during fire and heat attack that exceeds the melting temperature of electrically conductive materials, such as aluminum, zinc, copper, or steel. Conductor melt sites (recognized as fire-melting damage) are generally identified in the form of gross melting and/or globule features (**Figure 5**). They may exhibit, in part, a non-uniform surface and shape, no clear lines of demarcation at the damage site, irregular melting features in and around the damage site, manufactured tool markings melted away from the damage site, and non-uniform porosity within the damage site.



Figure 4
Example of electrical conductor arc melting damage²⁶.



Figure 5
Example of electrical conductor fire melting damage²⁶.

Alloying Site (Subset of Fire Melting)

Alloying sites (mixed metal) are generally recognized as a fire-melting feature that occurs by the mixing or alloying of dissimilar materials at elevated temperatures, causing melting at the damage site. The effect may occur due to electrical equipment, components, and wiring of different materials (such as copper, aluminum, lead, tin, and zinc) coming in contact during the course of a fire. Alloying sites may exhibit features similar in appearance to fire melt sites. The alloying site may have a brass and/or silver color appearance (**Figure 6**). Alloying sites are commonly mischaracterized as eutectic melting.

Mechanical Damage Site

Mechanical damage sites are generally recognized by fractured, impact, cracked, cut, sheared, stretched, or other damage from a mechanical action at the damage site (**Figure 7**). Mechanical damage can occur prior to the incident event or due to the excavation process involved in a scene investigation. Examples of this type of damage include: gouging/scraping of wires during installation or subsequent construction tasks; structural collapse causing conductors to stretch or break; or cutting by a tool.



Figure 6
Examples of electrical conductor fire melting damage (alloying). Fire melting copper and aluminum (A) and fire melting copper and zinc fire (B)²⁶.



Figure 7
Example of electrical conductor mechanical damage²⁶.

Subjective Methods of Characterizing Damage

Traditional methods of identifying electrical conductor or equipment damage sites at the fire scene have included, in part, visual and/or light microscopy surface analysis examination. NFPA 921 provides classic examples of the above types of damage sites that may be observed while performing the arc mapping methodology at the fire scene¹. The Bureau of Alcohol, Tobacco, Firearms and Explosives (ATF) Fire Research Laboratory issued a technical bulletin in 2012, describing visual characteristics of arc melting and fire melting on copper conductors that may visually assist the forensic fire investigation practitioner in identifying damage sites while performing an electrical survey and arc mapping methodology²⁷. Novak, together with nine other subject matter consultants, published “A Review of the Long-Standing Science Behind Arc Melting Identification”²⁸.

Skilled, trained, qualified, and competent forensic fire practitioners should be able to reliably recognize and distinguish the difference between electrical arc melting and fire melting at the fire scene. If the damage site is visually examined — and the damage type identification is disputed or otherwise identified as undetermined — additional

examination and analysis can be performed by implementing advanced methods. Additional examinations may involve laboratory analysis utilizing a scanning electron microscope (SEM) and/or by dissecting and examining the interior of the damage site to perform internal microstructure analysis (Figure 8 and Figure 9).

Buc researched and developed a laboratory examination methodology to characterize the damage site by grinding or cutting the arc site open and examining the internal structure³⁰. Buc’s research further distinguished the difference between arc melt and fire melt sites by examining the interior features of the damage site for microstructure, porosity, and internal lines of demarcation. Murray advanced metallurgical techniques for fire investigation. Murray’s findings were, in part: “As to the electrical damage, they revealed distinct characteristics. More precisely, macroscopically, damage was confined to a localized area, where the surrounding material showed the same condition than initially. Due to the fact that short-circuit phenomenon transfers to the metal an important amount of energy very

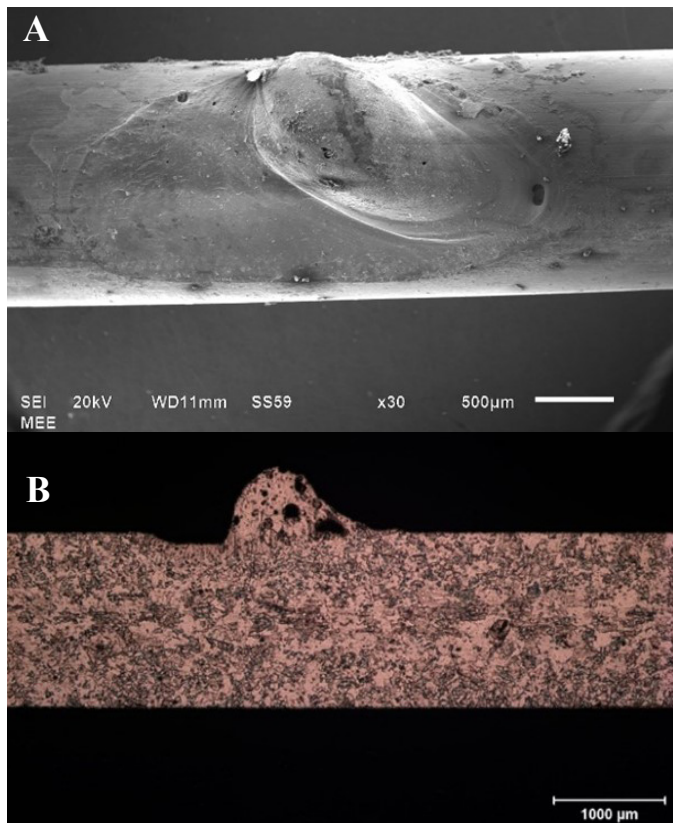


Figure 8

(A) Example of SEM arc melt surface features and (B) internal arc melt microstructure²⁹.

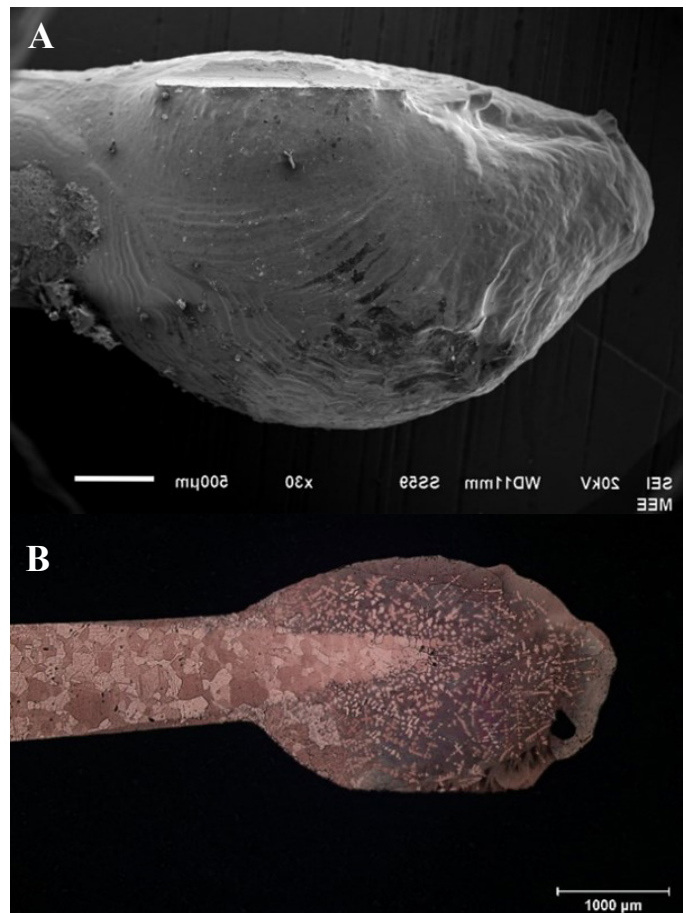


Figure 9

(A) Example of SEM fire melt surface features and (B) internal fire melt microstructure²⁹.

quickly, liquification and thus re-solidification are state changings that occurred very fast³¹.

If, during the electrical survey and fault evaluation, the fire investigation practitioners question the reliability of a damage site identification, they should identify the damage site as undetermined. Doing so will allow for expanding the size of the fire origin boundary as defined by the electrical system, thus leading to a fire origin hypothesis that is better defined and leads to a more reliable result.

Arc Mapping and X-Ray Techniques

Errors in fire origin determination may occur if the data collected is determined to be unreliable. Examples of unreliable eyewitness information, misinterpretation of fire patterns, and misapplication of fire dynamic principles can lead the fire investigation practitioner to inaccurately determine the area of fire origin and cause. Arc mapping has been challenged as an unreliable fire origin determination methodology¹⁸. Recent research has called into question whether arc melt sites or fire melt sites observed on post-fire damaged electrical conductors can be reliably distinguished from one another³².

It was reported that “it is not possible to distinguish between the beads formed on energized and non-energized wiring exposed to various thermal insults”³². There are instances where visual, non-destructive examinations of the damage sites may limit the ability of the forensic fire practitioner to accurately identify the type of damage found on the electrical wiring or equipment. Subsequent blind testing had revealed that experienced metallurgists can reliably distinguish between an arc melt site and fire melt site features by utilizing destructive means³³. However, neither NDT method nor protocol exists for distinguishing damage features observed on post-fire damaged electrical conductors.

X-Ray Radiographs and Computed Tomography (CT)

X-ray radiographs have been generally accepted and utilized by the professional welding industry for NDT examinations for almost 100 years. The American Society of Mechanical Engineers (ASME) provides guidelines for employers to establish certification programs for the qualification of NDT personnel.

The X-ray system is generally made up of a radiation source and imaging film or digital plate. Radiation from the source passes through an object or specimen, resulting in a captured two-dimensional image, known as

a radiograph. Most objects have an X-ray density, which will determine the ability of X-rays to pass through the material to the film or imaging plate.

Examination of radiographs taken for forensic examinations may reveal wiring, components, and parts that are not visible to the naked eye. For instance, by examining a radiograph of an electrical appliance, the forensic fire practitioner may determine if the device was “ON” or “OFF” or if wiring or component parts were damaged, out of place, or missing (**Figure 10**). Hansen agreed that X-ray analysis of electrical conduits can be helpful when attempting to document where electric arcs have occurred in relation to the fire origin area³⁴. However, Goodson reported that X-ray radiographs may have limitations (e.g., if an object has multiple components overlapping and/or at different levels of depth, the radiograph may not reveal a clear image)³⁵. Partial or complete disassembly of the object may be required to acquire a clear X-ray radiograph image.

X-ray imagery can be performed with either portable or fixed equipment (**Figure 11**). The resultant X-ray radiograph imagery is determined by the density of materials under examination.

X-ray radiographs can reveal internal features and structure (such as porosity) that are represented by varying gray scale values. For example, 10-bit grayscale, commonly utilized in digital radiograph (DR), ranges from one

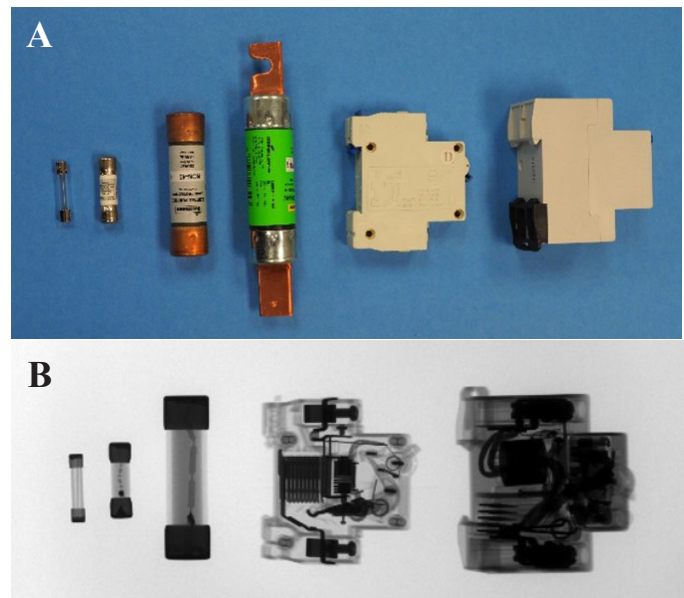


Figure 10
(A) Fuses and circuit breakers and (B) X-ray digital radiograph of fuses and circuit breakers²⁶.



Figure 11

(A) Portable X-ray digital system and
(B) fixed X-ray micro-focus CT²⁶.

to 1,024 different shades of gray/pixels. The human eye can detect 900 varying shades of gray/pixels. Generally, monochrome monitors only support 256 different shades of gray/pixels³⁶.

The shades of gray tests were developed to evaluate the ability to differentiate between shades of gray as required by American Society of Mechanical Engineers ASME V/SNT-TC-1A. **Figure 12** is a graphic example of 255 different shades of gray/pixels. Grayscale charts for visual comparisons are commonly available between 0 and 10 — where 0 is black and 10 is equal to white.

Advanced adaption of the two-dimensional X-ray radiograph was in the modern invention of CT, commonly utilizing a micro-focus, X-ray radiation source, rotating pedestal or stand and radiation detector, and generating a computerized three-dimensional representation of a scanned object. A 16-bit grayscale (commonly utilized in CT) ranges from 1 to 65,535 different shades of gray/pixels.

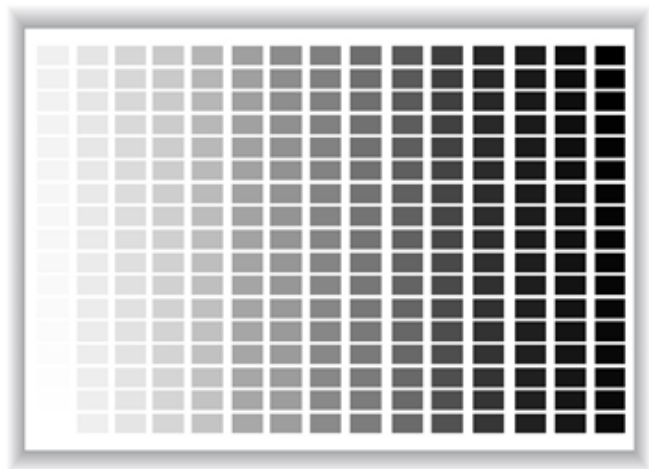


Figure 12

Graphic example of 255 shades of gray/pixels.

During the operation of a CT, the radiation source or object is rotated, thereby allowing each incremental image to be recorded by the detector. The data elements collected can be reconstructed to provide a three-dimensional image. The constructed image can be examined in all three dimensions externally and internally by stepping through or slicing through the object image. Goodson discussed additional history and theory of CT for fire investigation purposes in his research paper titled “The Application of CT X-Ray Analysis of Electrical Components”³⁵. Therefore, can X-ray technology be utilized for distinguishing damage features observed on post-fire damaged electrical conductors?

Methodology:

Part 1 – Generation of Datasets of Known Damage Full-Scale and Scaled Experiments

This empirical research represents a novel method of utilizing X-ray imagery to distinguish electrical conductor damage features. Post-fire electrical specimen samples were generated by field and laboratory experiments. North American copper #14 AWG (1.6 mm) non-metallic (NM) cabling and United Kingdom (UK) copper, 1.0 mm² and 2.5 mm², NM “Twin & Earth” cabling were utilized. Each cable type was utilized for repeated experiments. Specimens were generated by impinging heat and flame on energized and non-energized cabling as well as generating mechanical damage specimens. Both full-scale and scaled field experiments were performed as follows.

Series One Experiments

A total of 63 full-scale compartment fires were conducted at the United States’ Federal Law Enforcement, ATF fire training center (FLETC) located in Brunswick,

Georgia (**Figure 13**). The electrical distribution system under these tests was a 120/240VAC, single-phase, 15A electrical circuit. The available fault current at the point of fire impingement was calculated to be 210.9A.

Six #14 AWG (1.6 mm) diameter, NM copper electrical circuits (four energized at 120VAC, overcurrent protected at 15A and two non-energized electrical circuits) were installed at the ceiling level of each compartment. A fire was independently initiated by ATF personnel within each compartment. Each fire was allowed to develop based on controlled compartment fuel and ventilation characteristics that were determined by the ATF training parameters.

In total, 87.3% of the full-scale experiments went to post-flashover conditions. Electrical data in the form of voltage and short-circuit fault currents were recorded for future analysis. Although fire had reached post flashover conditions, only artifacts of arc melting were generated during the full-scale, FLETC burn cell experiments. However, additional arc melting, fire melting, and mechanical damaged artifacts were generated during a series of scaled fire impingement and non-fire experiments.

Series Two Experiments

No artifacts of fire melting were generated during the full-scale, FLETC burn cell experiments. As a result, two full-scale wooden compartments were constructed in Covington, Louisiana. Both Gulf Coast Fire Investigation and Fire Investigation Group personnel assisted with the construction, ignition, and collection of artifacts generated within these compartments. Non-energized electrical circuits were installed within the two burn cells. North Amer-

ican copper #14 AWG (1.6 mm) non-metallic (NM) copper cabling and United Kingdom (UK) copper, 1.0 mm² (1.1 mm) and 2.5 mm² (1.7 mm), “Twin & Earth” cabling were installed. Each compartment fire was allowed to burn until complete destruction of the compartment. Since no melting in these experiments could have been due to arc melting, a total of 60 non-energized electrical conductor artifacts were selected from the resultant dataset to be representative of fire melt sites.

Series Three Experiments

The third set of experiments was conducted at MSD Engineering laboratory located in Crystal Lake, Illinois. The purpose of these experiments was to perform scaled tests to generate electrical artifacts using a newly developed electrical testing apparatus that was designed and constructed to facilitate testing of electrical equipment and wiring under varying electrical, fire, and installation configurations. This newly designed test platform, called the Mark I – Arc Research Chamber (MARC – USPTO patent pending), included onboard flame/heat sources and instrumentation that can record voltage, current, temperature, heat flux data, and electrical fault current data.

A total of 42 scaled tests were undertaken. In each case, UK 1.0 mm² (1.1 mm), UK 2.5 mm² (1.7 mm) “Twin & Earth,” and North American #14 AWG (1.6 mm) NM copper cables were electrically connected to appropriately sized single-pole, overcurrent protection devices (OCPD) (6, 20 and 15A, respectively) and energized using an associated system voltage (UK “Twin & Earth” - 230VAC and North American NM 1.6 mm - 120VAC) that had sufficient electrical fault current to generate an arcing fault.



Figure 13

(A) Full-scale compartment fire testing at FLETC, (B) interior view of fire, and (C) post-flashover fire extending outside of compartment²⁶.

The arc artifacts generated using the MARC test platform were validated in terms of their characteristics and morphology against the artifacts generated under known conditions in the full-scale series one (arc melting) and series two (fire melting) fire tests. These experiments provided the opportunity to repetitively generate the arc and fire melt artifacts required for practitioner surveys and human factor research²⁶.

Carey Experiments

A total of 106 arc melting artifacts generated through Carey's research¹⁷ were also incorporated into the overall project dataset. These samples were generated using UK cables installed within full-scale compartments under real fire conditions. The inclusion of these samples enabled a direct comparison between the UK and North American samples to be made in terms of characterization of damage.

Part 2 — Examination and Analysis of Electrical Artifacts

The artifacts generated through the three series of experiments were examined and analyzed in several stages by numerous forensic engineers and technicians employed by both Materials Evaluation and Engineering (MEE) and MSD Engineering (MSD). Each artifact was documented based on the location, date of generation, and date of recovery. All artifacts were independently coded.

Samples were initially examined and cleaned, removing loose debris. When required, melted and charred insulation material was carefully removed. A Nikon, X-Tek XT H 225 DR & CT scanner was used for examining specimens. Key features of the X-ray machine included (in part): a 225 KV, micro focus X-ray source with 3 μ m focal spot size and a Varian Amorphous Si detector array that had 3 X 10⁶ individual pixels. This detector allows for high-performance image acquisition and volume processing. The CT had the capability of performing 3,600 scans per 360 degrees of specimen rotation. The Nikon micro focus X-ray source and movable turntable was able to provide an X-ray image in real time. This allowed for in-motion imaging as well as specimen magnification. The micro focus radiation source and stage also allowed it to be operated as an X-ray microscope. Specimens (in part) were examined, measured, compared, and contrasted between known electrical conductor damage at the University of Dundee, Scotland, United Kingdom and Avonix Imaging, Maple Grove, Minnesota.

Samples were mounted on the turntable located within the enclosure of the CT. Specimens could then be rotated

360 degrees about the axis of the turntable. Based, in part, on specimen size and density, DR & CT imagery was collected at 190KV. CT was conducted at 1,200 scans per 360 degrees of revolution. Additionally, DR real time imagery was captured utilizing varying levels of magnification.

NDT — X-Ray Examination

Thermal imagery, ultrasonic testing, and X-ray methodologies were considered. Initial X-ray examination revealed the most promise for damage site identification. X-ray examination of North American #14 AWG (1.6 mm) and United Kingdom (UK) copper, 1.0 mm² (1.1 mm) and 2.5 mm² (1.7 mm), "Twin and Earth" cabling revealed distinguishable features when compared to known artifacts or phantoms. Localized melting features, clear lines of demarcation, and uniform porosity were observed within an arc melt site (**Figure 14**).

In Buc's analysis of arc melt sites, Buc described this feature as a persistent porosity within the arc site³⁰. In contrast, fire melt sites revealed irregular melted globules or balls with non-uniform or non-persistent porosity (**Figure 15**). Mechanical damage sites revealed sharp lines of mechanical damage demarcation and no porosity (**Figure 16**). These experiments were repeated with the same identifiable, distinguishing features.

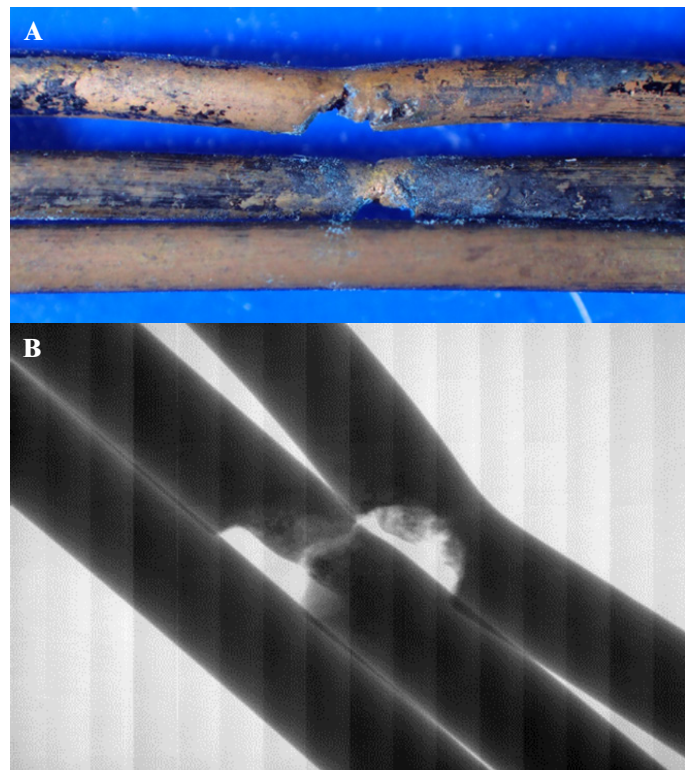


Figure 14

(A) Arc melting surface features and (B) X-ray digital radiograph²⁶.

Examination of the imagery acquired by NDT, utilizing both DR and CT for different types of damage sites, revealed distinguishable and measurable external and internal features. Currently, metallurgists use destructive methods to cut open and examine internal features to distinguish the difference between arc melting and fire melting. X-ray examination of damage sites along electrical conductors revealed measurable features from localized or non-localized melting along a specimen length. Internal features (in the form of porosity) were also clearly definable. Porosity was uniformly observed at arc melt sites (beads). However, porosity (if present) within the displaced mass was non-persistent and non-uniform within fire melt sites (globules).

Arc melting, fire melting, and mechanical damaged post-fire damaged electrical conductor's artifacts were examined and compared to a 0 to 10 grayscale chart. Comparison analysis revealed observable and measurable grayscale features within damaged areas of subject electrical conductors. Based on the collected data on a grayscale index of 0 to 10 (where 0 is black and 10 is white), arc melt sites had a mean grayscale index of 5.948 with a standard

deviation of 0.793; fire melt sites had a mean grayscale index of 2.25 with a standard deviation of 0.439; and mechanical damaged or non-damaged electrical conductors had a grayscale index of 2 with a standard deviation of 0 (Figure 17).

Characterization of Sample Artifacts

The following dataset table and figures (Figure 18 and Figure 19) represent an example of post-fire damaged electrical conductors with X-ray radiographs. X-ray imagery and grayscale analysis assisted in validating characteristic features of arc melting, fire melting, and mechanical damage sites observed on the tested post-fire damaged electrical conductors.

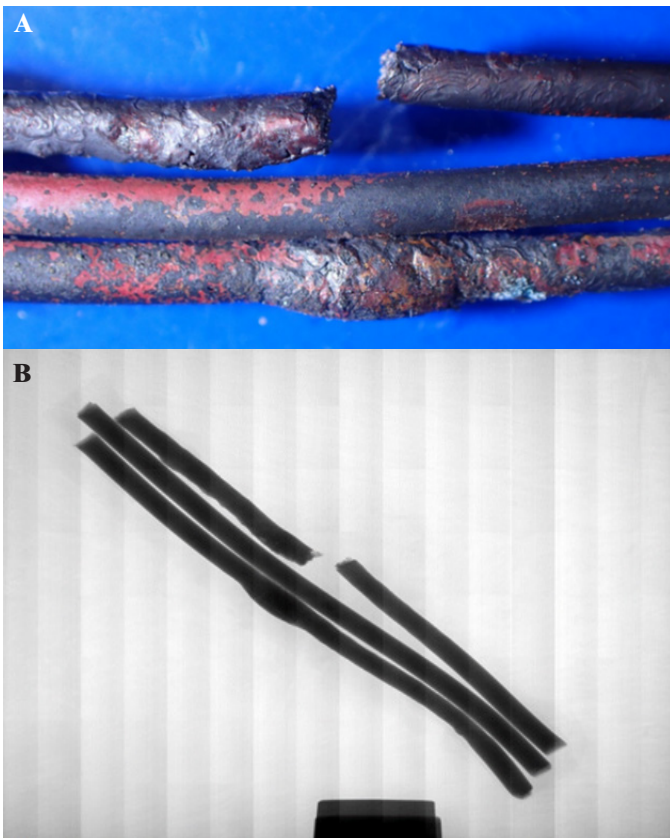


Figure 15

(A) Fire melting surface features and (B) X-ray digital radiograph²⁶.

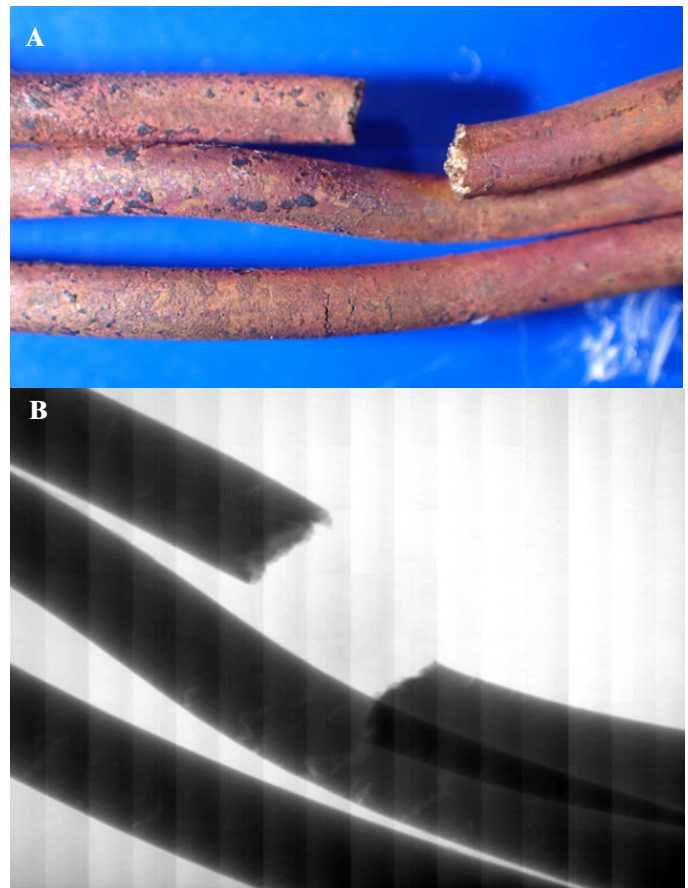


Figure 16

(A) Mechanical damage surface features and (B) X-ray digital radiograph²⁶.

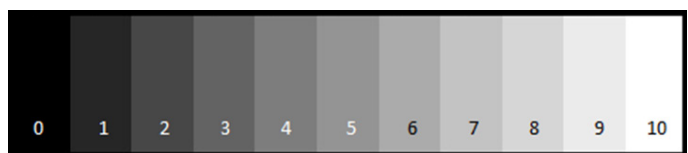


Figure 17

Grayscale chart (0-10), courtesy of MJ Svare.

| Survey Sample Identifier | Wire Type | Damage Type | Damage Size (mm) | Notes on Damage | Gray Scale Identifier | Corresponding Wire Identifier |
|--------------------------|------------------------|-------------|------------------|-----------------|-----------------------|-------------------------------|
| C-1 | UK 1.0 mm ² | ND | — | No damage | 2 | NC 54 |
| C-2 | UK 1.0 mm ² | MD | — | Mechanical | 2 | NC 19 |
| C-3 | UK 2.5 mm ² | AM | 3.44 | Arc melt | 5 | NC 21 |
| C-4 | UK 1.0 mm ² | FM | *>4.44 | Fire melt | 2 | MS 12 |
| C-5 | UK 1.0 mm ² | AM | 2.76 | Arc melt | 7 | NC 54 |
| C-6 | UK 2.5 mm ² | MD | — | Mechanical | 2 | MS 13 |
| C-7 | UK 1.0 mm ² | FM | *>10.37 | Fire melt | 2 | MS 14 |
| C-8 | UK 2.5 mm ² | AM | 2.84 | Arc melt | 7 | NC 48 |
| C-9 | UK 2.5 mm ² | AM | 2.70 | Arc melt | 7 | NC 98 |
| C-10 | UK 2.5 mm ² | FM | *>6.96 | Fire melt | 2 | MS 15 |

Figure 18

Example grayscale dataset (* = melted open)²⁶.

Surveys and Human Factors

Quantitative data was collected by surveying 912 participants within the fire investigation community to assess their ability to correctly identify arc-melting, fire-melting, and mechanical artifacts by applying arc fault data in a scenario-based context. Two surveys testing the participants' observations were administered.

Survey one participants were provided with post-fire damaged electrical conductor samples for visual observation without any additional data. The overall results revealed a mean examination score of 57% of distinguishing features observed on post-fire damaged conductors.

The ability to accurately identify conductor damage is a key step in any electrical evaluation, including the arc mapping methodology. The inability of participants to correctly identify damage on post-fire damaged electrical conductors indicated a knowledge gap within the fire investigation profession.

Survey two participants were provided with an additional one-hour training session on how to visibly identify and distinguish the different damage features of arc melted, fire melted, and mechanical damaged post-fire damaged electrical conductors, including through the interpretation of X-ray radiographs of the artifacts. Their ability to correctly identify the damage features observed on post-fire damaged conductors increased from an initial mean examination score of 45.6% to a mean score of 78.6% as a result of the training. Statistical evaluation further correlated that additional training had a significant positive effect in the participants' abilities to correctly attribute the damage observed.

Summary and Conclusions

When undertaking a fire investigation, a fire investigation practitioner may implement a similar electrical investigation methodology called arc mapping (or, more recently, termed an arc survey). The correct application of an electrical system-based origin determination methodology is dependent, in part, on the forensic investigation practitioner's ability to distinguish features observed on damaged electrical wiring and equipment.

Currently, fire investigation practitioners rely upon subjective visual observations to distinguish the difference between arc melting, fire melting, and mechanical features on post-fire damaged electrical conductors.

This empirical research represents a validated, novel, non-destructive methodology

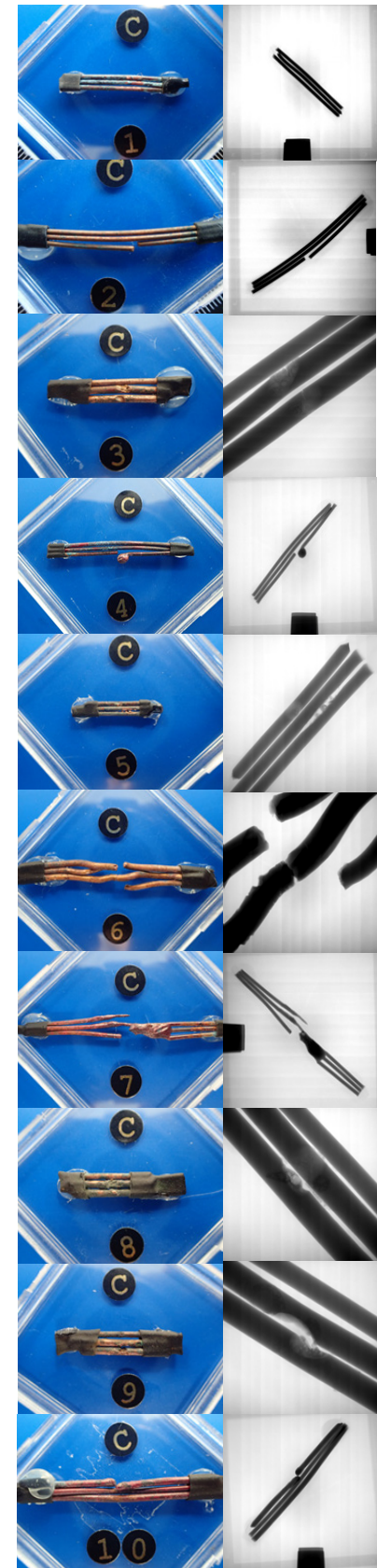


Figure 18

Sample set C1-C10 with corresponding X-ray radiograph²⁶.

for utilizing X-ray imagery and grayscale analysis to reliably distinguish characteristic conductor damage features observed on the tested post-fire damaged electrical conductors of the same size. Application of quantitative measurement of characteristic conductor damage features would further increase characterization reliability. However, additional testing may be required for different conductor sizes, materials, and fault current conditions.

Research Note: All FLETC full-scale experiments were performed in conjunction with ongoing ATF training programs; all research expenses for FLETC, Louisiana, Minnesota, Illinois, and United Kingdom location experiments and testing were funded by researcher Dr. Mark J. Svare, PE.

Acknowledgements

The authors wish to thank, in part, the Leverhulme Research Centre for Forensic Science, University of Dundee; University of Dundee (UK), Special Agents of the Department of Justice; Bureau of Alcohol, Tobacco, Firearms and Explosives (US); MSD Engineering (US), Gulf Coast Fire, LLC (US), Investigative Loss Services (US); and Materials Evaluation and Engineering (US) for their continued support. The author also wishes to acknowledge the following for their invaluable support: Dr. Nick Carey IAAI-CFI; Jeff Washinger, Sr. IAAI-CFI; Robert Schaal ATF (retired) & IAAI-CFI; Larry Hanke, PE; Neal Hanke, PE; Albert Bartolome i Regue Engineer & IAAI-CFI; Lester Rich ATF (former) & IAAI-CFI; Kerry Svare ATF (retired) & IAAI-CFI; Roberta Svare; Carol Severson EIT; and Erik Severson EIT.

References

1. National Fire Protection Association, 921 Guide for Fire and Explosion Investigations. NFPA, Quincy, MA, USA, 2021.
2. National Fire Protection Association, 921 Guide for Fire and Explosion Investigations. NFPA, Quincy, MA, USA, 2001.
3. National Fire Protection Association, 921 Guide for Fire and Explosion Investigations. NFPA, Quincy, MA, USA, 2004.
4. National Fire Protection Association, 921 Guide for Fire and Explosion Investigations. NFPA, Quincy, MA, USA, 2008.
5. V. Babrauskas, "Arc Beads from Fires: Can 'Cause' Beads Be Distinguished from 'Victim' Beads by Physical or Chemical Testing?," *Journal of Fire Protection Engineering* vol. 14, pp. 125-147, 2004.
6. H. Davy, *Elements of Chemical Philosophy: Part 1, Vol. 1*. Bradford and Inskeep, 1812.
7. H. Ayrton, *The Electric Arc*. London: "The Electrician" Printing and Publishing Company, 1903, pp. 20-96.
8. R. Lee, "The Other Electrical Hazard: Electric Arc Blast Burns," *IEEE Transactions on Industry Applications*, vol. IA-18, no. 3, pp. 246-251, 1982.
9. T. Gammon and J. Matthews, "The Application of a Current-Dependent Arc Model to Arcing at a Main Distribution Panel, a Sub-Panel and a Branch Circuit," *IEEE*, pp. 72-78, 2001.
10. T. Gammon and J. Matthews, "Instantaneous Arcing-Fault Models Developed for Building System Analysis," *IEEE Transactions on Industry Applications*, vol. 37, no. 1, pp. 197-203, 2001.
11. National Fire Protection Association, 70E Standard for Electrical Safety in the Workplace. NFPA, Quincy, MA, USA, 2021.
12. R. Straeter and C. Crawford, *Techniques of Arson Investigation*. Los Angeles, California: R. L. Straeter, 1955.
13. M. Delplace and E. Vos, "Electric Short Circuits Help the Investigator Determine where the Fire Started," *Fire Technology*, vol. 19, no. 3, pp. 185-191, 1983.
14. L. Rothschild, "Some Fundamental Electrical Concepts in Locating the Cause and Origin of a Fire," *National Academy of Forensic Engineers Journal*, vol. 3, no. 2, pp. 37-44, 1986.
15. R. Svare, "Determining Fire Point-of-Origin and Progression by Examination of Damage in the Single Phase, Alternating Current Electrical System," *Journal of People to People, International Arson Investigation Delegation to the People's Republic of China and Hong Kong*, pp. 4-8, 1988.

16. L. West and D. Reiter, "Full-Scale Arc Mapping Tests," *Fire & Materials*, pp. 325-339, 2005.
17. N. Carey, "Developing a reliable systematic analysis for arc fault mapping," Ph.D. Dissertation, Pure and Applied Chemistry, University of Strathclyde, Glasgow, UK, 2009.
18. V. Babrauskas, "Arc mapping: a critical review," *Fire Technology*, vol. 54, no. 3, pp. 749-780, 2018.
19. D. Icové and T. R. May, "State of the arc (mapping)," *Journal of the National Academy of Forensic Engineers*, vol. 38, no. 1, pp. 63-75, 2021.
20. J. McPherson, "FE Use of Arc Mapping / Arc Fault Circuit Analysis in a Residential Kitchen Fire Investigation," *Journal of the National Academy of Forensic Engineers*, vol. 39, no. 1, 2022.
21. C. L. Fortescue, "Method of Symmetrical Coordinates Applied to the Solution of Polyphase Networks," *Transactions of the American Institute of Electrical Engineers*, vol. 37, no. 2, pp. 1027-1140, 1918.
22. C. Miller, *Ugly's Electrical References*. Jones & Bartlett Learning, 2023.
23. Bulletin EDP- 1-3 - A Simple Approach to Short Circuit Calculations - Part 1, 2004, pp. 1-104.
24. *Short Circuit Current Calculations*, Cooper Bussmann, 2005, pp. 192 - 198.
25. N. Carey and N. NicDaeid, "The Metallic Damage to Electrical Conductors at Fire Scenes," presented at the Interflam 2007 Conference, Interscience Communications, University of London, Royal Holloway College, Egham, Surrey, 2007.
26. M. Svare, "A reliable systematic methodology for reconstructing the fire scene using the electrical system: analysing human factors," Ph.D. Dissertation, University of Dundee, Dundee, UK, 2022.
27. ATF Fire Research Laboratory, "Visual Characteristics of Fire Melting on Copper Conductors," ATF Fire Research Laboratory Technical Bulletin, no. Technical Bulletin 001, pp. 1-8, 2012.
28. C. Novak et al., "A Review of the Long-Standing Science Behind Arc Melting Identification," *Fire & Arson Investigator*, vol. 73, no. 1, 2022.
29. M. Svare and L. Hanke, "MEE - MSvare Research Images," ed, 2014, p. SEM and Microstructure Images.
30. E. Buc, D. Reiter, J. Battley, T. Sing, and T. Sing, "Method to Characterize Damage to Conductors from Fire Scenes," *Fire and Materials*, pp. 657-666, 2013.
31. I. Murray and F. Ajersch, "New Metallurgical Techniques Applied to Fire Investigation," *Fire and Materials*, pp. 857-870, 2009.
32. N. Hussain, "Forensic Investigation for Inspecting Electrical Conductors Involved in Fire for Arc and Melt Beads," Thesis for Master of Science, Department of Fire Protection Engineering, University of Maryland, 2012.
33. "MSD Engineering News Bulletin 001 - Empirical Blind Testing of Metallurgists," vol. 1, no. 001, p. 1.
34. Hansen, "Forensic Engineering Use of X-rays in Failure Analysis," *National Academy of Forensic Engineers (NAFE) Journal*, vol. 14, no. 2, pp. 1-7, 2002.
35. M. Goodson, "The Application of CT to Analysis of Electrical Components," *International Symposium on Fire Investigation Science and Technology*, pp. 293-303, 2012.
36. T. Kimpe and T. Tuytschaever, "Increasing the Number of Gray Shades in Medical Display Systems - How Much is Enough?," *Journal of Digital Imaging*, vol. 20, no. 4, pp. 422-432, December 2007.

Forensic Examination of Post-Fire Damaged Electrical Conductors by Quantitative Measurement

By Mark J. Svare, PhD, PE, DFE (NAFE 851M), Neal W. Hanke, PE (NAFE 1219A), and Niamh Nic Daeid, PhD

Abstract

During their course of work, forensic engineers and electricians may apply electrical engineering and scientific principles to forensic investigations by performing electrical surveys and electrical fault evaluations. When undertaking a fire investigation, an investigator may implement a similar electrical fault methodology called “arc mapping” or more recently termed an “arc survey.” The correct application of either of these methodologies is dependent, in part, on the forensic investigator’s ability to distinguish features observed on damaged electrical wiring and equipment. Experiments were conducted to generate a post-fire damaged electrical artifact dataset for this engineering analysis. Generated artifacts of arc melting, fire melting, and mechanical damage features were examined, measured, and quantified by applying metallurgical analyses, such as visual examination, measurement, light microscopy, SEM/EDS, X-ray, and/or metallographic examination. The results produced a novel proof of concept method of quantifying and reliably identifying electrical conductor damage features for forensic electrical fault (short circuit) and/or arc survey evaluations.

Keywords

Arcing, electrical, forensic engineering, fault, short circuit, fire investigation, conductors, copper, arc mapping, arc survey, melting, metallography, microstructure, porosity

Introduction and Background

Electrical engineers have been researching electricity, electrical systems, arcing faults, and arc flash for more than 100 years^{1,2}. Within the last 60 years, researchers have rigorously tested and published extensively on electrical distribution faults and arc flash analysis³⁻¹⁴. Power electrical engineers are aware of the hazards and risks associated with electrical arcing. They conduct electrical analyses as well as analytical and experimental studies to ensure proper overcurrent protection and coordination for safeguarding person(s) and property. Currently, both the electrical and fire investigation industries rely upon subjective observations to distinguish features of electrical damage in the form of arc melting, fire melting, or mechanical damage.

Low-Voltage Electrical Faults (<600VAC)

Location of a fault in the system/circuit, voltage, current, impedance, and duration of the event determines the electric arc plasma energy. These electrical variables can be derived from short-circuit calculations and evaluations¹⁵⁻¹⁸ (**Figure 1**). Unlike a low-energy spark generated

from static discharge, such as the capacitive discharge by touching a doorknob, the electrical energy released from a low-impedance electrical distribution system fault can lead to an arcing event that transfers significant amounts of electrical energy to surrounding materials. Additionally, variables (such as arc gap, arc location, impacted material properties, and exposure time) all factor into the resultant melting, burning, or vaporizing of the impacted material(s) within the area of origin of the electrical arcing fault.

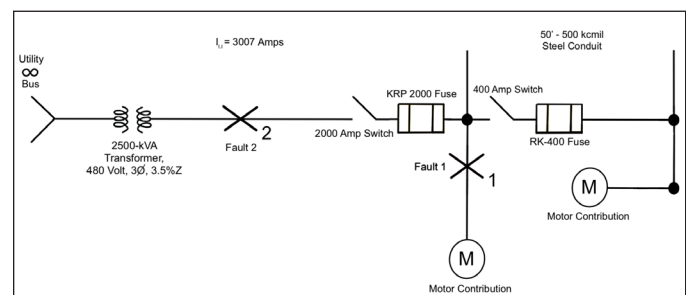


Figure 1

Example: one-line electrical diagram utilized for short-circuit (fault) evaluations.

Generally, low-voltage (<600VAC) arcs can result from a direct short circuit. Below 350VAC, an electric arc at one atmosphere will not jump an air gap greater than 50 μm¹⁹. Additionally, “below 350VAC, single-phase, sinusoidal electrical circuits will generally self-extinguish an arc at the 0VAC crossing point”⁷. Therefore, “the time dependent arcing event only generates a finite amount of energy to cause localized damage to electrical equipment and wiring”²⁰.

Electrical Distribution and Fire Investigation

Low-voltage (<600VAC) electrical distribution conductor damage is often observable. For example, storm-damaged electrical conductors resulting in an electrical arcing fault on an electrical distribution system are commonly located, identified, and repaired by qualified and competent electrical workers.

According to NFPA 921 and NFPA 1033, qualified and trained fire investigators should (as part of their fire investigation practice) be able to recognize and distinguish the differences between fire damage patterns, electrical damage patterns, and mechanical damage features at the fire scene by applying arc mapping (arc survey) for fire origin and cause determinations^{21,22}. The observable electrical artifact of the arcing fault (arc melt site) is in the form of physical evidence of localized melting of the electrical equipment or wiring.

Characteristic features of arcing damage include beading, notching, welding, or severing of the conductors. There may also be molten spatter or residue of vaporized metal immediately adjacent to the area of the arcing event. This may pose an effect on adjacent conductors or surfaces of other materials in close proximity²³⁻²⁶. A recent survey conducted of 317 participants revealed that investigators could reliably identify and characterize mechanical damage. However, survey participants had low probability overall (45.61%) of visually distinguishing the differences between arc-melting and fire-melting features²⁷.

Electrical Arcing and Metallurgy

From the time of initiation of the electrical arc until

extinguishment, the arc transfers electrical energy to surrounding materials. The transfer of energy may include all three heat transfer mechanisms of radiation, convection, and conduction. The transfer of energy in the form of heat causes impacted materials to increase in temperature, which, in turn, may lead to melting, burning, or vaporization of the materials.

Depending on the thermal energy generated by the electric arc, impacted materials (including metals such as steel, copper, aluminum, zinc, silver, gold, and tin) may undergo phase changes from a solid to a liquid, gas (vapor), and/or plasma. The phase change will depend upon the specific physical properties of the material. After the arc is extinguished, vaporized and melted materials will be quenched by the surrounding material and revert to a solid form. The solidification of the melted materials provides characteristic physical evidence (morphology) of the electrical event. The arc-melting data can provide important physical evidence related to how and where the electrical artifact was generated.

Phase Transition Properties of Copper

Copper materials are commonly utilized for electrical equipment and wiring. The heat required to raise the temperature of one gram of copper by one degree Celsius (known as the specific heat) is 0.386 J/g °C¹⁹. Additional phase transition properties of copper are listed in **Figure 2**.

Where: $T(C^{\circ}) = 5/9 \times [T(F^{\circ}) - 32]$

1 kJ/kg = 0.4299 Btu/lb = 0.23884 kcal/kg

Copper has loosely bound electrons that are able to easily transfer or conduct heat and electricity compared to other materials³. Alexander and Street described how the “pure copper metal is ductile and can be easily worked, rolled, and pressed into a variety of shapes”²⁸. “Copper is easily alloyed with other metals, such as tin, aluminium, or zinc, affecting the electrical conductivity. For example, the addition of 10% aluminium doubles copper’s physical strength but reduces the electrical conductivity of copper by one sixth”²⁸.

| Substance | Melting Point °C | Latent Heat of Melting (kJ/kg) | Heat Capacity C _{p,m} (J/mol C°) | Boiling Point — Vaporization Temperature °C | Latent Heat of Evaporation (kJ/kg) |
|-----------|------------------|--------------------------------|---|---|------------------------------------|
| Copper | 1083 | 207 | 24.7 | 2595 | 4730 |

Figure 2
Phase transition properties of copper¹⁹.

Within a fire scene, post-fire damaged electrical conductors may have characteristic damage features in the form of mechanical, fire melting, or arc melting. These have different morphology characteristics and are generally observable visually or with low magnification. There are instances where damage features may require specialized equipment and/or techniques to evaluate. The following damage types are generally recognized to describe observable damage features observed on post-fire damaged electrical wires^{21,26,29, 30}.

Mechanical Damage Sites

Mechanical damage sites are generally recognized by fracture, impact, cracks, cuts, shearing, stretching, or other damage from a mechanical action at the damage site. Mechanical damage can occur prior to the incident event, during the progression of the event or due to the excavation process involved in a scene investigation. Examples include gouging/scraping of wires during installation or subsequent construction tasks, structural collapse (causing conductors to stretch or break), or cutting by a tool.

Fire Melt Sites

Fire melt sites generally occur during heat or fire attack that exceeds the melting temperature of conductor materials, such as aluminum, zinc, or copper. Conductor melt sites identified as fire-melting damage features are recognized in the form of gross melting, globules, and/or balls. They may exhibit, in part, a non-uniform surface and shape, no clear lines of demarcation at the damage site, irregular melting in and around the damage site, and multiple or widespread areas of damage. Conductor manufactured tool markings (i.e., drawing lines) are generally melted at and away from the damage site, and no porosity or non-uniform porosity will be within the damage site.

Alloying Sites

Alloying sites, a subset of fire melting, are generally recognized by the mixing or alloying of dissimilar materials from elevated temperatures at the damage site. Electrical equipment uses many different materials that may alloy together, such as copper, aluminum, lead, tin, and zinc. Buc reported that alloying is a fire-melt feature that may exhibit features similar to an arc site; however, it is generally accepted that alloying of copper with other common materials, such as aluminum and zinc, exhibit visible features that are, respectively, silver and bronze in color and visually distinguishable from arc melt sites consisting of only copper materials³¹.

This type of damage site has been inaccurately broadly

identified as eutectic melting; however, “eutectic” is a specific metallurgical term that commonly applies to specific alloy systems and concentrations where the melting point of the mixture is lower than either of the involved materials individually. Thus, some mixtures (e.g., Cu-Al) exhibit eutectic behavior, but others (e.g., Cu-Zn) do not. “Alloying” encompasses any mixture of dissimilar metallic materials; therefore, it is a more appropriate general term.

Arc Melt Sites

When the heat of the fire is sufficient to compromise the electrical insulation of electrically energized (with sufficient available fault current) conductors, a fault or short circuit (arcing melting event) often occurs between the energized and/or earth (grounded or grounding) conductors.

The arcing event generates an arc-melt site(s) that can be identified by localized electrical arcing damage features that are generally identified on electrical wiring and equipment in the form of beads and/or notches. They may exhibit (in part) a smooth surface appearance, distinct lines of demarcation, internal uniform porosity between the different surface textures as well as obliteration of manufactured tool markings within the damage site. Conductor manufactured tool markings may be observed outside the damage site in some cases, but can also be obscured by post-event oxidation or damage. Furthermore, arc-melt sites are generated by electricity — not by fire.

Carbon Tracking

Carbon tracking, also known as arcing through char, is a subset of arc melting wherein electrical current can flow through a carbonized semi-conductive path. Sufficient electrical voltage and available current across the carbonized path may cause electrical current to flow between the carbonized materials and conductors. The carbon is formed from otherwise insulating materials by

Safety Note:

Electricity can be a dangerous occupational hazard. Forensic investigation practitioners may work in areas where this hazard exists. Prior to work, determine site-specific or foreseeable safety hazards, understand your employer’s health and safety program, and review safety documents related to workplace hazards. National Fire Protection Association’s NFPA 70E, “Standard for Electrical Safety in the Workplace,” which addresses safety-related work practices, can help reduce the risk of electricity-related workplace injuries²⁰.

impinged heat and flame.

Notable Fire Investigation Related Arc Melting and Fire Melting Research

Carey and Nic Daeid were able to visibly differentiate between arcing damage as a result of short circuit and arcing through char. They conducted 39 full-scale, electrically energized compartment fire test experiments. These tests enabled them to characterize nine types of post-fire, conductor arc-melt damage features that included combinations of arcing through char, severed ends, beading, notches and welding. No samples of fire melt were generated during their experiments²⁹.

Murray advanced metallurgical techniques for fire investigation. Murray's findings were, in part: "Electrical damage due to arcing revealed distinct characteristics. More precisely, macroscopically, damage was confined to a localized area, where the surrounding material showed the same condition than initially. Due to the fact that short-circuit phenomenon transfers to the metal an important amount of energy very quickly, liquification and thus resolidification are state changing that occurred very fast"³².

In 2012, Hussain's research called into question whether arc melt sites and fire melt sites could be reliably distinguished from one another. Hussain (as well as Roby and McCallister) reported that in their view, "it is not possible to distinguish between the beads formed on energized and non-energized wires exposed to various thermal insults"^{33,34}. Note: Hussain's research (and that of Roby and McCallister) present the same research/data but under different authorship.

In contrast to other researchers, Buc researched and developed a laboratory examination method to character-

ize the damage site^{31,35}, distinguishing the difference between arc melt and fire melt sites by examining the interior of the damage site for microstructure, porosity, and internal lines of demarcation. However, no quantifiable (measurable) research has been undertaken to distinguish between arc-melt and fire-melt features observed on post-fire damaged electrical copper conductors of 1.0 mm² to 2.5 mm². Thus, the following experiments were undertaken to generate electrical artifacts for study.

Methodology:

Part 1 – Generation of Datasets of Known Damage Full-Scale and Scaled Experiments

Post-fire electrical conductor arc melting, fire melting, mechanical damage, and non-damaged site specimens were generated within both laboratory and field experiment settings. North American copper #14 AWG (1.6 mm) non-metallic (NM) cabling and United Kingdom (UK) "Twin & Earth" type copper, 1.0 mm² and 2.5 mm², NM (where CD is the electrical conductor diameter) were used. Each cable type was used for repeated experiments as follows:

Series One Experiments

A total of 63 full-scale compartment fires were conducted at the United States Federal Law Enforcement (FLETC) ATF fire training center in Brunswick, Georgia (**Figure 3**).

The electrical distribution system under these tests, represented in a one-line diagram (**Figure 4**), included 120/240VAC, single-phase, 15A electrical circuits. The available fault current at the point of fire impingement was calculated to be 210.9A. Six #14 AWG (1.6 mm), NM, copper electrical circuits (four energized at 120VAC, overcurrent protected at 15A and two non-energized electrical circuits) were installed at the ceiling level of each compartment.



Figure 3

(A) Full-scale compartment fire testing at FLETC, (B) interior view of fire, and (C) post-flashover fire extending outside of compartment.

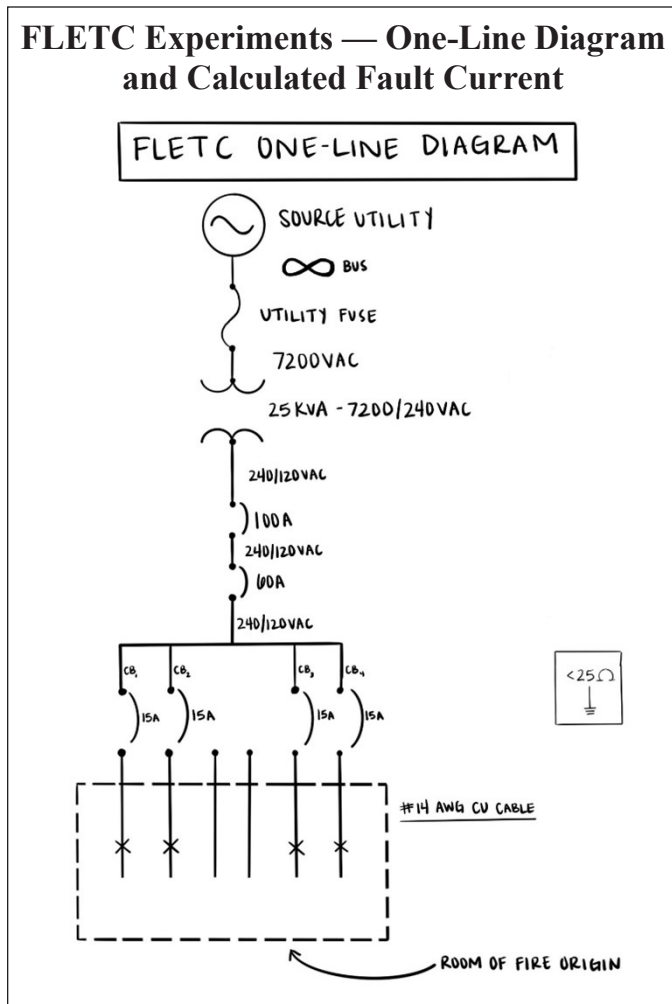


Figure 4

Electrical one-line diagram for FLETC experiments.

A fire was independently initiated by ATF personnel within each compartment. Each fire was allowed to develop based on controlled compartment fuel and ventilation characteristics that were determined by the ATF training parameters. A total of 87.3% of the full-scale experiments went to post-flashover conditions. Electrical data in the form of voltage and short-circuit fault currents were recorded for future analysis. Although fires had reached post flashover conditions, only artifacts of arc melting were generated during the full-scale, FLETC burn cell experiments. However, additional arc melting, fire melting, and mechanical damaged artifacts were generated during a series of scaled fire impingement and non-fire experiments.

Series Two Experiments

No artifacts of fire melting were generated during the full-scale, FLETC burn cell experiments. As a result, two full-scale wooden compartments were constructed in

Covington, Louisiana. Both Gulf Coast Fire Investigation and Fire Investigation Group personnel assisted with the construction, ignition, and collection of artifacts generated within these compartments.

Non-energized electrical circuits were installed within the two burn cells. North American copper #14 AWG (1.6 mm) non-metallic (NM) copper cabling and United Kingdom (UK) copper, 1.0 mm² (1.1 mm) and 2.5 mm² (1.7 mm), “Twin & Earth” cabling were installed. Each compartment fire was allowed to burn until complete destruction of the compartment. Since no melting in these experiments could have been due to arc melting, 60 non-energized electrical conductor artifacts with melting were selected from the resultant dataset to be representative of fire melt sites.

Series Three Experiments

The third set of experiments was conducted at MSD Engineering laboratory in Crystal Lake, Illinois. The purpose of these experiments was to perform scaled tests to generate electrical artifacts using a newly developed electrical testing apparatus, which was designed and constructed to facilitate testing of electrical equipment and wiring under varying electrical, fire, and installation configurations. This newly designed test platform, called the Mark I – Arc Research Chamber (MARC – USPTO patent pending), included onboard flame/heat sources and instrumentation that can record voltage, current, temperature, heat flux data, and electrical fault current data.

In total, 42 scaled tests were undertaken. In each case, UK 1.0 mm² (1.1 mm), UK 2.5 mm² (1.7 mm) “Twin & Earth” and North American #14 AWG (1.6 mm) NM copper cables were electrically connected to appropriately sized single-pole, overcurrent protection devices (6A, 20A, and 15A, respectively) and energized using an associated system voltage (UK “Twin & Earth” 230VAC and North American - 120VAC) that had sufficient electrical fault current to generate an arcing fault. The arc artifacts generated using the MARC test platform were validated in terms of their characteristics and morphology against the artifacts generated under known conditions in the full-scale series one (arc melt) and series two (fire melt) tests. These experiments provided the opportunity to repetitively generate the arc and fire melt artifacts required for practitioner surveys and human factor research²⁷.

Carey Experiments

In total, 106 arc melting artifacts generated through Carey’s research²⁸ were also provided for incorporation

into the overall project dataset. These samples were generated using UK cables installed within full-scale compartments under real fire conditions. The inclusion of these samples enabled a direct comparison between the UK and North American samples to be made in terms of characterization of damage²⁹.

Part 2 — Examination and Analysis of Electrical Artifacts

The artifacts generated through the three series of experiments were examined and analyzed in multiple stages by several forensic engineers/technicians employed by both Materials Evaluation and Engineering (MEE) and MSD Engineering (MSD). Each artifact was documented based on the location, date of generation, and date of recovery. All artifacts were independently coded. Samples were initially examined and cleaned, removing loose debris. When required, melted and charred insulation material was carefully removed. (Figure 5).

Each artifact was sectioned from the lengths of electrical cabling and examined using low power light microscopy where various visible features were characterized and compared to arc melt and fire melt images found within both ATF technical bulletin and NFPA 921^{30,36}. While visual examination revealed a difference in features between arc melt and fire melt, no protocol for the morphological examination of arc and melt damage has been published to date. The authors have developed a systematic methodology for the comparisons of post-fire features observed on fire-damaged electrical wiring³⁷:

Arc-melted and fire-melted artifacts were examined. Measurements were made using calibrated or validated handheld calipers, magnifying instrument(s), or light microscopy utilizing optical or digital Keyence microscope(s), as noted in Figure 6.

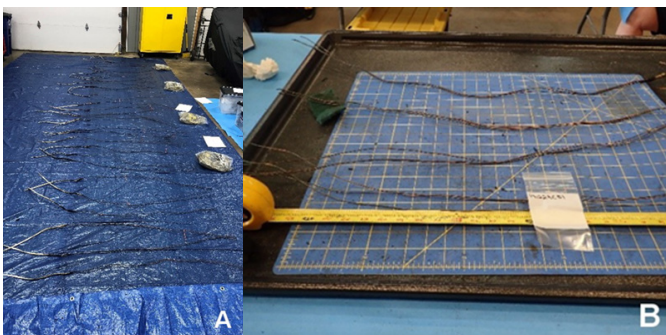


Figure 5

Post experiment examination of electrical artifacts. (A) post-fire damaged cable examination; (B) post-fire damaged collection and packaging of damage sites²⁷.

Each artifact was examined visually and/or with a microscope, and images were collected. The length of each area of displaced copper (in the form of beads, notches, globules, or other features indicating melting of the copper conductor) was documented. The maximum displacement was measured and recorded (Figure 7 and Figure 8). In cases where melted copper artifacts were grossly melted, melted open or discontinuous, a displaced material measurement of 50 mm was recorded for each artifact. Artifacts that exhibited multiple melt sites separated by greater than 100 mm were considered separate independent melting events.

Results and Discussion

In total, 721 artifacts were generated and categorized into 476 samples of electrical arc melting, 102 samples of fire melting, and 143 samples of fire-impinged, mechanical damage, or non-melted electrical conductors. Normalized diameter measurements of the displaced melted copper for both arc melt and fire melt artifacts were determined. The data revealed quantifiable and statistically significant Chi-squared, ($p = <0.00001$) differences between the measurable damage features and their comparison to the conductor diameters for arc melt sites and fire melt sites for all three cable types studied.

Arc Melt Sites

Localized melting features, clear lines of demarcation, and uniform porosity were observed within arc melt sites. Electrical arc-melt features generated had melted copper

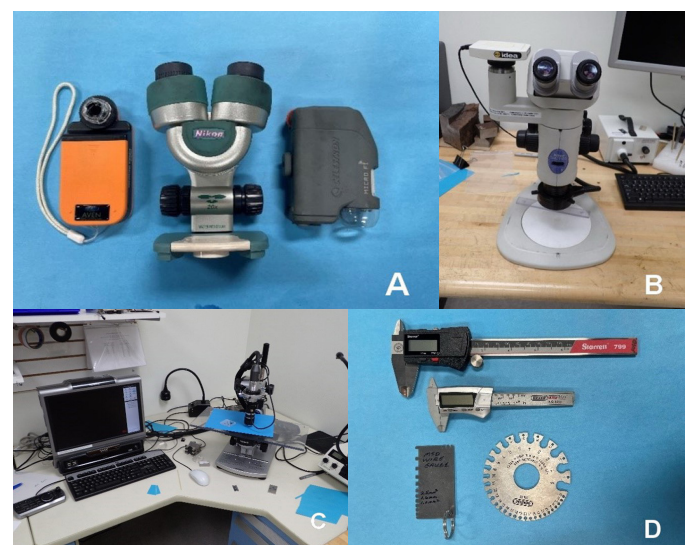


Figure 6

Examination equipment utilized for artifact examination. (A) portable microscopes for field light microscopy; (B) laboratory or bench optical light microscope; (C) digital light microscope for microscopy and measurements (calibrated); (D) digital caliper (top) and measurement gauges (bottom)²⁷.

displacement of less than or equal to four times the subject conductor diameter ($0 < AM \leq 4CD$). Arc melting scatter plots and normalized graphs for solid North American

(NM) 1.6 mm, (UK) 1.0 mm² and (UK) 2.5 mm² copper conductors are presented in **Figures 9** through **12**.




| Artifact ID | Wire ID | Conductor Diameter (mm) | Max Arc Melt Size (mm) | Artifact |
|--------------|---------------|-------------------------|------------------------|--|
| FLETC 150515 | Cell 5 Wire 2 | 1.6 | 4.01 |  |
| FLETC 150515 | Cell 3 Wire 1 | 1.6 | 2.53 |  |
| FLETC 150515 | Cell 1 Wire 3 | 1.6 | 2.37 |  |

Figure 7
Representative samples of series one – FLETC arc-melted artifacts²⁷.

Fire Melt Sites

In all cases, the generated fire melt sites had measurable melting features greater than four times the conductor diameter (FM>4CD). The sites exhibited melting, spherical balls (globules). Non-uniform or non-persistent porosity was observed within the mixed gas flame generated

globules and/or spherical ball fire melt sites.

Fire melt scatter plots and normalized graphs for 1.6 mm conductors are presented in **Figures 13** and **14**. The data analysis and findings for both 1.0 mm² and 2.5 mm² (UK) copper conductors were similar to the NM 1.6 mm




| Artifact ID | Wire ID | Conductor Diameter (mm) | Max Fire Melt Size (mm) | Artifact |
|-------------|---------|-------------------------|-------------------------|--|
| Louisiana 2 | 2 | 1.6 | 17 |  |
| Louisiana 2 | 3 | 1.6 | 32 |  |
| Louisiana 2 | 4 | 1.6 | >50 |  |

Figure 8
Representative sample of series two - Louisiana (LA) fire melt artifacts²⁷.

copper conductor results.

Additional Metallurgical Examination Techniques

The previously discussed methodology of quantifying displacement of melting observed on a post-fire damaged

electrical conductor provided high confidence in characterizing conductor melt sites by visual examination and quantitative measurement. This provides investigators with the ability to field deploy the methodology for characterizing electrical conductor melt sites. However, in instances of uncertainty with respect to whether an artifact is an arc melt or fire melt, further examination utilizing non-destructive X-ray examination³⁵ or destructive metallurgical techniques (such as metallography) can provide

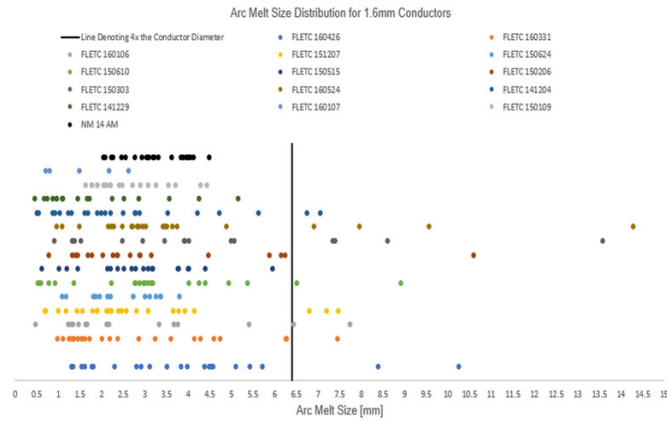


Figure 9

Scatter plot for Series One 1.6 mm arc melt size distribution. The vertical line represents the location of 4X the conductor diameter²⁷.

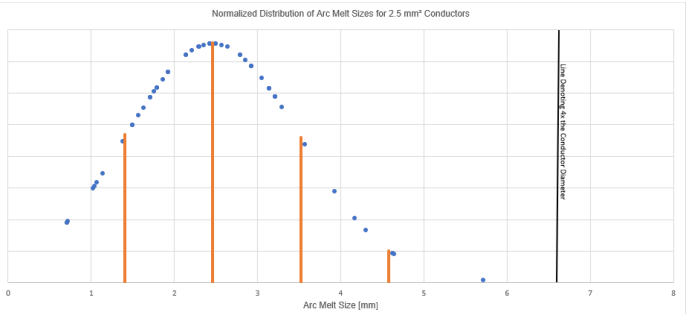


Figure 12

Distribution of the Series Two arc melt size generated on 2.5 mm² and the Carey samples (NC UK fire arc) size distribution. The vertical line represents the location of 4X the 2.5 mm² conductor diameter²⁷.

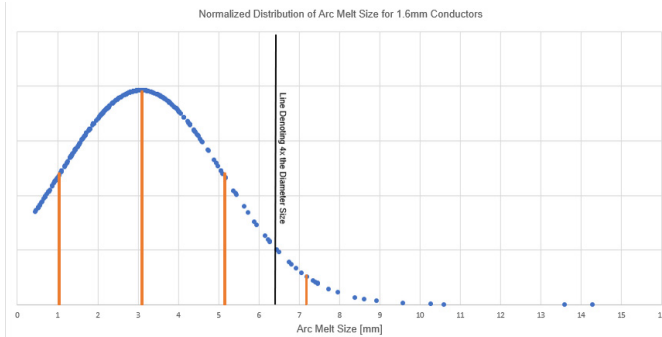


Figure 10

Distribution of the Series One arc melt size generated on 1.6 mm conductors. The vertical line represents the location of 4X the 1.6 mm conductor diameter²⁷.

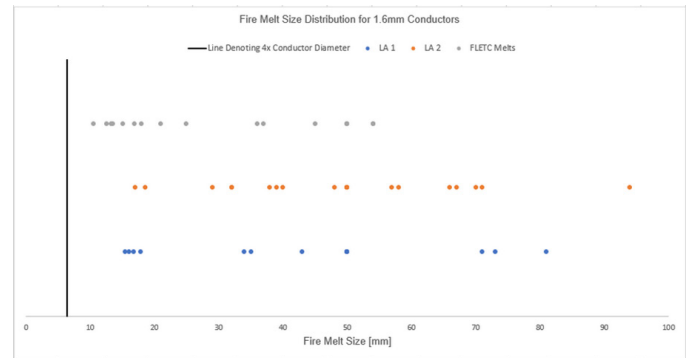


Figure 13

Scatter plot for 1.6 mm fire melt size distribution. The vertical line represents the location of 4X the conductor diameter²⁷.

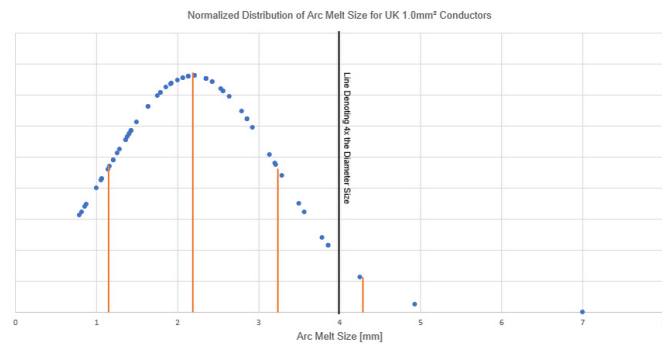


Figure 11

Distribution of the arc melt size generated on 1.0 mm² and the Carey samples (NC UK fire arc) size distribution. The vertical line represents the location of 4X the 1.0 mm² conductor diameter²⁷.

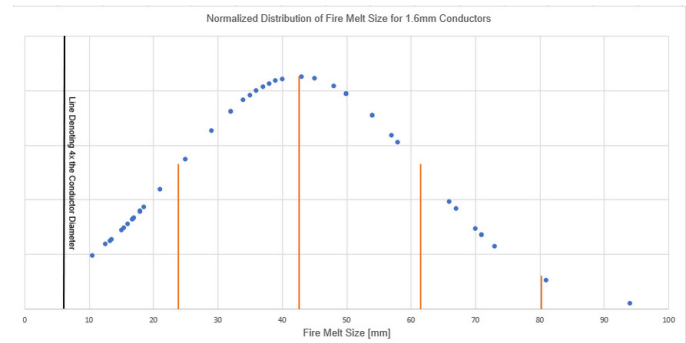


Figure 14

Normalized curve of 1.6 mm fire melt size distribution. The vertical line represents the location of 4X the 1.6 mm conductor diameter²⁷.

increased confidence and additional data to assist in the damage feature characterization.

To better understand the usefulness of many metallurgical techniques like metallography, a fundamental understanding of the structural configuration (grain structure) of metallic materials (in this case, specifically focusing on copper) is required.

The atoms in a solid copper material are arranged in an orderly structure, known as a face-centered cubic (FCC) lattice. Most commercial applications of copper (conductor) wire are polycrystalline materials. This means that the bulk wire material is comprised by discrete zones of the FCC lattice structure in various orientations (**Figure 15**). These zones are called grains, and their size/shape collectively constitute the material's "grain structure." Grain structure is one of the most useful aspects of characterizing melted conductors because the grain structure can change drastically due to the effects of various types of thermal exposure.

As copper materials cool from a liquid state (randomized atomic structure), the material will begin solidifying at many nucleation sites simultaneously³⁷. Each nucleation site is the origination point of a single grain; these grains continue to grow until they either run into another grain, or all of the liquid material is solidified³⁷. These solidified grains have a characteristic dendritic morphology, but become altered through further processing of the wire during subsequent manufacturing. The room-temperature grain structure of a typical copper conductor consists of very small grains. Levinson reported that the grains of copper become elongated during the manufacturing process

of drawing copper into wire³⁸. Copper wire for electrical purposes is commonly supplied in the annealed condition, which has a fine, equiaxed (i.e., non-elongated) grain structure. A representative example of the typical microstructure for a commercially available copper wire is shown in **Figure 16**.

Thus, through fundamental principles of metallurgy and direct observation of the specimens created during the course of the research presented herein, differences from this baseline structure observed in field specimens can be correlated to the thermal exposure condition for the subject conductor(s).

Conductor Characterization by Scanning Electron Microscopy

Characterization of a conductor surface by scanning electron microscopy (SEM) is typically non-destructive and a simple first step in a more comprehensive evaluation of a suspected arc site (**Figure 17**). As discussed previously, since an electrical arc is an extremely short-

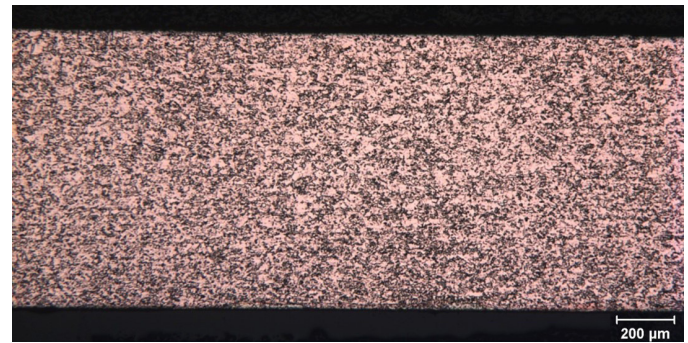


Figure 16

Typical material microstructure for a copper conductor as-manufactured (longitudinal section view)²⁷.

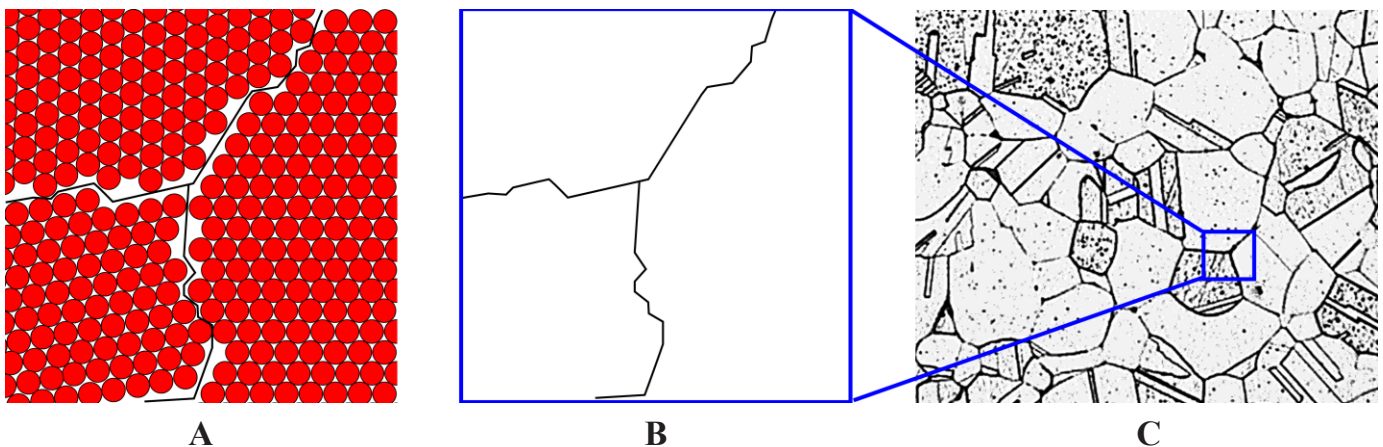


Figure 15

(A and B) schematic representation of a copper grain structure and (C) a typical micrograph of an actual grain structure for a copper material.

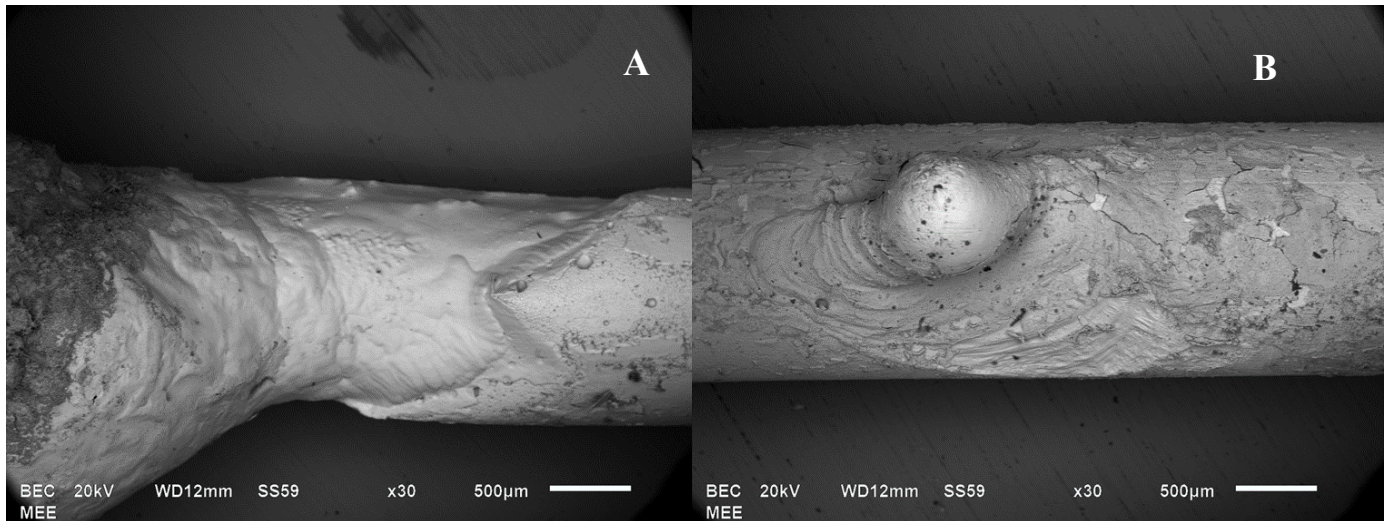


Figure 17

(A) and (B) SEM images of conductors showing boundaries between melted and non-melted regions.

duration but very high-temperature event³², the bulk wire material adjacent to the melted material does not experience sufficient heating to alter the grain structure, and the boundary between melted and resolidified material will be very sharply delineated. Examination by SEM can aid in characterizing the transition between resolidified material and the original conductor surface in very small regions that may not be as easily resolved by light microscopy.

In some cases — particularly after a fire and subsequent artifact extraction — the surface features in a suspected arc site may be more adequately characterized as mechanical damage or corrosion/oxidation. SEM examination is also useful in characterizing these features and can aid in distinguishing between the microscopic surface features that result from melting and re-solidification and surface features that result from mechanical damage, corrosion, or foreign material contamination.

A common companion technique to SEM is a method for elemental analysis known as energy dispersive x-ray spectroscopy (EDS), which is capable of identifying the elements comprising specimen surface features as small as a few microns.

As an example, one condition that can result in localized melting of copper conductors is alloying with lower-melting-point materials. As discussed previously, an alloy is a mixture of different metallic elements, and the melting point of alloys can be vastly different from the melting point of either material individually³⁹. For some metals, such as aluminum, lead, or tin, the melting point of a mixture with copper can be well below the temperatures sus-

tained during a fire event^{36,39}. Thus, melting can occur at conditions where the copper would normally be expected to be intact. EDS analysis is very useful for identifying elements (or the lack of elements) that could be responsible for melting due to alloying or the source of arcing to materials other than copper.

If surface level evaluations by SEM/EDS are still inconclusive, additional metallographic examination can be conducted to aid in further characterizing the damage.

Conductor Characterization by Metallographic Examination

Metallographic examination is a widely accepted and standardized method for characterizing the grain structure

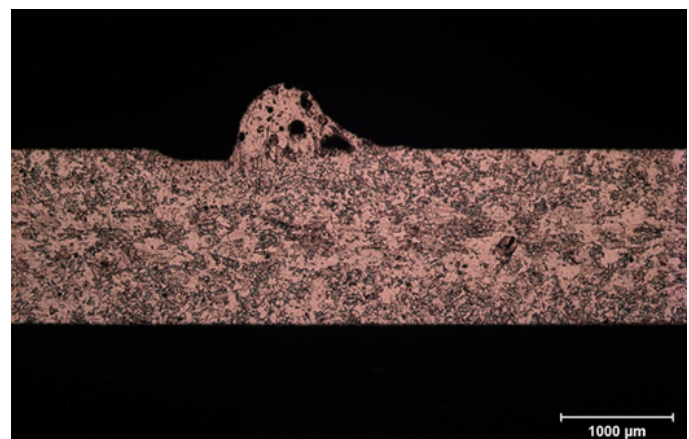


Figure 18

Light micrograph of a metallographically prepared specimen showing localized columnar grains, internal porosity, and a sharp boundary between the resolidified material and unaffected bulk material grain structure²⁷.

of a material⁴⁰. However, due to its destructive nature, it should be the last step in the characterization process. Since metallographic specimen preparation involves preparing a cross section through the conductor material to be studied, a primary benefit is that the internal structure of the material can be characterized. Once a metallographic section is prepared, the surface is chemically etched to reveal the grain structure and examined by light microscopy and/or SEM/EDS (**Figure 18**).

As discussed previously, melted and resolidified material will typically have a dendritic or columnar structure (unless there has been sufficient subsequent heating to recrystallize the material). Again, a clearly delineated boundary between the resolidified material and the bulk material and/or a lack of other indications of high temperature exposure for the damaged conductor is strong evidence of an extremely localized and rapid heating event (e.g., an electrical arc).

Resolidified material from an electrical arcing event is also characterized by a high concentration of porosity³¹. Levinson described how the “grain structure in copper changes when copper wire is heated through the melting point as well as the subsequent formation of copper oxide and the development of porosity”³⁸. Therefore, localized electrical arcing affects copper grain structure, the formation of copper oxide, and the formation of porosity.

Levinson³⁸ and Gray⁴¹ both reported that porosity was present, creating a “Swiss cheese” effect on the copper wire surface due to arc melting. However, surface-level examinations, such as those conducted by light microscopy or SEM, may not reveal internal porosity that is easily observed in a properly prepared metallographic section. Levinson theorized that “the porosity effect would be found if the wire was melted by the fire, the resistance effect of a gross overcurrent, or by arcing”³⁸. Levinson further theorized that this “porosity was a result of partial entrapment of gas pockets liberated from the copper wire”³⁸. Gray observed the effects of porosity within electrically arced conductor samples by utilizing an SEM⁴¹. Present empirical research continues to corroborate the findings of porosity within the resolidified material of an electrical arc melt site.

Converse to the characteristics of electrical arcing, conditions can also be observed that indicate more widespread, longer-term degradation due to high-temperature exposure. A gradual transition from a melted and resolidified zone to the bulk wire material grain structure indicates

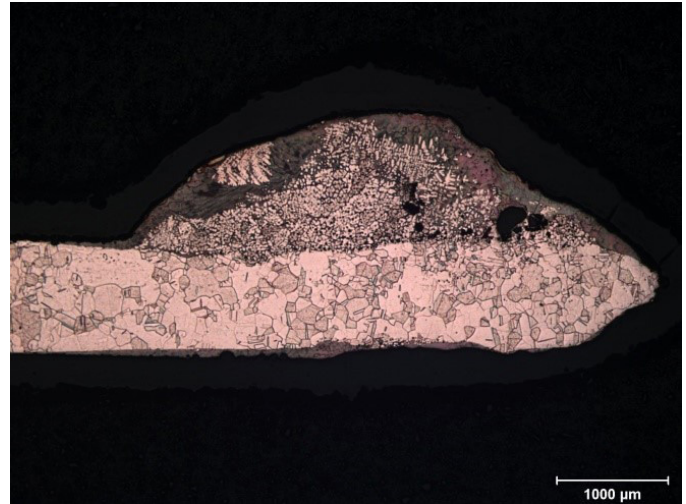


Figure 19

Light micrograph of a metallographically prepared specimen showing an irregular conductor profile, non-uniform melting, a more gradual transition between melted material and the bulk structure as well as a widespread enlarged grain structure²⁷.

non-localized heating that can be expected from the heat of a fire. Somewhat localized or gross changes in the fine-grained texture of the bulk material (e.g., grain growth) indicate prolonged exposure to elevated temperatures (**Figure 19**). The specific features observed, as well as their location, orientation, and/or coincidence with other artifacts, can be used to make a more conclusive determination of the conditions that resulted in the damage to the conductor.

Summary and Conclusions

During the course of their work, forensic electrical power engineers and electrician practitioners may apply electrical engineering and scientific principles to forensic investigations by performing electrical surveys and electrical fault evaluations. A fire investigation practitioner may implement a similar electrical investigation methodology called “arc mapping” or more recently termed an “arc survey.” The correct application of either of these methodologies is dependent, in part, on the forensic investigation practitioner’s ability to distinguish features observed on damaged electrical wiring and equipment.

Currently, practitioners rely upon subjective visual observations to distinguish the difference between arc melting, fire melting, and mechanical features on post-fire damaged electrical conductors. The experiments undertaken as part of this research generated an underpinning dataset of electrical conductors that exhibit arc melt, fire melt, and mechanical damage features. Examination and analysis of the data generated from this research resulted

in findings for tested conductors, in part:

- Post-fire damaged electrical conductor melting features in the form of arc melting and fire melting can be reliably distinguished from each other.
- Under fire conditions, arc melt sites were only observed on electrically energized electrical circuits, and arc melt sites were only located within the area of origin.
- Physical evidence in the form of both fire patterns from the effects of fire and electrical patterns in the form of arc melt sites were observable, distinguishable, and quantifiable throughout these experiments.
- Electrical arc melting features generated from these experiments had melted copper displacement of less than or equal to four times the subject conductor diameter ($0 < AM \leq 4CD$). Fire melt features had a copper displacement greater than four times the subject conductor diameter ($FM > 4CD$). This was a validated and repeatable characteristic across the dataset at 95% for both full-scaled and scaled experiments.
- The experiments revealed, in part, that NM 1.6 mm (#14 AWG) North American (U.S.) cables responded to fire in a similar manner as experiments conducted on UK 1.0 mm² and UK 2.5 mm² cabling experiments²⁷.
- Electrical experiments did not result in malfunction, damage upstream, or uncoordinated operation of overcurrent protective device(s) (OCPDs) that were electrically upstream from the OCPD protecting the circuit under test.
- Power electrical engineers and electricians can apply short-circuit/electrical fault analysis procedures during a fire investigation(s) whereby an electrical analysis of a one-line diagram in conjunction with arc fault analysis or arc survey may define a region of investigation interest, area of origin, and point of origin.
- Examination of non-energized electrical cabling recovered from the FLETC experiments had no observable melting.

- Adaptation of metallurgical techniques and methods, such as SEM, EDS, and microstructure analysis, further underpinned the ability to distinguish the different features of arc melting and fire melting.

This empirical research represents a validated novel methodology using quantified measurement to reliably distinguish the difference between arc melt and fire melt sites observed on the tested post-fire damaged electrical conductors of the same size. However, additional testing may be required for different conductor sizes, materials, and fault current conditions.

Acknowledgements

The authors wish to thank, in part, the Leverhulme Research Centre for Forensic Science; University of Dundee (UK), Special Agents of the Department of Justice; Bureau of Alcohol, Tobacco, Firearms and Explosives (US), MSD Engineering (US), Gulf Coast Fire, LLC (US), Investigative Loss Services (US) and Materials Evaluation and Engineering (US) for their continued support. The authors also wish to acknowledge the following for their invaluable support. – Prof. Susan Black, Dr. Nick Carey IAAI-CFI, Jeff Washinger Sr. IAAI-CFI, Robert Schaal ATF (retired) and IAAI-CFI, Larry Hanke, PE, Albert Bartolome i Regue Engineer & IAAI-CFI, Lester Rich ATF (former) & IAAI-CFI, Kerry Svare ATF (retired) and IAAI-CFI, Roberta Svare, Carol Severson EIT, and Erik Severson EIT.

These experiments were conducted and assisted by numerous companies and personnel further acknowledged. Additionally, all FLETC experiments were performed in conjunction with ongoing ATF training programs. All research expenses for FLETC, Louisiana, Minnesota, Illinois and United Kingdom locations were funded by researcher Dr. Mark J. Svare, PE.

References

1. H. Davy, Elements of Chemical Philosophy: Part 1, Vol. 1. Bradford and Inskip, 1812.
2. C. L. Fortescue, "Method of Symmetrical Coordinates Applied to the Solution of Polyphase Networks," Transactions of the American Institute of Electrical Engineers, vol. 37, no. 2, pp. 1027-1140, 1918.
3. R. Kaufmann and J. Page, "Arcing Fault Protection for Low-Voltage Power Distribution Sys-

- tems -Nature of the Problem,” Transactions of the American Institute of Electrical Engineers. Part III: Power Apparatus and Systems, vol. 79, no. 3, pp. 160-167, 1960.
4. R. Lee, “The Other Electrical Hazard: Electric Arc Blast Burns,” IEEE Transactions on Industry Applications, vol. IA-18, no. 3, pp. 246-251, 1982.
 5. R. Lee, “Pressures Developed by Arcs,” IEEE Transactions on Industry Applications, vol. IA-23, no. 4, pp. 760-764, 1987.
 6. T. Gammon and J. Matthews, “The Historical Evolution of Arcing-Fault Models for Low-Voltage Systems,” IEEE Industrial and Commercial Power Systems Technical Conference, pp. 1-6, 1999.
 7. T. Gammon and J. Matthews, “Arcing-fault models for low-voltage power systems,” in 2000 IEEE Industrial and Commercial Power Systems Technical Conference. Conference Record (Cat. No. 00CH37053), 2000: IEEE, pp. 119-126.
 8. T. Gammon and J. Matthews, “Instantaneous Arcing-Fault Models Developed for Building System Analysis,” IEEE Transactions on Industry Applications, vol. 37, no. 1, pp. 197-203, 2001.
 9. T. Crnko and S. Dyrnes, “Arcing Fault Hazards and Safety Suggestions for Design and Maintenance,” IEE Industry Applications Magazine, vol. 7, no. 3, pp. 23-32, 2001.
 10. T. Gammon and J. Matthews, “The application of a current-dependent arc model to arcing at a main distribution panel, a sub-panel and a branch circuit,” in Proceedings. IEEE SoutheastCon 2001 (Cat. No. 01CH37208), 2001: IEEE, pp. 72-78.
 11. T. Gammon and J. Matthews, “IEEE 1584-2002,” IEEE Industry Applications Magazine, vol. 11, no. 1, pp. 24-31, 2005
 12. T. Gammon and J. Matthews, “Conventional and Recommended Arc Power and Energy Calculations and Arc Damage Assessment,” IEEE Transactions on Industry Applications, vol. 39, no. 3, pp. 594-599, 2003.
 13. H. Land, “The Behavior of Arcing Faults in Low-Voltage Switchboards,” IEEE Transactions on Industry Applications, vol. 44, no. 2, pp. 437-444, 2008. [Online]. Available: vb.
 14. H. Land and T. Gammon, “Addressing Arc-Flash Problems in Low-Voltage Switchboards: A Case Study in Arc Fault Protection,” IEEE Transactions on Industry Applications, vol. 51, no. 2, pp. 1897-1908, 2015.
 15. Bulletin EDP-2 - Selective Coordination of Overcurrent Protective Devices For Low Voltage Systems, 1969, pp. 1-31.
 16. Bulletin EDP- 1-3 - A Simple Approach to Short Circuit Calculations - Part 1, 2004, pp. 1-104.
 17. Short Circuit Current Calculations, Cooper Bussmann, 2005, pp. 192 - 198.
 18. C. Miller, Ugly's Electrical References. Jones & Bartlett Learning, 2023.
 19. D. Lide, CRC Handbook of Chemistry and Physics, 79th ed. (Handbook of Chemistry and Physics). New York: CRC Press, 1998.
 20. National Fire Protection Association, 70E Standard for Electrical Safety in the Workplace. NFPA, Quincy, MA, USA, 2021.
 21. National Fire Protection Association, 921 Guide for Fire and Explosion Investigations. NFPA, Quincy, MA, USA, 2021.
 22. National Fire Protection Association, 1033 Standard for Professional Qualifications for Fire Investigator. NFPA, Quincy, MA, USA 2014.
 23. B. Beland, “Examination of Electrical Conductors Following a Fire,” Fire Technology, vol. 16, no. 4, pp. 252-258, 1980.
 24. B. Ettlting, “Arc Marks and Gouges in Wires and Heating at Gouges,” Fire Technology, vol. 17, no. 1, pp. 61-68, 1981.
 25. B. Ettlting, “Problems with Surface Analysis of Copper Beads Applied to the Time of Arcing,” International Association of Arson Investigators,

- pp. 23-26, 1998.
26. R. Svare, "Using the electrical system to help reconstruct the fire scene," in Proceedings of International Symposium on the Forensic Aspects of Arson Investigations, Federal Bureau of Investigation, Washington, 1995, pp. 103-116.
 27. M. Svare, "A reliable systematic methodology for reconstructing the fire scene using the electrical system: analysing human factors," Ph.D. Dissertation, Science and Engineering, University of Dundee, Dundee, UK, 2022.
 28. W. Alexander and A. Street, *Metals in the Service of Man*, 8th ed. Pelican Technology, 1982.
 29. N. Carey, "Developing a reliable systematic analysis for arc fault mapping," Ph.D. Dissertation, Pure and Applied Chemistry, University of Strathclyde, Glasgow, UK, 2009.
 30. ATF Fire Research Laboratory, "Visual Characteristics of Fire Melting on Copper Conductors," ATF Fire Research Laboratory Technical Bulletin, no. Technical Bulletin 001, pp. 1-8, 2012.
 31. E. Buc, D. Reiter, J. Battley, T. Sing, and T. Sing, "Method to Characterize Damage to Conductors from Fire Scenes," *Fire and Materials*, pp. 657-666, 2013.
 32. I. Murray and F. Ajersch, "New Metallurgical Techniques Applied to Fire Investigation," *Fire and Materials*, pp. 857-870, 2009.
 33. R. Roby and J. McAllister, "Forensic Investigation Techniques for Inspecting Electrical Conductors Involved in Fire," *Journal National Institute of Justice*, pp. 1-105, 2012.
 34. N. Hussain, "Forensic Investigation for Inspecting Electrical Conductors Involved in Fire for Arc and Melt Beads," Thesis for Master of Science, Department of Fire Protection Engineering, University of Maryland, 2012.
 35. E. Buc, "Metallurgy and Fire Investigation," International Symposium on Fire Investigation Science and Technology, pp. 137-148, 2012.
 36. National Fire Protection Association, *921 Guide for Fire and Explosion Investigations*. NFPA, Quincy, MA, USA, 2017.
 37. J. Davis, Ed. *Metals Handbook Desk Edition*. ASM International, 1998.
 38. D. Levinson, "Copper Metallurgy as a Diagnostic Tool for Analysis of the Origin of Building Fires," *Fire Technology*, vol. 13, no. 3, pp. 211-222, 1977.
 39. ASM International, *Alloy Phase Diagrams (ASM Handbook)*. ASM International, 2016.
 40. *Standard Guide for Preparation of Metallographic Specimens, E3-11 (Reapproved 2017)*, ASTM, 2017.
 41. D. Gray, "Investigation of Electrical Fires," MSc in Fire Engineering Dissertation, University of Edinburgh, 1982.

Application of Matchmoving for Forensic Video Analysis with Recorded Event Data

By Richard M. Ziernicki, PhD, PE, DFE (NAFE 308F) and Ricky Nguyen, PE, DFE (NAFE 1223M)

Abstract

A fatal collision involving a pedestrian struck by a public train at a rail station located in a major U.S. metropolitan city was investigated. The train was equipped with an event data recorder that recorded valuable empirical data related to the collision, such as the train speed, braking, and acceleration inputs. However, the original digital version of the data was not available to analyze, and only a single screenshot of the data in an analog graph format was available. The subject train was equipped with multiple video cameras at various vantage points that recorded video footage of the collision. Using the process of “matchmoving” — and with the assistance of three-dimensional LiDAR scanning of the station and train — video footage was analyzed to spatially determine the location of the train in three-dimensional space. The process of matchmoving is an established scientific process used to calibrate a virtual camera to “match” the movement and optic properties of the real-world camera that captured the video. Further analysis was performed to determine the train’s kinematics (such as its speed and deceleration rates) leading up to the collision. The accuracy of the matchmoving analysis was then verified with the available event data.

Keywords

Train, pedestrian, matchmoving, LiDAR, 3D high-definition scanning, event data recorder, photogrammetry, accident reconstruction, forensic engineering

Introduction

Around midnight, a pedestrian on the passenger loading platform at a public rail station was waiting alone for a train to board. Due to medical issues, the pedestrian inadvertently fell onto the train tracks. The pedestrian laid on the tracks with minor movements from his arm for several minutes before a train arrived at the station, running over him. As a result of this collision, the pedestrian suffered fatal injuries. In deposition testimony, the train operator stated that during his arrival to the train station, he had observed a foreign object on the train track, but he was unable to tell this was a pedestrian until he got closer. He then testified that once he realized there was a pedestrian on the train tracks, he applied the emergency brakes to attempt to stop the train in an effort to avoid colliding with the pedestrian.

The train was equipped with an event data recorder (also commonly referred to as a “black box”), which recorded valuable digital data related to the incident, including the train’s speed, acceleration, and brake application. However, the data in its original format was no longer

available at the time of the investigation. The data was limited to a single screenshot of an analog graph. Furthermore, the screenshot of the graph had more than 10 minutes of data compressed and printed onto a single 8.5-inch (in.) by 11-in. PDF document (**Figure 1**).

The train was also equipped with several video cameras that recorded footage at the time of the incident, one of which was located at the train’s front car recording a forward view from the train (approximately from the viewpoint of the train operator). The camera recorded video footage at a rate of 5 frames per second (fps) and showed the train approaching the train station. As the train entered the station, a foreign object (determined to be the pedestrian who had fallen on the train tracks) could be observed. The footage then showed the train colliding with the pedestrian before coming to a complete stop (**Figures 2, 3, 4, and 5**).

The train operator testified that his training as well as his employer’s written policy required him to avoid colliding with any foreign object on the train tracks. He further

testified that the policy was put in place so that train operators do not assume the object could just be trash or debris — that it could actually be a dangerous object or a person instead.

The attorneys representing the estate of the pedestrian on the track theorized that the train operator should have been able to apply the emergency brakes sooner, avoiding the collision. However, the attorneys representing the

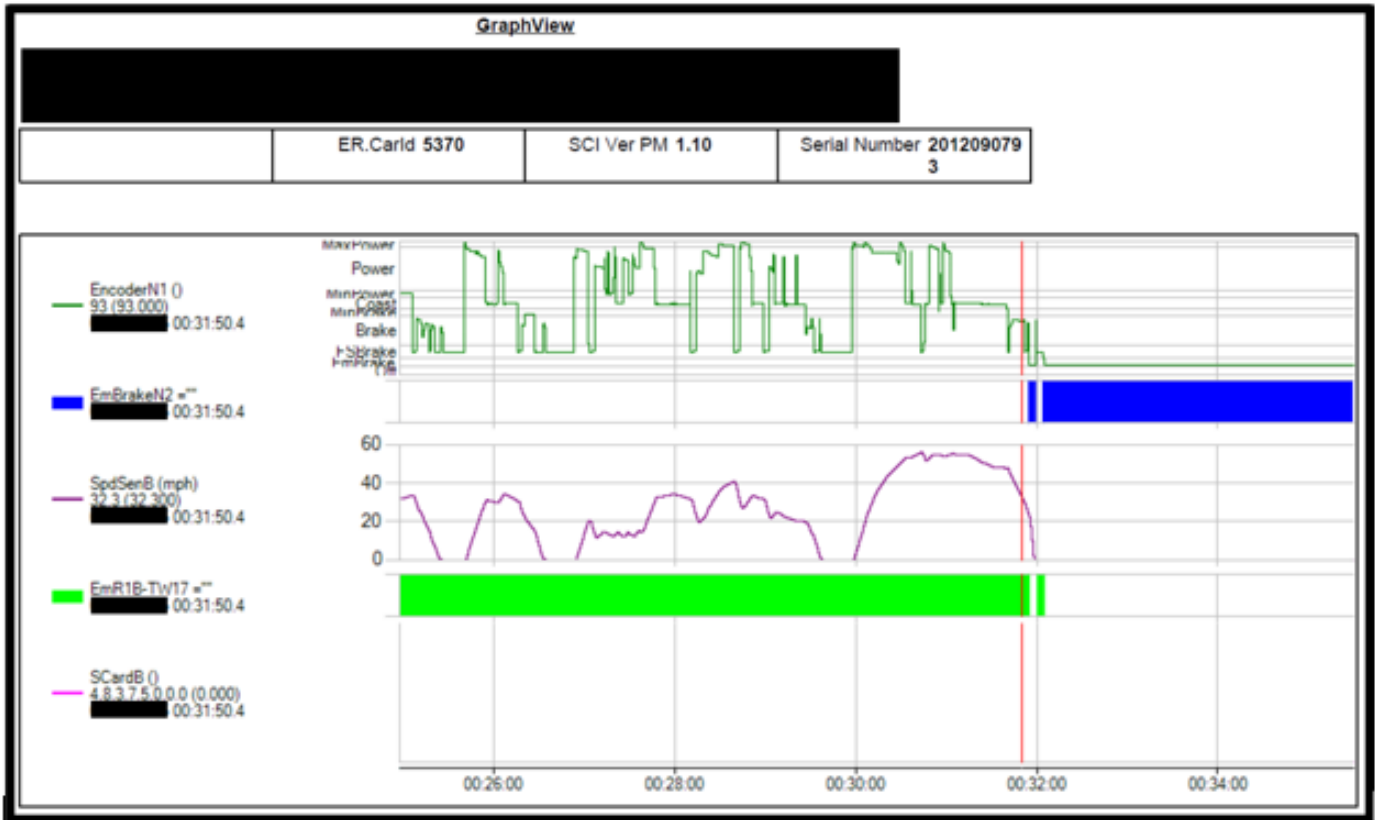


Figure 1

The original screenshot of the graphs that were generated from data recorded by the train’s event data recorder at the time of the incident. The graph data traces include the train’s speed profile (purple curve), the train’s acceleration/service brake input position (dark green curve and light green bar) and the application of the train’s emergency brakes (blue bar) as a function of time in minutes.

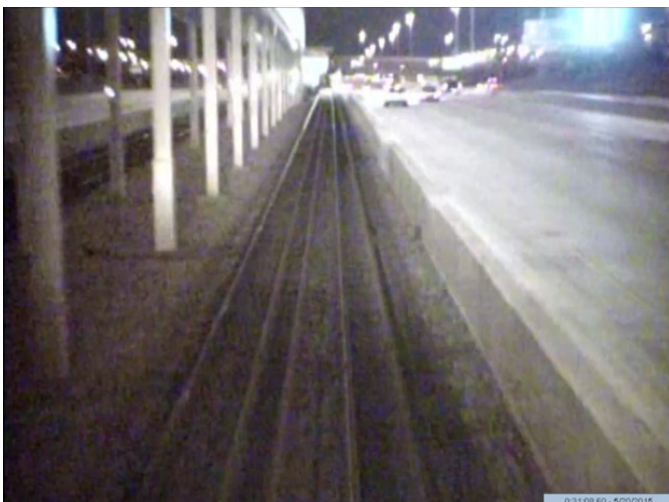


Figure 2

A screenshot from the footage recorded from the front camera of the train at the time of the incident, showing the train approaching the station.

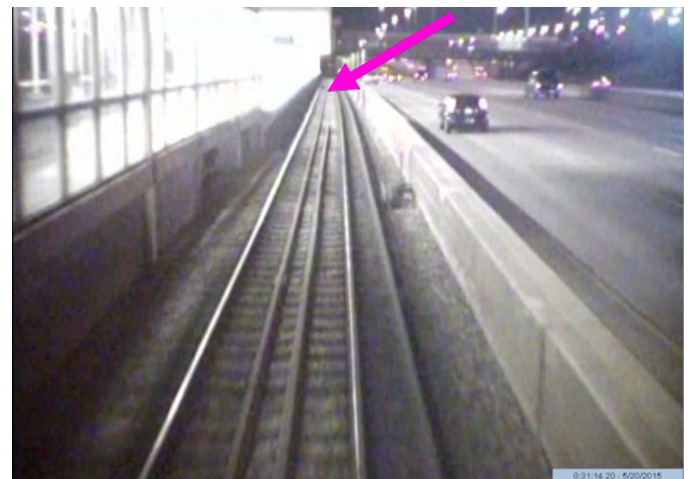


Figure 3

Another screenshot from the footage recorded from the front camera of the train at the time of the incident, showing the train approaching the station’s passenger loading platform. The magenta arrow was added to show the position of the pedestrian lying on the train tracks.



Figure 4

Another screenshot from the footage recorded from the front camera of the train at the time of the incident, showing the pedestrian lying on the train tracks. This was the last frame in which the pedestrian was visible before the train collided with him. The magenta arrow was added to show the position of the pedestrian lying on the train tracks.



Figure 5

Another screenshot from the footage recorded from the front camera of the train at the time of the incident, showing when the train came to a stop after colliding with the pedestrian.

train company and the train operator asserted the video and event data clearly showed that the operator did apply the emergency brakes in a timely manner to try and avoid the pedestrian — and that there was simply not enough time and distance to react and avoid an impact.

The authors were tasked with an engineering investigation and analysis of the incident to determine the kinematics of the train during the incident, including how fast the train was traveling when it entered the station, when the train's service brakes and emergency brakes

were applied, and when the emergency brakes would need to be engaged to avoid the impact.

The attorneys requested engineering assistance because the point of impact was not clearly known in the event data. In addition, the portion of the data that was of interest, which was approximately a 20-second window leading up to the collision, made up a very small portion of the available graph. Furthermore, the video footage that showed the collision between the train and pedestrian did not include relevant information, such as the train's speed or when its various braking systems were applied. In addition, the timestamp in the event data was offset and out of sync from the timestamp in the video.

Methodology and Analysis

Inspection of the incident site and exemplar train

In conducting the forensic investigation and analysis, the authors inspected an exemplar train car and the subject train station where the collision occurred (**Figure 6** and **Figure 7**). The inspection consisted of taking photographs and performing a high-definition three-dimensional laser scan of the train and the crash site with a high-definition 3D light detection and ranging (LiDAR) scanner. More than 300 million data points were scanned/collected for the exemplar train, and more than 2 billion data points were scanned/collected for the crash site.

Matchmoving Analysis of Video Footage

The photogrammetric process of matchmoving was performed to analyze the recorded footage from the forward-facing camera mounted on the front of the train which documented the subject incident. The process of



Figure 6

Photograph of the train station where the subject incident occurred. The station was inspected and 3D laser scanned. The laser scanner is shown in the foreground.



Figure 7

A photograph of the exemplar train car that was inspected and 3D laser scanned.

matchmoving is an established scientific process used to calibrate a virtual camera to “match” the movement and optic properties of the real-world camera that captured the video. In conjunction with the established technology of high-definition 3D laser scanning^{10,12,13}, the process can be used to virtually analyze the movement of objects (e.g., vehicles, pedestrians, etc.) visible in the video captured

by moving cameras with high precision. The above process has been peer reviewed and accepted in the forensic engineering industry^{1,2,3}. In summary, using principles and techniques based upon photogrammetry^{4,5,6,7,8,9,11}, each frame of the video can be analyzed to determine the object’s position, path, average speed, and average acceleration between video frames.

For this investigation, a 3D point cloud model of the train station, passenger platform, and pedestrian bridge was generated based on 3D high-definition scan data collected during the inspection of the train station. The point cloud model was used to track the train’s forward-facing camera through its approach to the train passenger platform and impact with the pedestrian.

The author’s firm used widely and publicly available software (Syntheyes) to perform the matchmoving process. First, two-dimensional points (or features) were identified and tracked through multiple frames of the video. Each feature represents a specific point on the surface of some fixed objects of the train station (i.e., structural columns, signs, passenger platform corners, etc.). Each tracked feature was then assigned and constrained to the feature’s corresponding three-dimensional coordinates (x, y, z) as defined by the train platform point cloud (**Figure 8**).



Figure 8

Screenshot showing a sample of the three-dimensional (x, y, z) coordinate data from the train station point cloud model used to constrain the corresponding two-dimensional trackers.

Using the two-dimensional trackers and their given three-dimensional x, y, z coordinate constraints, the software mathematically solved for (or “calibrated”) a virtual camera (relative to the train platform point cloud) that emulates the lens characteristics and movement of the real-world camera used to record the footage.

With the virtually calibrated camera and the train station point cloud model imported into the 3ds Max software by Autodesk, the authors were able to view the original footage through the virtual camera and track the position of the pedestrian on the tracks. This position, along with the movement of the camera, allowed the authors to determine the train’s movement and distance over time, as it approached the passenger platform to the point of impact and to the train’s resting position (**Figure 9** and **Figure 10**).

Since the framerate of the video was known to be 5



Figure 9

The video footage (center and red box) overlaid onto the 3D point cloud model of the train station, showing how the footage matches up with reference features, such as the station’s structural columns, signs, passenger platform corners, and the barrier separating the train from the road highway.

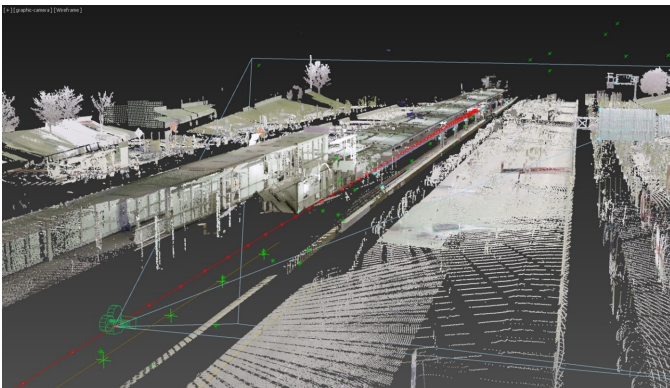


Figure 10

Screenshot from the computer software showing the path (red line) of the camera (green camera icon) mounted on the train in the 3D point cloud model of the train station, determined through the process of matchmoving.

fps, the train’s average speed between each video frame was then determined based on the matched positions of the train at each frame and the frame rate of the video with the below calculation:

$$S = \frac{\sqrt{(\Delta X)^2 + (\Delta Y)^2 + (\Delta Z)^2}}{\Delta t}$$

Where:

S = Speed of the train for that video frame

$\Delta X, \Delta Y, \Delta Z$ = The train’s change in distance between the current frame and the previous frame in the three-dimensional space (X, Y, Z).

Δt = the elapsed time between video frames or the inverse of the video’s framerate.

The speed profile of the train at the time of the incident was then graphed as a function of time (**Figure 11**).

To verify the train’s speed profile that the authors determined through the matchmoving process, the speed profile graph from the train’s event data recorder was transformed by scaling and zooming in so that the time and speed scales were the same (**Figure 12**). The two independent speed profiles were then overlaid onto each other so that the profiles could be compared (**Figure 13**). The comparison of the speed profiles showed the train’s speed (determined through matchmoving) closely matched the speed recorded by its event data recorder. The above analysis and verification with event data determines that the matchmoving process when used with recorded video footage can analyze the movement of the train with accuracy, resulting in a reliable method to determine the train’s

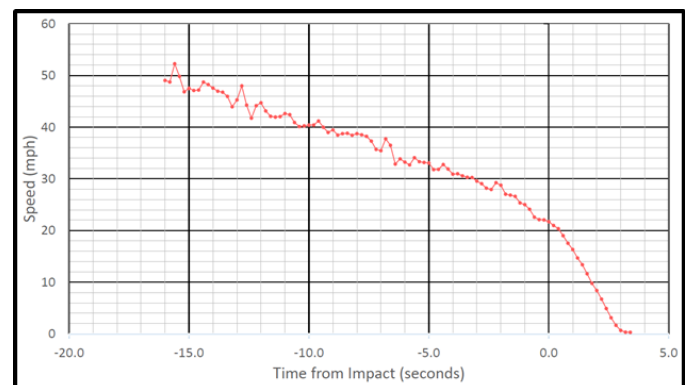


Figure 11

The train’s speed profile determined through matchmoving analysis. Impact with the pedestrian occurred at “time from impact” = 0 seconds.

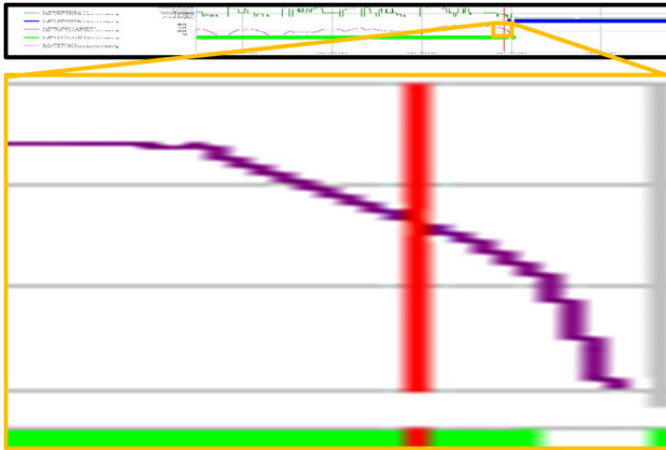


Figure 12

The graph generated by data recorded from the train’s event data recorder scaled to match the speed and time scale of **Figure 11** (black boxed). The speed profile graph zoomed in to the portion of interest and to compare with **Figure 11** (orange box). It should be noted that the speed profile appears distorted/blurry because the graph was zoomed into and scaled so that the time and speed scales of the speed profiles could be matched up.

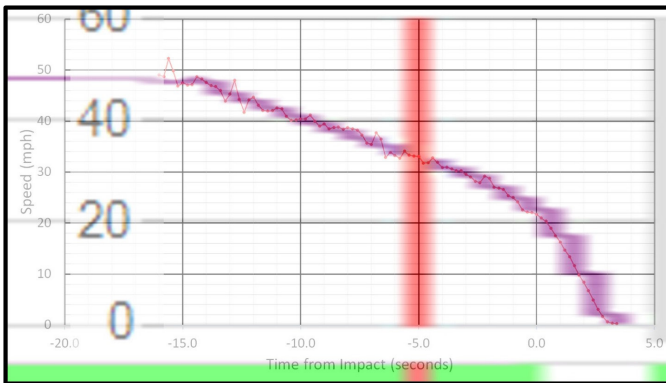


Figure 13

The train’s speed profile determined through the matchmoving analysis (**Figure 11**) overlaid onto the speed profile generated by the train’s event data recorder (**Figure 12**).

kinematics.

Train Braking Analysis

The train was equipped with three independent braking systems. Based on the train’s specifications provided by the train operating company, the following is a description of each of the braking systems and their maximum specified deceleration rates:

1. *Electric brake* — The train is equipped with electric motors. Depending on the position of the throttle control, the polarity to the motors can provide acceleration or deceleration to the train. The electric brake acts as the train’s service brakes during

normal operation and has a specified maximum deceleration rate of 2.8 miles per hour per second (or 0.13 g).

2. *Friction brake* — Similar to disc brakes seen on automobiles, the friction brake has a specified maximum deceleration rate of 2.5 miles per hour per second (or 0.11 g).
3. *Track brake* — Magnetically decelerating the train with an electromagnet that acts on the train’s rails, the track brake has a specified maximum deceleration rate of 1.0 miles per hour per second (or 0.046 g).

The train operator can also activate the train’s emergency braking system, which simply applies all three of the train’s braking system simultaneously. The train operating company specified the train’s maximum theoretical deceleration rate was the summation of the deceleration rates for each individual braking system. Therefore, during emergency braking, the train’s effective specified maximum theoretical deceleration rate was 6.3 miles per hour per second (or 0.29 g).

From the train’s speed profile determined through the matchmoving process, the train’s deceleration rate during the incident was determined with the following calculation:

$$a = \frac{\Delta S}{\Delta t}$$

Where:

a = acceleration of the train in a specific time frame (negative value is deceleration)

ΔS = the change in the train’s speed in a specific time frame

Δt = the elapsed time between a specific time frame

From the above analysis, the authors determined that as the train approached the passenger platform, the train decelerated at an average rate of approximately 1.81 miles per hour per second (or 0.082 g). Since the deceleration rate was about 64 percent of the specified maximum deceleration rate of 2.8 miles per hour per second (or 0.13 g) for the service brakes, the train was decelerating at a rate below the maximum rate that the service brakes could provide. This was consistent with the train gradually slowing

down to a planned stop at the station.

At approximately 0.8 seconds before the train collided with the pedestrian, the train decelerated at a much higher rate until it was brought to a complete stop at approximately 3.4 seconds (or 53 feet) after impact. The deceleration rate in the above time frame was approximately 5.7 miles per hour per second (or 0.26 g), which is well above the maximum rate the service brakes could provide and just below the emergency brake's specified maximum theoretical deceleration rate of 6.3 miles per hour per second (or 0.29 g). Therefore, the above analysis showed the emergency brakes were not engaged until approximately 0.8 seconds before the train collided with the pedestrian — or when the train was approximately 26 ft from the pedestrian (see **Figure 14**).

As previously discussed, the train's event data recorder recorded the train's service brake and emergency brake application at the time of the incident. Like the speed profile recorded by the event data recorder, the brake input data was used to verify the deceleration calculations above. The braking input graphs had line and bar traces that showed when each of the braking systems were applied as a function of time. Also like the speed profile, the

braking input traces were overlaid onto the train's speed profile determined through the matchmoving process, and the graphs were scaled until the time scales were the same (**Figure 15** and **Figure 16**). The event data recorder

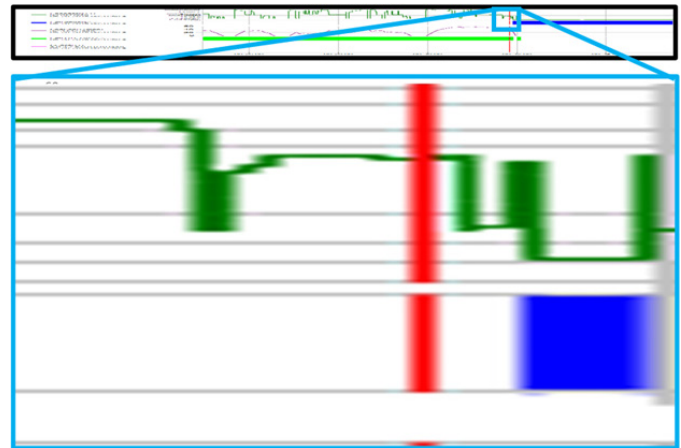


Figure 15

The graph generated by data recorded from the train's event data recorder scaled to match the time scale of **Figure 11** (black box). The service and emergency braking graph zoomed in to the portion of interest and to compare with **Figure 11** (blue box). The braking input traces appear distorted/blurry because the original graph was low resolution, and the graph was zoomed into and scaled so the time and speed scales of the speed profiles could be matched up.

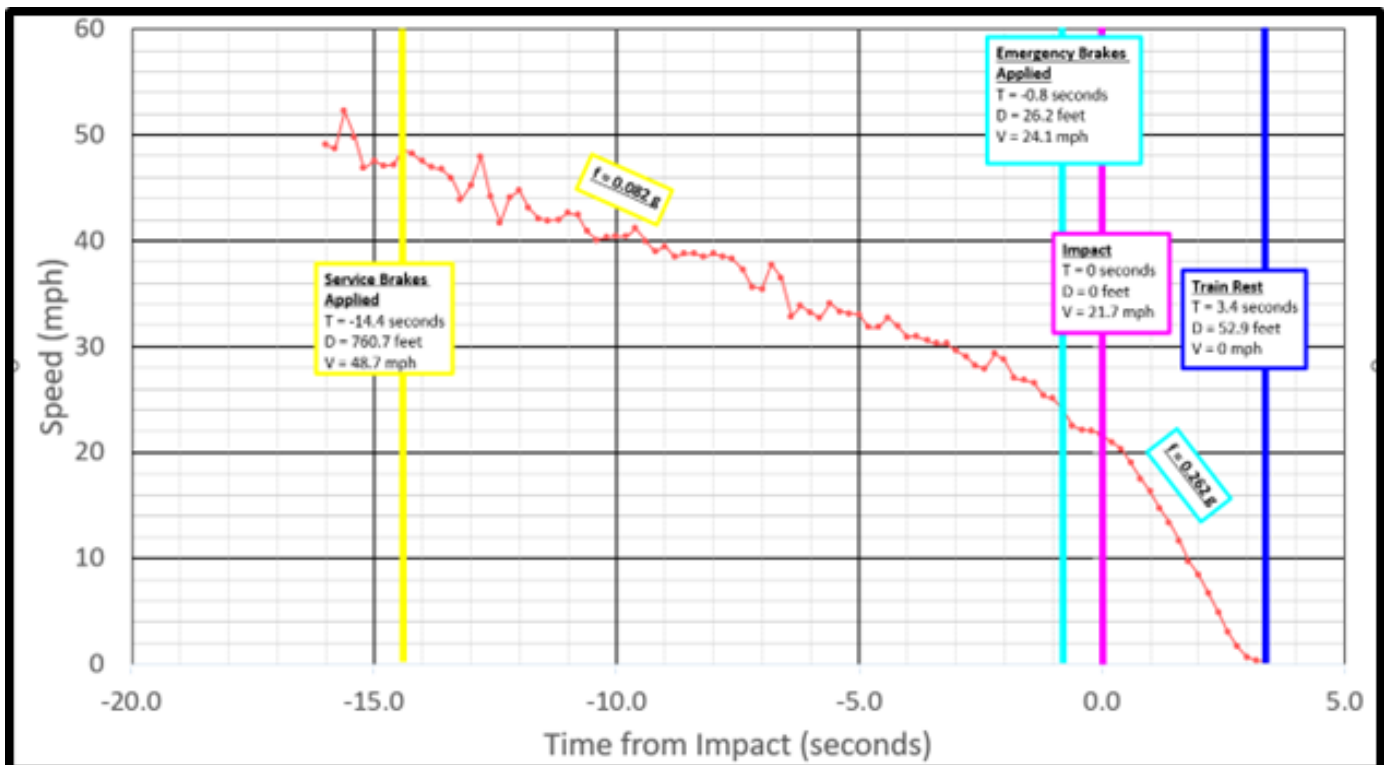


Figure 14

The train's speed profile determined through the matchmoving analysis with callouts showing when the train's service and emergency brakes were engaged in relation to the point of impact with the pedestrian.

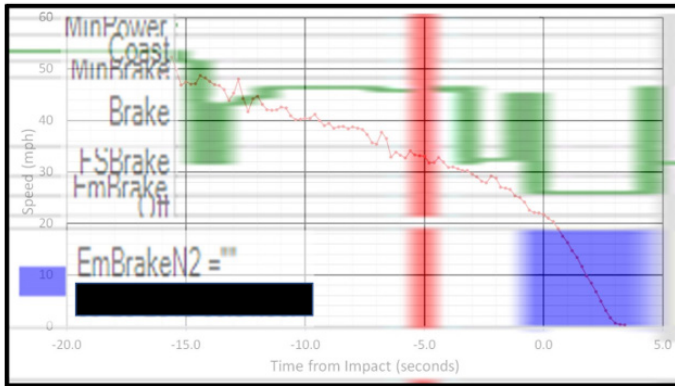


Figure 16

The speed profile determined through the matchmoving analysis (Figure 11) overlaid onto the service and emergency braking input traces generated by the train’s event data recorder (Figure 15). The train’s service brake input indicated with the dark green line and the application of the train’s emergency brakes indicated with the blue bar.

verified and confirmed the authors’ analysis, which showed the train’s service brakes were applied as the train approached the station, but the emergency brakes did not engage until approximately 0.8 seconds before the train collided with the pedestrian.

Further analysis was performed to determine the points in time that the emergency brakes could be engaged to bring the train to a complete stop and avoid colliding with the pedestrian. Absent of perception-reaction time,

the following formula was used to determine the distance the train would need to stop with the emergency brakes engaged based on a given speed:

$$d_{\text{brake}} = \frac{S^2}{(2 * f * g)}$$

Where:

d_{brake} = the distance it takes for the train to come to a complete stop

S = Speed of the train at the given time

f = the train’s emergency braking deceleration rate, 0.26

g = gravitational constant

The calculation was performed at every video frame to determine the distance the train would need to decelerate to a stop and to avoid impacting the pedestrian. Based on the above calculations, the authors determined the emergency brakes would need to engage when the train was at least 3.0 seconds from impact (or at least 114 ft from the pedestrian) to avoid the impact. The train was traveling approximately 30 mph at this time (Figure 17).

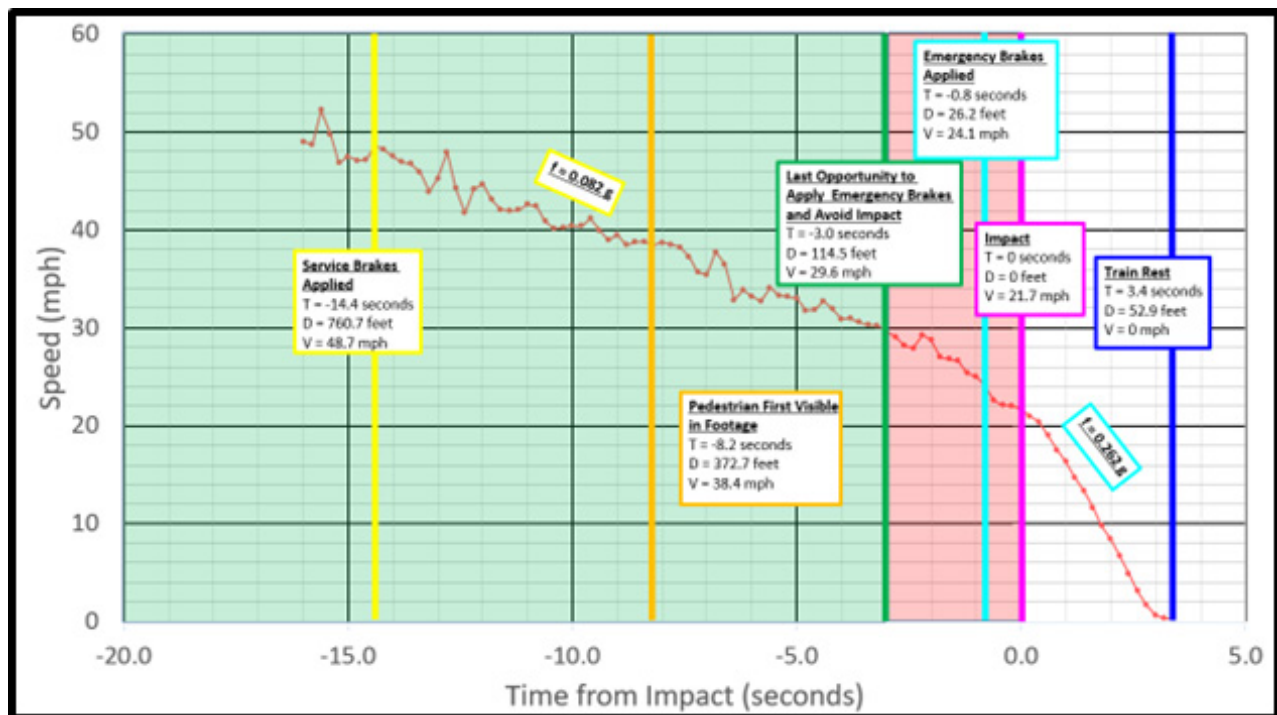


Figure 17

The train’s speed profile determined through the matchmoving analysis with callouts showing when the pedestrian was first visible in the footage and the points in time the impact was avoidable (green) and unavoidable (red) had the emergency brakes been engaged at that time.

The authors then overlaid the train's speed, time to impact, distance to impact, type of braking system applied, and whether the collision would have been avoidable had the emergency brakes been engaged sooner at each frame in the video. Below are screenshots showing when the emergency brakes were applied and what points in the footage the collision was avoidable had the emergency brakes been engaged sooner (**Figure 18**).

Discussion and Conclusions

This paper demonstrates that using video footage from moving objects with sufficient visual detail for identifying reference points/features, allows for the determination of positions, speeds, and acceleration rates of the moving object and stationary objects using the photogrammetric method of matchmoving. In addition, through verification and confirmation with data by the train's event data recorder, the paper further validates that the process of matchmoving is a highly accurate and reliable methodology in the field of accident reconstruction and forensic engineering.

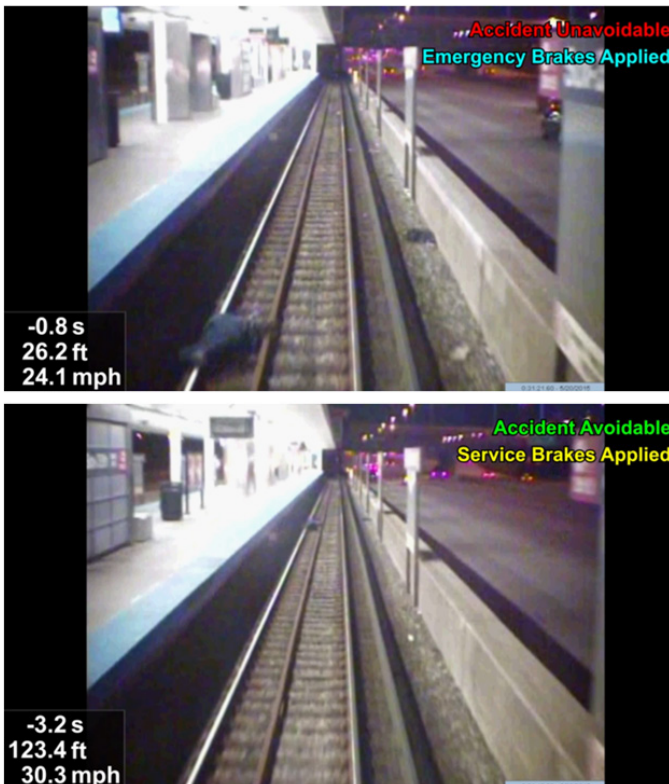


Figure 18

Screenshots of footage recorded from the front of the train at the time of the incident with the train's speed, time to impact, distance to impact, which braking system was applied, and whether the collision would have been avoidable at that moment in time. These screenshots show the moment that the operator applied the emergency brakes during the incident (top) and when the collision was avoidable — had the emergency brakes engaged sooner (bottom).

The above methodology is not limited to analyzing the kinematics of trains and pedestrians; it can be applied to other moving objects, such as automobiles, motorcycles, bicycles, aircrafts, and marine vehicles. Providing valuable data and information for triers of fact, this process can be especially useful in reconstructing accidents when a video of the incident is available but there is a lack of physical evidence or when recorded event data is limited or no longer available/accessible.

References

1. R.M Ziernicki, et al., "Forensic Engineering Application of the Matchmoving Process," *Journal of the National Academy of Forensic Engineers*, vol. 35, no. 2, December 2018.
2. R.M. Ziernicki, et al., "The Application of Matchmoving for Forensic Video Analysis of a Fatal Sprint Car Accident: Part 1." *Journal of the National Academy of Forensic Engineers*, vol. 38, no. 1, June 2021.
3. R.M. Ziernicki, et al., "The Application of Matchmoving for Forensic Video Analysis of a Fatal Sprint Car Accident: Part 2." *Journal of the National Academy of Forensic Engineers*. vol. 38, no. 1, June 2021.
4. S. Fenton and R. Kerr, "Accident Scene Diagramming Using New Photogrammetric Technique," SAE International Congress and Exposition, SAE Technical Paper no. 970944, 1997.
5. S. Fenton, et al., "Determining Crash Data Using Camera Matching Photogrammetric Technique," SAE Automotive and Technology Congress and Exposition, SAE Technical Paper no. 2001-01-3313, 2001.
6. W. Neale, et al., "A Video Tracking Photogrammetry Technique to Survey Roadways for Accident Reconstruction," SAE 2004 World Congress and Exhibition, SAE Technical Paper no. 2004-01-1221, 2004.
7. R.M. Ziernicki and D. Danaher, "Forensic Engineering Use of Computer Animations and Graphics," *Journal of the National Academy of Forensic Engineers*, vol. 32, no. 2, 2006.
8. R.M. Ziernicki, et al., "Forensic Engineering

- Evaluation of Physical Evidence in Accident Reconstruction,” *Journal of the National Academy of Forensic Engineers*, vol. 24, no. 2, 2007.
9. T. Dobbert, *Matchmoving - The Invisible Art of Camera Tracking*, 2nd ed., Indianapolis, Indiana: John Wiley & Sons, Inc., 2012.
 10. D. Tandy et al. “Benefits and Methodology for Dimensioning a Vehicle Using a 3D Scanner for Accident Reconstruction Purposes,” SAE 2012 World Congress and Exhibition, SAE Technical Paper no. 2012-01-0617, 2012.
 11. R.M. Ziernicki et al., “Forensic Engineering Usage of Surveillance Video in Accident Reconstruction,” *Journal of the National Academy of Forensic Engineers*, vol. 31, no. 2, 2014.
 12. C. Coleman et al., “Applying Camera Matching Methods to Laser Scanned Three-Dimensional Scene Data with Comparisons to Other Methods,” SAE 2015 World Congress and Exhibition, SAE Technical Paper no. 2015-01-1416, 2015.
 13. R. M. Ziernicki and A. Leiloglou, “Advanced Technologies Utilized in the Reconstruction of an Officer-Involved Shooting Incident,” *Journal of the National Academy of Forensic Engineers*, vol. 34, no. 2, 2017.

Nondestructive Forensic Investigation of a Scissor Lift Fatality

By Michael Stichter, PhD, PE, DFE (NAFE 1162M), Zachary Ball, PhD, PE, Carl Jewell, PhD, and Wade Lanning, PhD

Abstract

After a worker was found fatally pinned between the top rail of a scissor lift and an overhead beam, rescue attempts were frustrated by unresponsive lift controls. In the investigation of this fatal accident, certain lift controls did not function or functioned intermittently. The intermittent nature of the malfunction indicated that the evidence was sensitive — likely to be disturbed if the device was disassembled using typical destructive techniques. Therefore, nondestructive techniques were required. This study discusses how X-ray imaging, computed tomography (CT), electrical testing, and engineering analysis of the lift and control system were used to investigate the causes and contributing factors of this fatal accident without disturbing sensitive evidence.

Keywords

Nondestructive, failure analysis, accident investigation, exemplar testing, scissor lift, control panel, lift controls, electrical, damage, safety devices, forensic engineering

Introduction and Background

Two construction workers (the victim and his colleague) were welding steel plates to overhead beams in a permit-required confined space (**Figure 1**). In order to reach the overhead beams, each worker was provided with a rented scissor lift. The workers were taking turns performing different tasks. One would weld while the other acted as “fire watch” and/or repositioned their lift to

prepare for their turn at welding. No other workers were present in the confined space.

The accident occurred while the victim’s colleague was welding; he did not directly observe the accident. While the colleague was welding, the victim was expected to be on fire watch and/or repositioning his lift. After completing a series of welds, the colleague noticed that the victim’s lift was not moving. Further investigation revealed the victim was unresponsive and appeared to be pinned between the lift and an overhead beam. The colleague lowered his lift and ran to get help.

After a brief delay in getting access to the confined space, other construction workers and medical responders arrived and attempted to use the base controls on the scissor lift to lower the platform and rescue the victim. Unfortunately, the lift did not lower in response to the rescuers’ attempts to use the base controls. The colleague got back in the other scissor lift, raised it to reach the victim, and found the victim with his head pinned between the top rail of the lift and an overhead beam and his hand pushing against the upper control console joystick. The colleague moved the victim’s hand off of the joystick; then he operated the controls of both scissor lifts simultaneously to lower them to the ground. The victim died of severe crushing injuries to the head.



Figure 1

Photo from the incident scene showing the subject scissor lift (red arrow), the other lift used in rescuing the victim, and the overhead beams involved in entrapping the victim.

The authors and other investigators were tasked with evaluating the incident and determining how the victim became entrapped and why the subject lift's base controls were unresponsive during rescue attempts.

Post-Accident Interview

Investigators conducted interviews of witnesses. The victim's colleague was able to describe the position of the victim's body prior to freeing him from entrapment between the lift and the beam. The colleague described the position of the victim as if he was trying to look over the edge of the platform at the wheels of his scissor lift. When the colleague used his own lift to reach the victim, he found one of the victim's hands pressing the joystick on the upper control console in the forward/raise direction. The upper control console was positioned on the top rail of the lift platform (**Figure 2**). The colleague moved the victim's hand off of the controls; then he used the controls on both lifts simultaneously to lower them.

The joystick is designed to either make the lift platform raise/lower or the chassis move forward/backward, depending on the position of a selector switch. The colleague suggested that, while investigating control malfunctions, the victim had mistakenly attempted to move the lift forward — not realizing that the selector switch was in the raise/lower position, which resulted in the lift raising unexpectedly. The colleague also reported that, prior to the accident, the upper lift controls would sometimes “hesitate” or exhibit other malfunctions.



Figure 2

Photo from the accident scene, showing the control console of the subject scissor lift mounted on the top rail. The rail of a second scissor lift, used in an attempt to rescue the victim, is in the foreground. The top rail of the subject scissor lift is bent downward from the force exerted between the scissor lift rail, the victim, and an overhead beam.

Initial Inspection and Functional Testing of the Subject Lift

After the incident, the subject scissor lift was removed from the site, stored in a warehouse, and then examined/ tested by investigators several months later. One of the upper rails was bent downward (**Figure 3**), indicating the contact point between the rail, the victim's body, and the overhead beam. Witness testimony and maintenance records indicated that the rail was not bent until after the incident. The force exerted by the lift during the incident bent the top rail and caused the victim's injuries.

The incident unit was an electric-powered machine with a bay of four 6V batteries wired in series, which had to be replaced prior to testing (due to the old batteries having run down while in storage). Replacing the batteries was the only modification performed prior to the functional testing, which was deemed appropriate. This was due to the fact that the batteries were very unlikely to be a direct or indirect cause of the incident because the lift was able to raise at the time of the incident — low or defective batteries would have provided an inability to raise that is contradictory to all of the available evidence.

The investigators began the functional testing of the subject lift by following the pre-start checklist provided in the manufacturer's manual, which is fairly standard across manufacturers. This checklist was chosen because it is designed to notify the user of any issues with the unit prior to operation. During pre-start functional tests, the lift's electric motor was found to have failed. The motor was replaced in order to complete the functional tests. The original motor was preserved, and later examination determined that the motor failure was due to corrosion of the brushes while it was in storage. At the time of the incident, the subject lift was able to raise with sufficient force to



Figure 3

Photo from inspection of the lift several months after the accident. The top rail was bent downward where the victim was entrapped between the rail and an overhead beam.

bend the top rail and fracture the victim's skull. The effect of the motor or battery failures discovered at later inspections would have made the lift unable to raise, preventing the incident. Thus, the condition of the motor could not have contributed to the incident.

After replacing the motor, functional testing continued. Investigators found that the control console was unable to cause the steering wheels to steer to the right, but could make the wheels steer left. Swapping the subject control console for an exemplar console corrected the problem, narrowing the cause of the issue to the subject control console. The subject control panel was preserved for nondestructive examination.

Investigators conducted electrical continuity tests between components of the control console and the pins in the console connector plug. As a result, they found a fault in the control for the lift to steer to the right. The steering switch itself functioned properly: it was normally open and connected its central pole to either the "steer right" or "steer left" terminals. The "steer left" terminal had normal electrical connectivity to a corresponding pin in the connector plug. However, there was no electrical connectivity between the terminal steering switch's "steer right" terminal and its pin in the connector plug. This testing narrowed the cause of the steering malfunction to a connectivity fault somewhere between the control console cable and its connector plug.

Photographs from the incident scene showed the subject scissor lift's front wheels were steered to the right (**Figure 4**). At the time of the accident, the lift was able to steer to the right. However, during functional testing, the incident control box was unable to steer the wheels to the right. This indicated an intermittent malfunction, of the lift's steering mechanism. An intermittent malfunction was consistent with the victim's colleague referring to "hesitation" and other (non-specific) control malfunctions prior to the incident.

As described earlier, rescuers claimed to have attempted to lower the scissor lift using the base controls, but the lift did not respond. Ultimately, the colleague used another lift to reach the victim and found him pinned against the control lever and platform rail with his right hand pressing the lever in the forward/raise position. Investigators found that the manufacturer of the subject lift issued a service bulletin approximately four years after the subject incident to scissor lift dealers describing a design flaw in the model and serial number of scissor lift involved in the incident.



Figure 4

Photograph of the incident scene taken shortly after the incident, showing the subject lift's wheels turned to the right.

When the upper controls were held in the UP position, the flaw made the lower controls unable to lower the platform. This design defect explained why rescuers were unable to use the lower controls to rescue the trapped worker.

Rescuers claimed to have attempted to use the mechanical emergency lowering valve to lower the platform when it was stuck in the raised position, but were unable to get the platform to come down. In functional testing, investigators did not find any fault or malfunction with the emergency lowering valve.

As far as investigators were able to determine, the rescuers were unfamiliar with the lift's emergency lowering procedure. Before the emergency lowering valve could be used, a holding valve manual override knob on the lift cylinder had to be engaged. In interviews, rescuers did not demonstrate awareness of the holding valve manual override. Most likely, the rescuers failed to engage the holding valve manual override, which is why the emergency lowering valve did not cause the platform to come down. Rescuers did not attempt other means of lowering the platform, such as relieving pressure in the cylinder. Similarly, after initial failed attempts to use the lower controls to lower the platform, rescuers did not use the lower controls; instead they used the upper controls to lower the platform and free the trapped worker.

Investigators disagreed on how to proceed with investigation of the lack of electrical continuity found between

control console and the pins in the connector plug. Some investigators wanted to proceed with destructive disassembly; others were concerned about preservation of the condition of the evidence and wanted to further document the condition of the plug and cord before risking disturbing evidence. The decision was made to not disassemble any additional components prior to the completion of 2D X-ray radiographs and CT scans.

Nondestructive examination methods were critical because the position of any loose or damaged conductors could be easily disturbed and raise questions about whether any faulty connections were the result of the disassembly process. The presence of intermittent electrical connections was indicated by witness testimony and the discrepancy in steering function observed between functional testing and scene photographs. However, the cause of the intermittent connections might be difficult to preserve while disassembling the components.

Nondestructive Radiography of the Control Console

Investigators performed nondestructive 2D X-ray radiography of the subject scissor lift platform control console. In the 2D X-ray radiographs (Figure 5), some of the wires in the cable connector appeared off-center relative to the pins, suggesting that they were not fully inserted into their terminals.

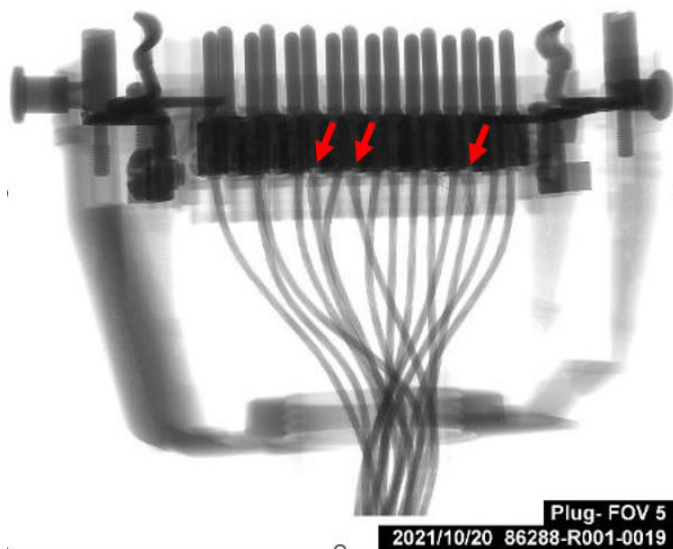


Figure 5

2D X-ray radiographs of the platform control console cable connector. Some of the wires appeared off-center relative to the pins, suggesting possible loose or detached connections. Further radiography was required to resolve the positions of the wires and identify which control functions were affected.

Investigators ordered a nondestructive 3D CT scan of the platform control console cable connector in order to better resolve the locations of the wire terminations in three dimensions. In the CT scans of the cable connector, the wires behind pins number 1 through 8 appeared to be fully inserted into the pin screw terminals (shown, but not labeled, in Figure 6 and Figure 7). However, the wires behind pins 10, 11, and 15 were not secured in the pin screw terminals at all — they were either free-floating or resting against the outside of the terminals (Figure 6 and Figure 7). Pins 12, 13, and 14 were partially withdrawn

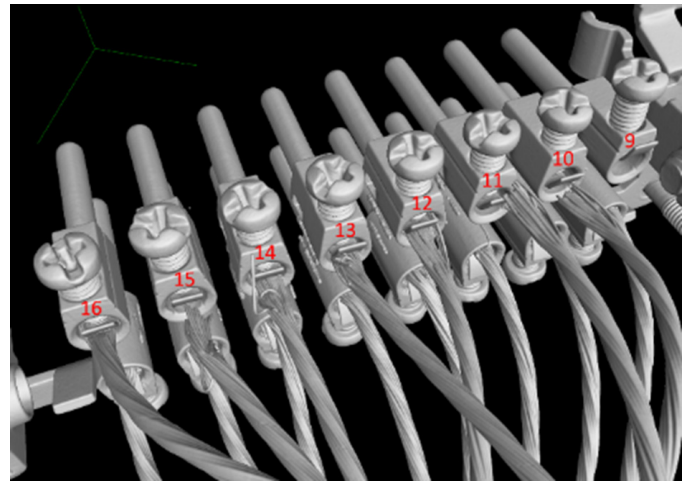


Figure 6

Top view of 3D CT scan of the subject platform control console cable connector. Numbers in red have been added to identify individual pins. Pins 1 through 8 (not numbered, located below pins 9 through 16 in this view) appeared fully secured within the screw terminals. Pins 10 to 15 were loose and withdrawn from the screw terminals. Pin 9 was left empty and had no corresponding wire.

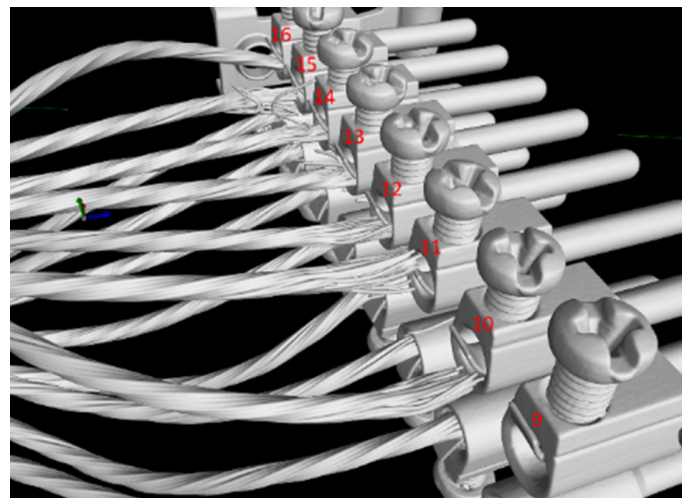


Figure 7

Side view of a 3D CT scan of the subject platform control console cable connector. Numbers in red have been added to identify individual pins. Pins 10 through 15 exhibited varying degrees of being withdrawn from the screw terminals.

from their screw terminals. Out of pins 9 through 16 of the cable connector, only the wires behind pins 14 and 16 appeared fully inserted into and secured within the screw terminal. Pin 9 was not used (by design).

A slice of the 3D CT scan was used to measure the heights of the screws (i.e., how far they were tightened down) as shown in **Figure 8**. The threaded depth of the screw is directly correlated to clamping force of the wire as the screws for each wire connection were all the same size, and the wires were all the same gauge. The largest gap was the unoccupied pin 9 (measuring 3.4 mm between the top of the screw terminal and the bottom of the head of the screw). The next largest gaps were pins 15, 10, and 11 (measuring 2.31 mm, 2.28 mm, and 2.20 mm, respectively).

The reduced clamping force in the affected screw terminals would have made it easier for the wire to be pulled out from the terminal. Additionally, pin 14 was still partially inserted into the terminal, even though pin 13 and pin 15 on either side of it were more withdrawn from their respective terminals (**Figure 8**). If the sole cause of the withdrawal of the wires from the terminals was an excessive force, then one wire would not be expected to remain connected while the wires on either side failed. The fact that only some of the wires were withdrawn from the terminals indicates that those wires were not as firmly secured as the others in the connector.

Electrical connectors are typically designed with “strain relief” features that provide a mechanical connection between the cable and the connector. In this case, the two primary forms of strain relief were the “cable gland”-style connector that gripped the exterior of the cable as it entered the connector and the screw terminals that clamped



Figure 8

Slice of a 3D CT scan of the subject platform control console cable connector with threaded depth of the screws marked. Pins 1 through 8 had relatively tightly connected crew terminals. Pins 10 through 15 had relatively loose screw terminals with partially or fully withdrawn wires. The distance labels also correspond to the pin numbers.

the ends of the stranded wires in place. Cable glands (like those in the subject plug) grip the exterior of the cable insulation and transfer stress from the insulation to the body of the connector plug. Screw terminals grip the ends of the wire, forming a mechanical link from the wire to the plug pins. After nondestructive radiography of the console plug, the cable gland connector was disassembled, revealing evidence that the cable had been pulled through the cable gland (**Figure 9**).

Some, but not all, of the wires inside the connector in the subject platform control console pulled out of the screw terminals used in the cable connector (**Figure 6** and **Figure 7**). The screw terminals in pins 10, 11, and 15 had wires that withdrew completely, and pins 12, 13, and 14 were partially withdrawn. These pins did not provide adequate strain relief to hold their wires in place, but the other screw terminals successfully retained their wires. Pins 10 through 15 were not properly secured to the connector. If they were properly secured, then the connections between the cable and connector (the cable gland and the screw terminals) should have been stronger than the cable and its wires. When a properly secured connector fails, the cable and/or the wires fail rather than the strain relief. No such breakage or damage was visible in the 2D radiographs, CT scans, or physical inspection.

Each wire in the platform control console cable conveyed a different command from the platform control console to the lift. Investigators used wiring diagrams from the lift’s service and maintenance manual to identify the platform control console functions that were associated with the improperly secured wires found in the platform



Figure 9

After nondestructive radiography, the cable gland connector on the control console plug was disassembled. The cable exhibited evidence of tension on the cable, such as movement of the cable within the gland and a tear in the outer insulation.

control console connector. Pins 10 through 15 in the platform control console cable connector had wires that were not properly secured, and, as a result, were partially or fully withdrawn from the screw terminals connected to the pins (**Figure 6** and **Figure 7**).

The base controls were designed to override the platform control console in accordance with the requirements of ANSI/SAIA A92.6 (2006). The subject lift's override was accomplished by turning a key located at the base controls from a "platform control" position to a "base control" position. This would disable the platform controls and enable the base controls. However, due to an uncorrected design flaw, the platform control console was able to override the base controls if the platform control console joystick was in the up/forward position.

Since the wires to pins 10 through 15 were not properly connected to the screw terminals, the connection through those pins was interrupted, weak, or intermittent during operation of the lift. This affected a variety of signals sent from the platform control console to the lift, including:

- The speed with which the lift moved (raise/lower or forward/reverse) in response to the joystick (pin 12, withdrawn from terminal but still touching).
- The ability of the lift to move forward or up in response to the joystick controls (pin 10, withdrawn from terminal but still touching).
- Steering to the left (pin 14, partially inserted into terminal).
- Steering to the right (pin 15, fully withdrawn from terminal and not touching).
- Steering common, + voltage (pin 11, fully withdrawn from terminal but still touching).

Interruption of the connection on these pins would interfere with the operator's ability to control the lift from the platform control console and make the lift unpredictable and dangerous to operate. The console might work properly at times when the wires make contact, but malfunction when the wires were moved and would break contact with the terminals. This is consistent with statements that, prior to the accident, the lift controls would sometimes "hesitate" or malfunction.

Due to the intermittent nature of the connections, malfunctions could appear sporadically during inspections, functional tests, and use of the machine. For instance, the console could not steer to the right during functional testing because the wire to pin 15 was completely separated from its terminal, but the lift could still move forward because the wire to pin 10 was touching the terminal, even though it had been pulled loose. Because of the loose wires in the plug, important control console functions, including moving upward, movement speed, and turning right, would respond unpredictably. The steering malfunction is notable because, according to the colleague, the victim's body was positioned as if attempting to look over the edge of the platform down at the wheels. The victim may have been trying to look at the wheels in response to a steering problem.

Intermittent connections on the joystick pulse width modulation (PWM) output on cable connector pin 12 would have created a dangerous condition. PWM uses a series of digital pulses (i.e., a voltage that is either zero or maximum) that are processed in a microchip to achieve what is effectively an analog output (i.e., a voltage at a desired value between zero and maximum). The PWM output controlled how quickly the lift moved when either raising/lowering (by controlling a hydraulic proportional valve) or moving forward/backward (by controlling the drive system). An intermittent connection would interrupt and reconnect the signal to the speed control, causing the lift to move at unpredictable rates. The loose connection on pin 12 may have resulted in an unexpected rate of motion of the scissor lift's up/down movement and contributed to the victim being pinned against the ceiling beam.

These findings highlight the value of performing non-destructive testing prior to any disassembly of components when their condition is both sensitive and critical to the investigation. Had the connector been disassembled during the functional testing, the status of the wires prior to disassembly would have been suspect as it may have been hypothesized that they became loose during the disassembly. Even if great care was taken during disassembly, the CT scans and 2D radiographs were valuable in documenting the state of the evidence — establishing that the loose wiring connections were present prior to disassembly. Nondestructive radiography was key to gathering forensic information while preserving the evidence.

After radiography, the connector was subsequently disassembled for further inspection, and wiring diagrams were used to identify the controls affected by loose and broken connections found in the connector. After removal

of wires 1 through 8 from the cable terminal block by backing out each of the terminal screws, wires 10 through 15 were free without applying tension to the wires or backing out their respective screws (**Figure 10**).

Biomechanical Analysis of Injuries in the Subject Incident

The pattern of the victim's injuries and signs of external trauma indicated that he sustained a significant compressive force to his mandible and face¹¹. The primary mechanism for bilateral laminar fractures in the cervical spine is a compressive force applied during extension¹²⁻¹⁵. The mechanism of injury for the victim's multiple facial fractures involved blunt force trauma to the face. The bones of the face are more resistant to fracture in frontal impacts as opposed to lateral¹¹. The nasal bones are the most fragile bones of the face with reported tolerance levels for minor fractures as 25 to 75 pounds (lb)^{6,11}. The maxilla (140 to 445 lb) and zygomatic arch (208 to 475 lb) show greater tolerance than the nasal bones, while the mandible (upward of 425 lb) is capable of withstanding greater amounts of force¹¹. Given the pattern of injuries sustained by the victim, the sustained compressive force was most likely directed from the front as well as upward and laterally toward the left side of his face — most probably in excess of 400 lb.

Standards for Preventing Sustained Involuntary Operation (SIO) Accidents

Scissor lifts like the one involved in this case are one kind of mobile elevating work platform (MEWP), a machine for moving workers, tools, and materials to elevated

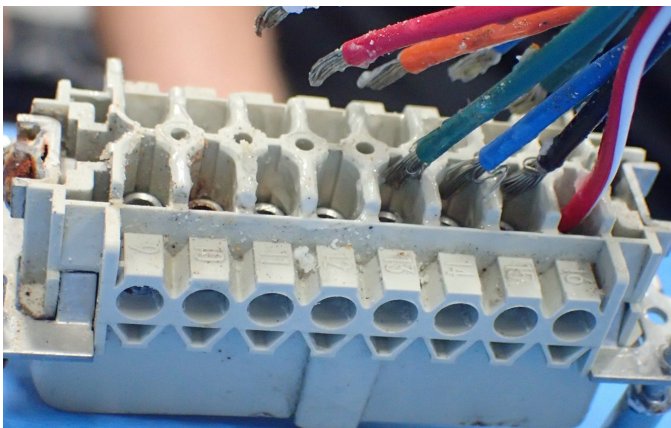


Figure 10

After nondestructive radioactivity, the cable terminal block was disassembled. The wires in terminals 1 through 8 were removed by backing out the screws on each terminal. Upon backing out the screw for terminal 8, the wires in terminal 10 through 15 slipped out of their respective terminals without applying tension to the wire or backing out the terminal screws.

working positions. The accident in this case was an entrapment accident, where an occupant became trapped between the machine and another object or structure. Entrapment accidents are one of the most common causes of reported fatalities involving MEWPs, along with falls from the platform, electrocutions, and equipment over-turns¹⁶.

This specific type of entrapment accident is referred to as sustained involuntary operation (SIO)¹⁷⁻¹⁹. In an SIO accident, the operator is pushed against the controls. The operator's body engages the controls, causing the MEWP to move, which further entraps the operator and jams the controls, creating a feedback loop. Since operators are unable to stop the motion of the lift or to free themselves, SIO accidents often make rescue of the operator difficult and result in fatal crushing and/or suffocation injuries.

The modern versions of standards, such as ANSI/SAIA A92.20 and ISO 16368, require design features such as overload protection, control console guards, and/or interlocks to interrupt the SIO feedback loop and reduce the likelihood and severity of SIO-type accidents²⁰⁻²³. However, the subject scissor lift did not have these features.

Multiple standards govern the design and safety features included on scissor lifts, including:

- ANSI/SAIA A92 series of standards (USA, Scaffolds and Access Industry Association)
- ISO 16368 standard (international)
- BS EN 280-1 (Europe / UK)
- CSA B354.6 (Canada)

The ANSI/SAIA A92 standards are the primary American standards for MEWPs, and major recent revisions include additional requirement for anti-SIO guarding. Historically, the ANSI/SAIA A92 standards were published as separate standards for different classifications of machine. These included ANSI/SAIA A92.3 (manually propelled lifts), A92.5 (boom lifts), A92.6 (self-propelled/scissor lifts), and A92.8 (vehicle-mounted bridge inspection/maintenance lifts). However, ANSI/SAIA published a new suite of A92 standards that combined the standards for different types of machines, instead dividing them by topic. ANSI/SAIA A92.20 (design, safety, and testing), A92.22 (safe use), and A92.24 (training) were issued in December 2018 to replace the machine-specific ANSI/

SAIA A92.3, A92.5, A92.6, and A92.8, which were withdrawn in June 2020²⁰. The stated reason²³ for the change was to combine the requirements for MEWPs with similar configurations/uses and to bring the ANSI/SAIA standards into closer agreement with existing international standards such as ISO 16368²².

The subject lift was manufactured in 2013 after international ISO 16368 standard began to explicitly require anti-SIO guarding but before ANSI/SAIA A92.20, which explicitly addressed anti-SIO guarding. Pre-A92.20 requirements were potentially relevant to preventing unintentional activation of controls but did not explicitly address the relevance of such guarding to prevent operator entrapment. ANSI/SAIA A92.6-2006, “American National Standard For Self-Propelled Elevating Work Platforms” has requirements for the controls.

The upper controls at the platform shall:

- 4.7.1(5) be protected against activation other than that initiated by the operator.
- 4.7.1(3) include a separate control that shall be continuously activated by the operator for upper directional controls to be operational, which can be released by the operator independently from the directional controls and render the upper controls inoperative when released.

The lower controls shall:

- 4.7.2(1) override upper controls for powered functions.
- 4.7.2(2) be provided for all powered functions except drive and steering.
- 4.7.2(4) be protected against activation other than that by the operator.

The newer ANSI/SAIA A92.20, “Design Calculations, Safety Requirements and Test Methods for Mobile Elevating Work Platforms,” which replaced A92.6, has more explicit requirements for anti-SIO design:

- 4.7.1.2. All controls shall be designed to protect against inadvertent operation (any operation other than that intentionally initiated by the operator). Hand-operated controls in the platform shall be protected against sustained involuntary opera-

tion. This protection should either prevent further movement of the machine in the direction of trapping or allow the operator to reverse or stop the trapping movement.

- 4.7.1.3. The upper controls shall include a separate device(s) that shall be continuously activated by the operator for directional controls to be operational. This device(s) shall be capable of being released by the operator independent of the directional controls. When released, this device(s) shall render the directional controls inoperative.
- 4.7.3.1. The control devices shall be located on the work platform. Duplicate controls for all powered functions of the extending structure shall be provided at the base or ground level, except for drive or steering, and shall override control devices situated on the work platform. Control devices shall be readily accessible to the operator. Control boxes not permanently attached shall have their normal location and orientation clearly marked.

The subject lift was manufactured in 2013 — before the ANSI/SAIA A92 standards were restructured and language was added explicitly addressing the SIO hazard. Thus, features that would have detected an SIO event and stopped or reversed motion of the lift were not yet required by the applicable American standard when the subject lift was made. However, the lift did not meet the existing A92.6 requirements related to inadvertent activation of the upper controls.

- The joystick on the upper controls extended above the small handle/guard (**Figure 2**), making it inadequately guarded against inadvertent activation as required by A92.6 Section 4.7.1(5).
- Although the joystick did have an activation switch, it was integrated into the joystick grip rather than being a separate control. It is debatable whether a button on the joystick satisfies A92.6 Section 4.7.1(3). In the incident, the victim did not release this control even after he was entrapped.
- Due to a flaw in the wiring design, the lower controls could not override the upper controls as required by A92.6 Section 4.7.2(1), which delayed rescue of the victim.

The international ISO 16368:2010(E) standard was

published in 2010 (prior to manufacture of the subject lift), and includes similar requirements to ASTM A92 for a separate activation control and protection of controls from inadvertent activation (Section 4.7.1) and for lower controls that override upper controls (Section 4.7.3). ISO 16368:2010(E) also requires that all signal-transmitting wiring be protected against damage (Section 4.11.3.2), which the exposed control cable of the subject lift (**Figure 2**) did not meet.

ISO 16368:2010(E) has additional requirements in Section 4.4.1.2 relevant to SIO incidents. All MEWPs are required to have a load-sensing system that activates when it detects a load between 100 percent and 120 percent of the machine's rated capacity. The system activates warning lights and an audible alarm. If the system is activated when the lift is raised 1 meter or 10 percent of its lift height (whichever is greater), then the system must prevent further upward motion once excessive load is detected. The standard notes that some means of moving the lift must still be available in order to release a trapped person²³. Section 4.4.1.2.1 of ANSI/SAIA A92.20 duplicates the requirements for a load-sensing system from ISO 16368²³. The subject lift did not have a load-sensing system.

Exemplar Testing of Alternative Design

Testing of an exemplar — a machine of identical design to the subject lift — allowed investigators to probe the design of the machine without risk of disturbing evidence. Even though testing can be potentially destructive to the exemplar, it is nondestructive with regard to the subject machine. The investigators also built and tested a technologically and economically feasible alternative design that would guard against the hazard of sustained involuntary operation (SIO) per the hierarchy of controls when designing a new product²⁴⁻²⁷. Before designing and adapting the alternative solution, testing on an exemplar was required to characterize the hazards associated with SIO in an unmodified exemplar scissor lift.

Investigators conducted testing of an exemplar lift matching the model and year of manufacture of the subject lift. They found that in the lowered position, the lift could exert in excess of 900 lb of force when raising the platform into contact with an overhead obstruction. Based on the test results at a 136.5-inch height, the lift could exert in excess of 2,100 lb of force when encountering an overhead obstruction. The increase in force was due to a change in the angle of the hydraulic actuators (lift cylinders) relative to the lift's "scissor" lift mechanism, which increased the magnitude of the moment (torque) created by the actuator

acting on the scissor mechanism.

Because the moment is proportional to the perpendicular component of force acting on a lever arm, the magnitude of the moment increased as the scissor mechanism raised, causing the hydraulic actuators to rotate from an oblique angle to a more perpendicular angle with the arms of the scissor mechanism, increasing the resulting moment (torque) on the scissor arms and the total force exerted by the lift. The lift reached maximum force approximately 1 second after encountering an obstruction. **Figure 11** shows the orientation of the lifting cylinder and the cylinders when in the fully lowered and a partially raised position. The lifting cylinder becomes more vertical as the scissor lift mechanism extends.

The forces measured in testing the exemplar violated relevant ANSI and ISO standards. The subject and exemplar had a rated capacity of 550 lb. ISO 16368:2010(E); 4.4.1.2 requires lifts to be equipped with a "load-sensing system" that would activate if a force above the rated load and before 120 percent of the rated load is exceeded. The lift involved in the accident did not have such a system.

Testing of an exemplar lift revealed that the type of lift involved in the accident could exert dangerous levels of force too quickly for the operator to react and save himself. In order to test whether a safety device could have prevented the accident, investigators designed and built a simple anti-SIO device that triggered the lift's emergency stop when a pressure sensor on the top rail was activated (**Figure 12**), motivated by the Design Order of Precedence²⁷. The device stopped the lift and reduced the force exerted on the overhead obstruction to 50 to 225 lb of force, depending on how far forward the control joystick was pressed. Note: The angle of the joystick controlled a pulse width modulation (PWM) signal that modulated the

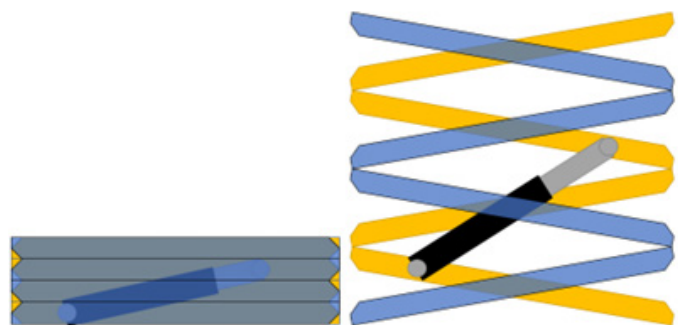


Figure 11

Sketch of a scissor lift mechanism in the lowered (left) and raised (right) position. Note that in the raised position, the lift cylinder and scissor arms rotate to be more nearly perpendicular to one another.

position of the hydraulic proportional valve — and thus the speed with which the platform moved upward or traveled forward or reverse.

The investigators determined that the absence of an anti-SIO device was a contributing factor to the accident — and that if such a device was equipped, it would have reduced the severity of the victim's injuries and increased his chances of survival. Although an anti-SIO device as described above is not explicitly required by the ANSI/SAIA standards, at the time of manufacture the testing showed, in conjunction with biomechanical analysis of the injuries sustained in the subject incident, that the upward force developed by the subject lift was well above the force necessary to cause fatal injuries to the head without this device and is limited to survivable forces when such a device is implemented.

Summary

A witness at the scene stated that the victim was positioned as though he was looking down at the wheels on the lift. This would be consistent with the victim reacting to a steering malfunction by observing the lift wheels while the victim manipulated various controls to see which responded.

Faulty connections in the upper control console plug would result in unpredictable changes in the speed of the lift's motion in response to the joystick. It is likely that the accident was the result of the lift moving upward faster than expected, pinning the victim between the lift and an overhead beam. The victim's body was trapped such that it pushed the joystick forward, causing the lift to continue to

move upward and resulting in SIO of the lift controls and fatal injuries to the victim. The lift lacked control guarding against inadvertent activation that would reduce the likelihood of trapping the operator in an SIO feedback loop.

A design flaw in the lift's wiring prevented the lower controls from overriding the upper controls, as required by ISO and ANSI standards applicable at the time the lift was manufactured. The lift also lacked overload protection features required by ISO and later ANSI standards. Testing of an exemplar lift found that a raised scissor lift could exert in excess of 2,100 lb when encountering an obstruction — and that a simple anti-SIO device could reduce the force to 225 lb or less, greatly decreasing the risk of injury or death.

Conclusion

Conducting a forensic failure analysis of an intermittent malfunction requires special care to avoid losing vital evidence. In this case, nondestructive radiography allowed investigators to detect and document evidence that would have been disturbed by disassembling the part for visual examination. This would have left investigators in doubt of the significance of finding loose screw terminals.

Nondestructive radiography revealed that wires had been withdrawn from the screw terminals without altering the condition of the plug. This case illustrates that nondestructive radiography can be an effective strategy for investigating intermittent failures or malfunctions. The investigator must consider that whatever causes a failure to be intermittent or difficult to reproduce may also leave sensitive evidence that is best examined by nondestructive

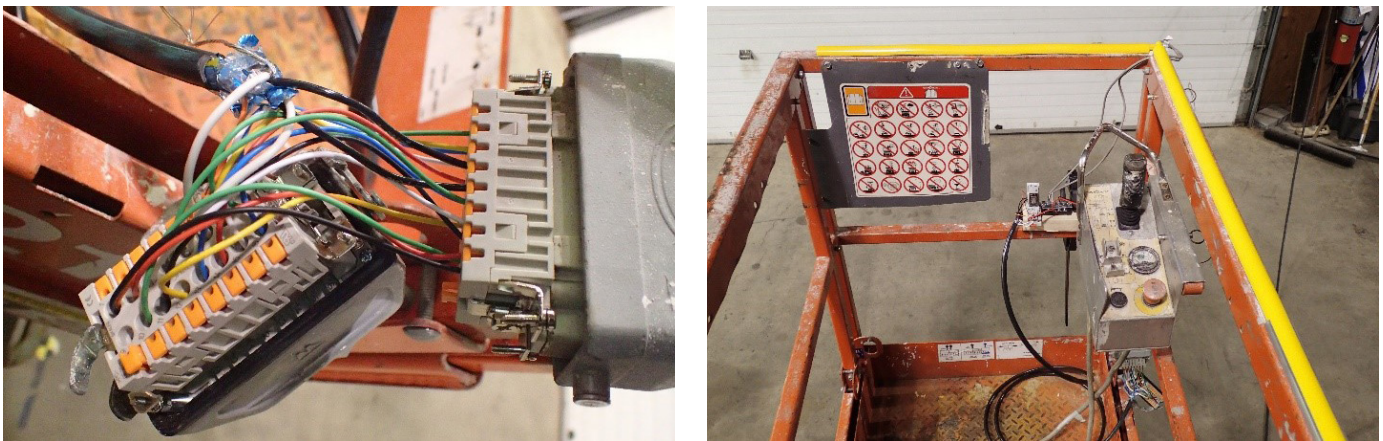


Figure 12

Exemplar test setup including left and upper guardrail sensors and circuitry to cut off power. The alternative solution allowed for a plug-and-play connector along with a force sensor signaling to a basic circuit that stopped the upward movement of the lift when it came into contact with a hazard.

means to avoid losing valuable information. While this case study focused on loose wiring connections, the same principles can be applied to other types of failures, such as blockages in hoses, stuck/seized valves, and other conditions where disassembling the part would cause the investigator to disturb the as-found condition and lose potentially critical information.

Acknowledgements

The authors would like to acknowledge Jeremy Robbins of ARCCA with assistance in testing the exemplar scissor lift and assembling the anti-SIO safety device.

References

1. K. U. Schmitt, P. F. Niederer, and F. Walz, *Trauma Biomechanics: Introduction to Accidental Injury*. Berlin: Springer, 2004.
2. W. C. Whiting and R. F. Zernicke, *Biomechanics of Musculoskeletal Injury*. Leeds: Human Kinetics, 2008.
3. E. A. Luce, T. D. Tubb, and A. M. Moore, "Review of 1,000 major facial fractures and associated injuries," *Plastic and Reconstructive Surgery*, vol. 63, no. 1, pp. 26–30, 1979. doi:10.1097/00006534-197901000-00005.
4. C. St. Hilaire et al., "Facial fractures and associated injuries in high- versus low-energy trauma: All are not created equal," *Maxillofacial Plastic and Reconstructive Surgery*, vol. 42, no. 1, 2020. doi:10.1186/s40902-020-00264-5.
5. N. Yoganandan and F. A. Pintar, "Biomechanics of temporo-parietal skull fracture," *Clinical Biomechanics*, vol. 19, no. 3, pp. 225–239, 2004. doi:10.1016/j.clinbiomech.2003.12.014
6. J. Cormier et al., "The tolerance of the nasal bone to blunt impact," *Annals of advances in automotive medicine/Annual Scientific Conference*, vol. 54, pp. 3-14, 2010.
7. D. Raymond, C. Van Ee, G. Crawford, and C. Bir, "Tolerance of the skull to Blunt ballistic temporo-parietal impact," *Journal of Biomechanics*, vol. 42, no. 15, pp. 2479–2485, 2009. doi:10.1016/j.jbiomech.2009.07.018.
8. T. L. Jackson, "Effect of American football helmet chin strap placement on measures of blunt impact," Honors Theses, University of Southern Mississippi, 2018. [Online]. Available: https://aquila.usm.edu/honors_theses/606.
9. M. Vander Vorst, J. Stuhmiller, K. Ho, N. Yoganandan, and F. Pintar, "Statistically and biomechanically based criterion for impact-induced skull fracture," *Annual Proceedings Association for the Advancement of Automotive Medicine*, vol. 47, pp. 363 – 381, 2003.
10. C. Chang, Y. Chen, S. Noordhoff, and C. Chang, "Maxillary involvement in central craniofacial fractures with associated head injuries," *The Journal of Trauma: Injury, Infection, and Critical Care*, vol. 37, no. 5, pp. 807–811, 1994. doi:10.1097/00005373-199411000-00017.
11. B. Pappachan and M. Alexander, "Biomechanics of cranio-maxillofacial trauma," *Journal of Maxillofacial and Oral Surgery*, vol. 11, no. 2, pp. 224–230, 2012. doi:10.1007/s12663-011-0289-7.
12. R. R. Crowell et al., "Cervical injuries under flexion and compression loading," *Journal of Spinal Disorders*, vol. 6, no. 2, 1993. doi:10.1097/00002517-199304000-00013.
13. D. J. Maiman et al., "Compression injuries of the cervical spine," *Neurosurgery*, vol. 13, no. 3, 1983. doi:10.1097/00006123-198309000-00007
14. A.A. White III, M. M. Panjabi, *Clinical Biomechanics of the Spine*, Philadelphia: J.B. Lippincott Company, 1990.
15. F. A. Pintar et al., "Dynamic characteristics of the human cervical spine", *Proceedings Stapp Car Crash Conference*, vol. 39, pp. 195–202, 1995.
16. "IPAF Global Safety Report" International Powered Access Federation, 2022. [Online]. Available: <https://www.ipaf.org/en-us/resource-library/ipaf-global-safety-report>.
17. C. Leah, D. Riley, A. Jones, "Mobile elevated work platform (MEWP) incident analysis", *Research Report RR961*, Health and Safety Laboratory for the Health and Safety Executive, United Kingdom, 2013.

18. “SAIA - Secretariat for the A92 Series of Standards,” SAIA, <https://www.saiaonline.org/a92> (accessed Jan. 27, 2023).
19. A. Jones, S. Bates, “Mobile elevated work platforms”, Research Report RR960, Health and Safety Laboratory for the Health and Safety Executive, United Kingdom, 2013.
20. Self-Propelled Elevating Work Platforms, ANSI/SAIA A92.6-2006, 2006.
21. Safety Requirements for Industrial Scissor Lifts, ANSI MH-1:2012, 2012.
22. Mobile Elevating Work Platforms – Design, Calculations, Safety Requirements and Test Methods, ISO 16368:2010, May 2010.
23. Design, Calculations, Safety Requirements and Test Methods for Mobile Elevating Work Platforms (MEWPs), ANSI/SAIA 92.20-2018, 2018.
24. “Hierarchy of controls,” Centers for Disease Control and Prevention, <https://www.cdc.gov/niosh/topics/hierarchy/default.html> (accessed Aug. 11, 2022).
25. Guidelines for Addressing Occupational Hazards and Risks in Design and Redesign Processes, ANSI/ASSE Z590.3-2011, R2016.
26. F. A. Manuele, On the Practice of Safety. Hoboken, NJ: John Wiley & Sons Inc., 2013.
27. R. L. Brauer, Safety and Health for Engineers. Hoboken, NJ: Wiley, 2016.

Forensic Analysis of Roof Deterioration Due to Condensation

By James R. Drebelbis, AIA, PE, DFE (NAFE 938S)

Abstract

Corrosion of the structural steel roof deck of large warehouses resulted in several invasive forensic investigations to determine the cause and mechanism of the corrosion. The warehouse roof investigation presented in this paper is one of many similar warehouses located near the Gulf of Mexico and along the Southern Atlantic Seaboard experiencing corroded roof decks when constructed using fiberboard roof insulation made from sugarcane fiber called bagasse. Consensus exists among individuals studying this phenomenon that the fiberboard became saturated with water, which dissolved formic and acetic acid from the fiberboard. The steel deck corroded when it came in contact with the acidic solution. There was little consensus regarding the mechanism by which water intruded into the roof assembly. Invasive investigation of the low-slope roofs of buildings with various types of insulation (including bagasse fiberboard) and observation of physical commonalities between the instances led to the following conclusion: Water in the roof assemblies did not result from leaks through a compromised roof membrane but rather from humid air infiltrating the roof assembly and condensing on the underside of the roof membrane.

Keywords

Low-slope roof, condensation, roof membrane, structural roof deck, fiberboard, bagasse, acetic acid, formic acid, corrosion, wind load, Gulf of Mexico, Atlantic Seaboard, vapor barrier, destructive testing, humidity, roof leaks

Introduction

Although wood fiberboard insulation has been used for years as an inexpensive roof insulation, in the last several years, metal roof decks supporting low-sloped roofs (primarily located near the Gulf of Mexico and the South Atlantic Seaboard) began to fail due to corrosion. Investigating engineers agreed that the deck corroded when exposed to acidic solution of formic, and acetic acid dissolved from bagasse fiberboard insulation.

Bagasse is the fibrous material that remains after sugar is squeezed from sugar cane. Lacking is consensus about the mechanism by which moisture occurs in the roof assembly. The following case focuses on a forensic investigation in Texas near the Gulf of Mexico involving a low-sloped roof insulated with bagasse fiberboard where the corrosion of the metal deck occurred. The water intrusion was not unique to low-sloped roofs insulated with bagasse fiberboard; similar moisture conditions, without the severe corrosion, occur in roofs with other types of roofing insulation when exposed to similar environmental conditions.

Important consideration is given here to the characteristics of the fiberboard insulation itself, common environmental conditions, and the mechanism by which water saturated the insulation. This paper refers to these insulation boards made from wood pulp and bagasse collectively as “fiberboard.” Reference to “roof assemblies” means the composition of insulation boards sandwiched between a roofing membrane and a structural deck.

Background

Since the early part of the 20th century, the construction industry has used panels called “fiberboard” made from wood fibers for various building components, including wall sheathing, cover boards (a thin substrate on the insulation to which the roof membrane is adhered), and roof insulation¹. Fiberboard is produced through a wet process where the fibers are first washed, then the lignocellulosic fibers are combined with water and binders to create a slurry that is fed onto a moving screen to create sheets of various thicknesses whose fibers become interfelted as water leaves the boards². The material is then heated to drive out the moisture and sometimes pressed or laminated

before the panels are cut into boards³.

In the early 21st century, the roofing industry became aware of premature roof deck corrosion on roofs insulated with fiberboard⁴. The corroded roof decks occurred in states bordering the southern Gulf Coast and southern Eastern Seaboard. Along with the similarity of construction (i.e., low-sloped roofs supported on metal deck), other investigators identified the common component in the failed roof assemblies as fiberboards made from “bagasse” fibers that remain after the sugar-manufacturing-process crushes sugarcanes to extract sugar³.

Bagasse fiberboards have been produced since 1921 and used for roof insulation for 80 years as an inexpensive insulation material³. Although the insulation value of fiberboards insulation is relatively low (e.g., in the range of 3.0 per inch (in.) for fiberboard versus values exceeding 5.0 per in. for polyisocyanurate insulation), fiberboard insulation is appropriate for buildings such as warehouses that have minimal need for environmental control. One can visually differentiate fiberboard made using bagasse fibers from those made with wood fibers because bagasse fibers are slightly more coarse than wood fibers⁴.

After earlier investigations associated bagasse with the corrosion of steel decks, controversies arose between investigators and the North American Fiberboard Association (NAFA) regarding the corrosive elements in bagasse fibers. The team of Chuck Marvin and Bruce Bryne proposed that fiberboard manufacturers poured liquid chlorine onto the unprocessed fibers to prevent mold⁵. The chlorine that remained in the fibers eventually leached onto the steel roof decks, causing corrosion. By contrast, Hopmann and Steiner opined that the findings of Marvin and Bryne did not account for the presence of other corrosive agents in fiberboard, such as carboxylic acid, acetic acid, and formic acid⁶.

In March 2012, Mark S. Graham, executive director of the National Roofing Contractors Association (NRCA), published a paper expressing concern about this premature corrosion of steel decks. Graham stated that the corrosion of steel roof decks appears to be confined to roofs insulated with bagasse fiberboards⁴. In an undated publication, Louis Wagner, executive director of NAFA, denied that fiberboards were currently being manufactured with bagasse fibers⁷. That document states that the only manufacturer of bagasse fiberboards ceased production in 2006.

Typical roof construction affected by corrosion consists

of a membrane roof (e.g., built-up bituminous, modified bituminous, or single-ply roofing) over a single, 1½-inch to 2-in. layer of fiberboard insulation mechanically attached or otherwise adhered to the structural steel deck. The economy of the fiberboard products over other insulation boards made this a popular insulation system for buildings such as warehouses and manufacturing plants where environmental control was less important. Eventually, however, in the early 21st century, awareness that roofs insulated with bagasse fiberboard were associated with corrosion of the structural steel decks eliminated bagasse fiberboards from use as a roof insulation board, although wood fiberboard insulation is still manufactured and readily available for use as wall sheathing.

In the subject case and similar cases, controversy remained over how moisture intruded into the bagasse-insulated roof assemblies. Intuitively, one expects that water leaks into the roof system when the roof membrane is breached, soaks the insulation, and then wets the steel deck.

The presence of multiple tears in the membrane led to one line of thinking that the fiberboard shrunk and tore the roof membrane. A second line of thinking concluded that the membrane failed because foot traffic caused joints over ribs (valleys in the deck profile) to deflect and collapse, ripping the roof membrane. The presence of linear tears with spacing that matched the dimensions of the fiberboard reinforced the foot-traffic explanation. Of the two explanations, the failure of the roof membrane at unsupported seams appeared more plausible. It is unlikely that the fiberboards shrunk and tore the roof membrane. Heat applied during the manufacturing process drives moisture out of the boards, causing them to shrink. Instead of shrinking, once installed, the fiberboards (as all wood products) absorb moisture from the air and expands. Adding to the controversy is the absence of similar corrosion failures in fiberboard-insulated roofs in northern states.

Location of Investigations

The subject investigation occurred in the southern region of Texas near the Gulf of Mexico. The description of corrosion in this study is similar to instances of corrosion of structural steel decks insulated with bagasse fiberboard that the NRCA reported in the southern and eastern coastal regions of the United States⁴. Buildings investigated in other matters involved warehouse facilities or warehouse portions of office/warehouse facilities that experienced partial or widespread deterioration of the structural decks within 10 years of construction. Due to the extent of loss to

the buildings and the potential cost of remediation, the resulting litigation included multiple parties associated with the design and/or construction processes, each represented by an investigation team of architects, engineers, and attorneys. The investigations generated competing theories about causation.

Description of Case Study Site and Building

The subject of this investigation is a 360,000-square-foot warehouse located near Houston, Texas and the Gulf of Mexico. Its 900-foot-long axis is oriented in the east-west direction, and its 400-foot dimension is oriented in the north-south direction (**Figure 1**). Dock doors are located along the south and north faces of the building.

Construction of the building consists of concrete tilt wall exterior panels with a structural steel frame interior. A Type B steel roof deck rests on steel bar joists supported by the structural steel frame. The low-slope roof has a ¼-in.-per-foot pitch that drains from the ridge of the building (oriented in the east-west direction) down



Figure 1
Aerial view of the subject warehouse.



Figure 2
Fractures in the roofing membrane running parallel to the south side of the warehouse. The arrow points to the south edge of the roof.

to gutters on the north and south edges of the roof. The roof assembly consisted of built-up bituminous asphalt roofing membrane on a single, 1½-in. layer of fiberboard insulation mechanically attached to the steel deck.

Within 10 years of original construction, the roof membrane of the warehouse began to fail. Splits formed in the roofing membrane with concentrations of deterioration near and parallel to the south and north sides of the roof (**Figure 2**).

Initial Hypotheses

Investigations of other warehouse facilities where the roofs deteriorated in the same manner as the subject roof preceded this investigation. Chemical analysis performed during those investigations established that the steel decks corroded when exposed to aqueous solutions containing acetic and formic acid. The design teams generally accepted this explanation of the cause of the corrosion. Disagreement remained about the source and mechanism of water intrusion.

Experts assigned to investigate this warehouse advanced different explanations about the sequence of events that introduced water into the roof assembly. Consistent with the theories of deterioration previously described in this matter, the hypotheses included the roof membrane splitting when the fiberboard shrinks after installation and foot traffic depressing the roof at unsupported joints in the insulation located over ribs in the steel deck. Either hypothesis would result in the roof membrane splitting and admitting rain water to enter the system. A third hypothesis proposed that condensation was the mechanism by which water collected in the roof assembly.

Site Investigation

To evaluate the substrate, contractors engaged by the plaintiff systematically removed areas as large as 4 feet (ft) by 8 ft (roof cores) in 31 locations. In performing each roof core, after the roof membrane was removed, the insulation was observed and then removed to expose the underlying steel deck. With the removal of each layer, experts observed, photographed, and sampled the materials. Observed conditions at most (but not all) roof cores included damage to the roofing membrane, corroded steel decks, and water saturated fiberboard (**Figure 3**).

During the investigation of the roof, the plaintiff's experts directed most of the invasive investigation focusing on areas where splits and repairs occurred in the roofing membrane. A request was made to conduct similar coring



Figure 3

Corrosion of the structural steel roof deck exposed by removal of roofing membrane and fiberboard insulation during destructive testing. Note standing liquid and prevalence of corrosion in the ribs of the steel deck.



Figure 4

Undamaged roofing membrane being removed. The long dimension of the roof membrane being removed is oriented north-south, and the view looks southwest across the roof.



Figure 5

Fiberboard insulation exposed after removal of the roof membrane seen in **Figure 4**. Note darker areas around the seams of the fiberboard insulation on the south end of the exposed roof that indicate the presence of moisture absorbed by the insulation.

where the roof membrane showed no evidence of damage (**Figure 4**).

Once the roof membrane was removed — exposing the insulation at the requested location where the roofing membrane showed no signs of deterioration — the insulation appeared wet (**Figure 5**). Removal of the fiberboard revealed that corrosion of the steel deck generally coincided with the joints in the insulation (**Figures 6 and 7**).

As shown in **Figures 6 and 7**, corrosion of the steel deck was pervasive, regardless of the condition of the overlying roof membrane. The roof investigation discovered that some insulation boards were installed with the joints between the fiberboard panels abutting over the ribs instead of resting on the flutes of the steel deck. This gave validity to the explanation that foot traffic



Figure 6

South end of the exposed roof deck. Corrosion of the structural steel deck beneath the fiberboard insulation layer seen in **Figure 4** and **5**. This shows corrosion coinciding with the seams in the insulation and confirms that corrosion can occur beneath undamaged roof membrane.



Figure 7

North end of the exposed roof deck. Corrosion of the structural steel deck beneath the fiberboard insulation layer seen in **Figure 4** and **5**. This illustrates that corrosion occurs beneath undamaged roof membrane and coincides with seams in the insulation. Corrosion is greatest in line with the damaged adjacent roofing seen in **Figure 4** and **5**. Areas of corroded and uncorroded decking suggest that although the moisture is pervasive across the plane of the roof, the insulation is not uniformly wetted.

may have deflected the unsupported ends of the boards and damaged the roof membrane (**Figure 8**). It was still unexplained, however, why more roof failures occurred near the edges of the north and south perimeter of the building, why the steel deck corroded beneath undamaged roof membrane, and why some steel deck was not corroded. Once the roof membrane fractures, water can penetrate the roof membrane through those fractures. However, the presence of corrosion where no roof membrane damage occurred suggests that water entered the

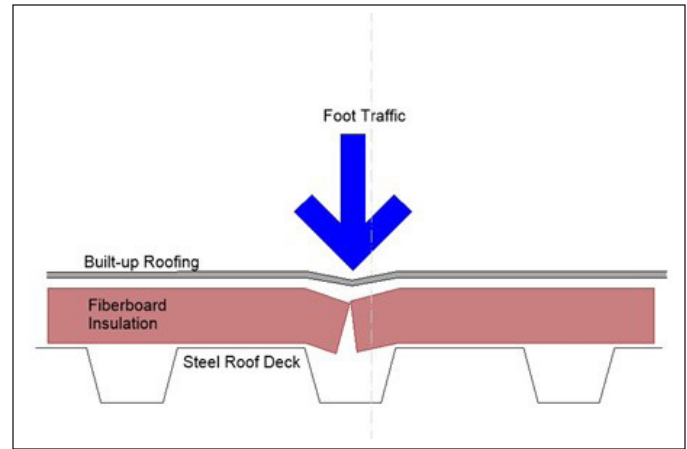


Figure 8

Illustration of the mechanism by which foot traffic damages unsupported joints that abut over the rib of the structural steel deck.

roof assembly by means other than through fractures in the roof membrane. The prevalence of distress at the north and south sides of the building indicates that the moisture intrusion is not necessarily uniform across the roof plane.

Chemical Analysis of the Fiberboard

Chemical analysis by laboratories engaged by the plaintiff verified the presence of acetic acid and formic acid in the fiberboard. In other similar cases, Hopmann and Steiner report elevated levels of chlorides, carboxylic acid, acetic acid, and formic acid in bagasse fiberboard⁶. Wood products naturally contain acetic and formic acid. Elevated temperatures, such as one finds in a roof assembly exposed to direct sun, accelerate the emission of volatile forms of acetic and formic acid in the wood,⁸ lending credibility to this line of thinking. By contrast, in the manufacture of wood fiberboard, the washing process preceding placement of the wet slurry onto a screen is intended to remove most of the corrosive material⁹.

The investigating teams were provided no documentation regarding the manufacturing process — specifically the washing of the fibers — of the bagasse fiberboard installed on the subject building. Since bagasse fiberboards were produced and used for years preceding the discovery of the corrosion resulting from their use, wood fibers used to make fiberboard also contain acetic and formic acid, and the corrosive fiberboard insulation appeared to be associated with one manufacturer, it was hypothesized that the corrosive materials in the bagasse may remain in high concentrations as a result of the manufacturing process used by the fiberboard manufacturer.

General Observations

In all buildings investigated, a single layer of bagasse fiberboard insulation was a common construction component. The reported prevalence of the moisture issue along the southern and eastern seaboard suggests that the deterioration of the steel deck, in all likelihood, relates to a combination of factors including the climate conditions, the bagasse material, and/or the roof assembly construction.

Climate Conditions

In all probability, finding corroded roof deck beneath undamaged roof membrane leads to the conclusion that moisture did not necessarily intrude through fractures in the roof membrane, but may have collected in the roof assembly due to condensation of water vapor in the roof assembly. This explanation is consistent with the technical memo issued by the NRCA concerning problems with fiberboard and with discussion in the NRCA Roofing Manual regarding condensation in roof assemblies where outside winter temperatures fall below 40°F, and the relative humidity of interior spaces exceeds 45 percent¹⁰.

Climate conditions in southern coastal states are consistent with conditions noted by the NRCA that result in condensation forming in roof assemblies. Despite mild temperatures through the winter months in the southern coastal part of the country, it is not unusual for evening temperatures to drop below 40°F, combined with year-round humid conditions due to the proximity of southern coastal regions to large bodies of water, environmental conditions of temperature and humidity exist that result in condensation in roofing assemblies.

For example, in the Southern coastal region of the United States, during the winter daytime temperatures average 40°F to 50°F, and nighttime temperatures regularly drop to 30°F to 40°F¹¹. Formation of condensation in this manner occurs due to seasonal or nightly drop in temperature¹². Exposed to ambient temperatures, during the evening, the temperature of the roof membrane can fall below the dew point of air trapped in the roof assembly. February 11, 2010 represented typical noontime conditions during winter in the Houston. During the day when the interior of the warehouse is exposed to outdoor conditions due open dock doors, daytime temperatures were in the low 40s, the relative humidity was 93 percent, and the dewpoint temperature was 37°F to 39°F. At night, the ambient temperature fell to 37°F, below the dewpoint of air infiltrated from the exterior during the day. Not only is the roof membrane

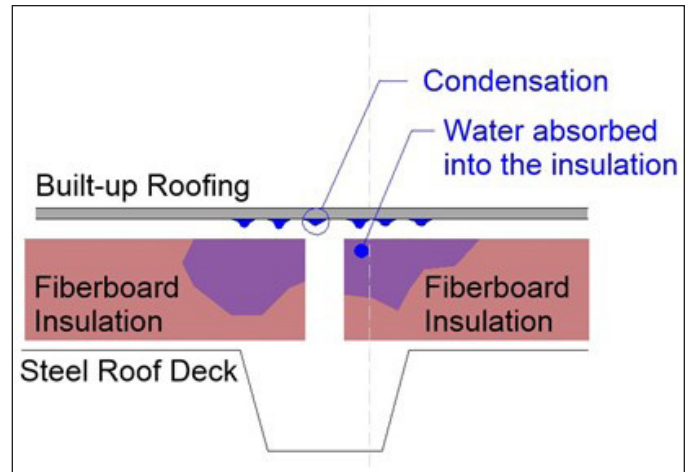


Figure 9

Illustration of the mechanism by which moist air condenses within the roof assembly.

cooled by the ambient temperature, but during the night, the surface of the roof also radiates heat to the sky. When this occurs, moist air trapped in the roof assembly that contacts underside of the cool roof membrane condenses (Figure 9).

Evaluation of climate conditions in the northern United States provides information that explains the lack of reports of corrosion on warehouses constructed similarly to warehouses in the southern coastal states. In summary, the climatic conditions in the north differ from those in southern coastal states — and do not encounter to the climatic conditions associate with corrosion of steel roof decks stated by the NRCA. Northern cities experience extended periods of nighttime temperatures below 40°F. Daytime temperatures are also low. However, even when the daytime relative humidities are high (because of the low temperatures), the capacity of the cold air to absorb moisture remains low. Even in the spring (when the climatic conditions might be expected to approximate those of wintertime in the Southern states), there is less difference between daytime and nighttime temperatures in Northern states. For example, a typical temperature range is illustrated by temperature and humidity at noon on March 31, 2010 in Chicago where the temperature was 72°F, but the relative humidity was 37°F. On that day, nighttime temperatures dropped only to the 60s — higher than the dewpoint temperature where condensation forms¹³.

External and Internal Air Flow

The direct effects of air flow in buildings are caused by wind-induced pressures, stack-effect, and mechanical ventilation¹⁴. The operators of the subject warehouses

typically close the doors of the facilities at night. In the case of the subject warehouse and other similar warehouses, the interior is heated during winter months. Experimentation and analysis by Stathopoulos, Surry, and Davenport found that internal pressures in buildings due to wind loads fluctuate significantly, varying the most near dominant openings in buildings and peaking when the wind direction is perpendicular to dominant openings¹⁵.

The south-facing dock doors were used more frequently to manage product, exposing the interior of the warehouse to southerly Gulf winds. As the wind loads against the warehouse exterior vary, air pressure of the warehouse interior fluctuates (**Figure 10**). Aside from pressure due to wind forces, the stack-effect from rising warm air increases the interior air pressure slightly against the upper portion of the warehouse. Stacking-effects vary with the difference in temperature between the interior and exterior and with the increased elevation above the floor (i.e., at the rate of 0.2 Pascals per meter of building height or approximately 0.00001 psi per foot of building height)¹⁶.

Consistent with the findings of Stathopoulos, Surry, and Davenport, the most severe roof damage to the subject building occurred along the south and north perimeters of the building where internal air pressures would be greatest. In addition, the storage racks located beyond the perimeter loading area block the flow of incoming air to the interior space¹⁷, resulting in more infiltration of warm humid air and higher air pressures at the perimeter of the warehouse (**Figure 10**).

Migration of Air into the Roof Assembly

The Second Law of Thermodynamics states that

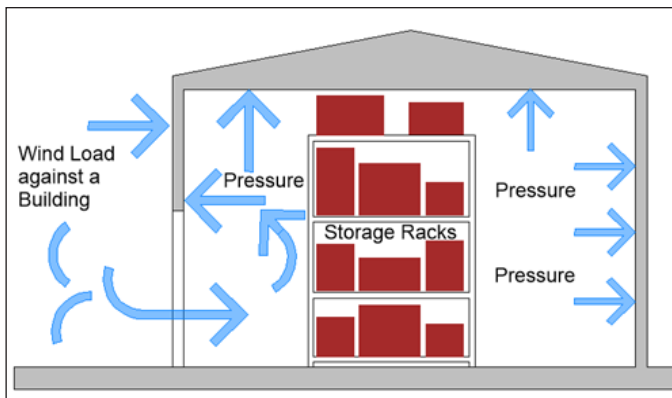


Figure 10

Wind-induced pressure in the building due to wind load on one face resulting in higher air pressure at the perimeter of the building next to the opening through which the wind enters the building.

matter and energy move from a higher potential to a lower potential and explains, in engineering terms, the mechanism by which air from the interior of the building moves into the roof assembly and how moisture moves within the roof assembly. Air moves from higher pressure to lower pressure, non-gaseous material moves from higher elevation to lower elevation, and moisture migrates from wet to dry. By this means, air from the interior of the warehouse is either pushed into, or pulled from, the roof assembly, and liquid from condensation drains to the ribs of the steel deck.

The interstitial space between the steel roof deck and the roof membrane has a series of voids created by the ribs of the steel deck and joints between the fiberboard panels¹⁸. The pathway for air to migrate from the warehouse into the roof assembly is through the laps and other openings in the steel deck (**Figure 11**). As air pressure fluctuates, air migrates into and out of the roof assembly from the warehouse through the openings in the steel deck. Air is pushed into the interstitial space of the roof assembly as air pressure in the warehouse increases and leaves the interstitial space as the air pressure in the warehouse decreases. On buildings covered with a mechanically attached single-ply membrane roof, the membrane will lift as wind blows across the roof surface, creating negative pressure in the interstitial space of the roof assembly. This acts as a bellows and pulls air into the interstitial roof space (**Figure 12**).

The air below the steel roof deck has elevated humidity since the rising warm air absorbs and carries moisture with it¹⁹. Once inside the roof assembly, this humid air can move through voids in the ribs of the deck and through the seams in the insulation until it reaches the underside of the roof membrane. If the surface of the roof membrane is at or below the dew point, condensation occurs, and the

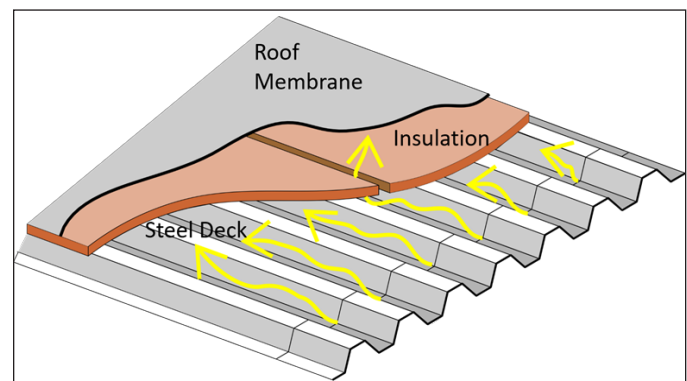


Figure 11

Illustration of the path of air infiltrating the structural steel deck and the fiberboard insulation.

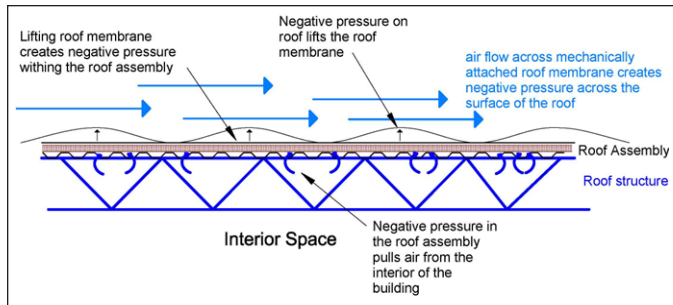


Figure 12

Wind across the roof surface lifts a mechanically fastened single-ply roof membrane.

liquid water is absorbed by the hydrophilic fiberboard (**Figure 9**).

Other Instances of Condensation in a Roof Assembly

In a separate matter in Louisiana, the plaintiff’s expert diagnosed moisture in a roof assembly as a roof leak. The roof assembly in this case consisted of a thermoplastic polyolefin (TPO) single-ply roofing membrane over polyisocyanurate insulation on a structural steel roof deck. The consultant never verified that a breach in the TPO membrane caused moisture in the roof assembly. For example, the consultant could have used a common toilet plunger to create a vacuum over suspected defects in the roof membrane. Instead, the roofing consultant removed large areas of the roof membrane, exposing the insulation.

The exposed insulation revealed moisture concentrated around fastener penetrations and along the seams of the insulation panels (**Figure 13** and **14**), reminiscent of observations in the subject warehouse case. The subject building in this case has apartment units heated/cooled using PTAC wall



Figure 13

Removal of a TPO roof from polyisocyanurate insulation board. Notice the dark areas indicating moisture due to condensation.

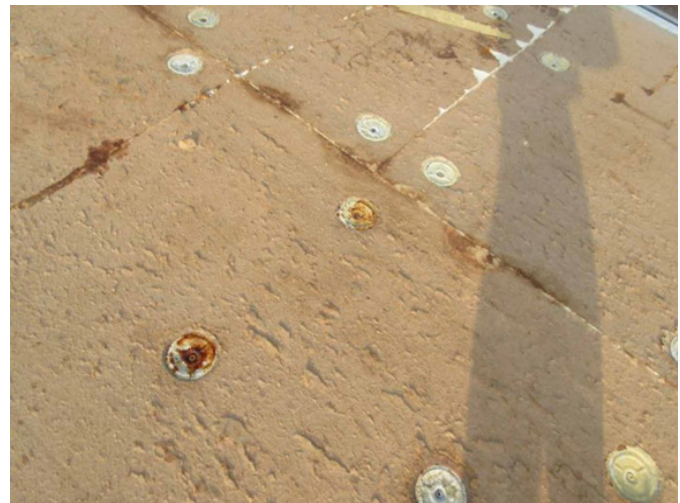


Figure 14

Detail of moisture in the polyisocyanurate insulation. Notice the concentration of moisture around seams in the insulation boards and around the mechanical attachments.

units. Air pressure in the units increases due to mechanically induced pressure when the PTAC units run and force outside air into the space. The apartments have no finished ceilings. The floor and roof structural members are exposed along with the steel deck. On the upper floor, air from the occupied room can be exchanged with air in the roof assembly through laps and penetrations in the steel deck.

Rather than a defective roof membrane causing water to collect in the roof assembly, the photographic evidence showed that warm, humid air from the heated interior spaces infiltrated the roof assembly, where it condensed on the underside of the TPO membrane next to seams in the insulation and around mechanical roof fasteners. Moisture due to condensation was interpreted as a roof leak.

Prevention of Condensation in Roof Assemblies

The need to prevent, or minimize, condensation in roof assemblies within low-sloped roofs has been known since the 1970s²⁰. However, there is no consensus regarding the use of vapor retarders. Although the current building codes require vapor retarders under various conditions for walls, slabs-on-grade, and crawl spaces, the building codes do not require vapor retarders in low-sloped roofs²¹. ASHRAE²⁰ and other sources¹² advise caution in the application of vapor retarders in low-sloped roofs, as it is almost impossible to prevent infiltration into the roof assembly²². Once condensation forms within the assembly, it is difficult to remove moisture from the roof assembly²². Removal of moisture from low-slope roof assemblies can only be accomplished by diffusion or wind-induced ventilation — neither of which is effective²².

Recommendations for managing condensation in low-slope roof assemblies include:

1. Either prevent the entry of water vapor or create a system to remove the vapor or condensation²².
2. Locate vapor retarders in the roof assembly below the point of the theoretical dewpoint temperature²³.
3. Seal the vapor retarders at the edges of roofs, at vertical projections and around penetrations to prevent short-circuiting of air barriers²⁴.
4. On steel decks, install low-R-value, fire-resistant insulation beneath vapor retarders to protect the vapor retarder from damage²⁴.
5. Install two layers of insulation with joints in the insulation offset to minimize leakage and to increase the rigidity of the insulation layer²⁴.
6. Install roof vents to relieve pressure due to temperature changes and provide a means for moisture to escape from the assembly.

Conclusions

The aforementioned investigations — reinforced by the principles of thermodynamics and wind engineering — support the theory that warm, humid air infiltrates into low-sloped roof assemblies. Low-sloped roof assemblies consisting of roof membrane over rigid insulation and steel roof deck allow warm moist air to migrate through the components of the roof and condense on the underside of the roofing membrane. Regardless of the type of insulation used, the condensation is absorbed by, and retained within, the insulation. However, when the insulation board contains corrosive constituents, such as acetic and formic acid found in bagasse fiberboard, the moisture dissolves the corrosive material, and the accumulation of acidic solution deteriorates the steel deck and fasteners at an accelerated rate.

The condition most conducive to moisture collection in the roof assembly is characterized by cool roof surfaces over warm, humid interior spaces. This suggests that the phenomenon may not be confined to southern, coastal portions of the United States but may also occur where the interior space is artificially heated and humidified. Based on these findings, the recommended construction for low-sloped roof assemblies consisting of a layer of

rigid insulation sandwiched between a roof membrane and a steel deck should be as follows:

- Install two layers of the insulation board with their seams staggered and taped. This increases the rigidity of the roof membrane where the insulation boards abut over the ribs of the deck, making the roof more resistant to damage from foot traffic and blocks the pathway from the steel deck to the roof membrane.
- Prevent the infiltration of air from the interior of the building into the roof assembly by installing a vapor barrier on top of the steel deck and/or seal joints and laps in the steel deck.
- Add pressure relief valves through the roof membrane to prevent buildup of pressure due to heating and cooling and to vent any moisture that collects in the roof assembly.

If these modifications to the roof assembly design had been employed in the assemblies investigated in this case, damage to the roofs insulated with bagasse insulation may have been avoided — and bagasse fiberboard might still be available as a viable, sustainable, and economic insulation material. Regardless of how low-sloped roofing systems are insulated, moisture in the assembly deteriorates the roofing components. Based on the findings of this investigation, managing condensation in low-sloped roof assemblies requires rigorous attention to the design of roof assemblies and consideration of local climatic conditions.

References

1. W.C. Lewis and S.L. Schwartz. “Insulating Board, Hardboard, and Other Structural Fiberboards,” August 1965. Distributed by U.S. Forest Service, Research Note FPL-077.
2. “Hardboard and fiberboard manufacturing.” Active: <https://www.epa.gov/sites/default/files/2020-10/documents/c10s0604.pdf>.
3. “Corrosion issues related to Bagasse Fiberboard Roof Insulation in the Gulf States Region of the United States,” International Institute of Building Enclosure Consultants, Technical Advisory, IIBEC-TA-010-2016.
4. Mark S. Graham. “A concern with fiberboard insulation.” www.professionalroofing.net, March

- 2012 Available: doi <https://www.google.com/search?client=firefox-b-1-d&q=A+concern+with+fiberboard+insulation>.
5. Chuck Marvin, RRC and Bruce Bryne. "Back to the Future: Roof Decks Quickly Corroded by Insulation." Interface RCI, Inc. January 2011.
 6. Mark H. Hopmann, P.E. and Kimberly Steiner. "Premature Metal Roof Deck Corrosion: Difficult to Detect and Diagnose." Distributed by WJE.
 7. Louis Wagner, Executive Director. "A concern with inaccurate allegations regarding wood fiberboard." Distributed by the North American Fiberboard Association.
 8. Signe Hjerrild Smedemark, Morten Ryhl-Svendesen, and Alexandra Schieweck. "Quantification of formic acid and acetic acid emissions from heritage collections under indoor room conditions. Part I: laboratory and field measurements," Distributed by Heritage Science. Available: <https://doi.org/10.1186/s40494-020-00404-0>.
 9. Sarah Hunt, Josep Grau-Bove, Eleanor Schofield, and Simon Gaisford. "Effect of Polyethylene Glycol Treatment on Acetic Acid Emissions from Wood," *Forests* 2021,12, 1629. Available: <https://www.mdpi.com/1999-4907/12/12/1629>.
 10. The NRCA Roofing Manual, National Roofing Contractors Association 10255 W. Higgins Road, Suite 600, Rosemont, IL 60018-5607, 2010, p. 164.
 11. National Weather Service. Monthly Lowest Min Temperatures for Houston Area, TX 2000 to 2022, Available: <https://www.weather.gov/wrh/Climate?wfo=hgx>.
 12. "Moisture Control in Low Slope Roofs" APA Engineered Wood Systems, R525B, January 1999, p. 2.
 13. National Weather Service. NOAA Local Climatological Data. Available: <https://www.ncei.noaa.gov/cdo-web/datasets>.
 14. Fariboz Haghghat, Henrik Brohus, Jiwu Rao, "Modelling air infiltration due to wind fluctuations – a review." Department of Building, Civil and Environmental Engineering, Concordia University, Montreal, Quebec, Canada H3G 1M8, Building and Environment 35, May 25, 1999. p. 377.
 15. T. Stathopoulos, D. Surry, and A.G. Davenport, "Internal Pressure Characteristics of Low-Rise Buildings due to Wind Action." "Proceedings 5th International Conference on Wind Engineering, Colorado State University, July 8-14, 1979. P. 461.
 16. Andrew K. Persily and Steven J. Emmerich, "Effects of Air Infiltration and Ventilation." *Moisture Control in Buildings*, 2nd Edition, © 2009 ASTM International. p. 111.
 17. ASCE 7 – 16 Minimum Design Loads and Associated Criteria for Buildings and Other Structures. American Society of Civil Engineers, 1801 Alexander Bell Drive, Reston, VA 20191-4382, 2016, p. 375.
 18. Joseph Lstiburek, P.Eng., PhD, "Pressures in Buildings." Building Sciences Corporation. BSD-109. 1-15-2014. p. 2.
 19. Thomas J. Taylor, PhD, "3 Types of Moisture in Low Slope Roofing Systems." *Building Science*. 12-14-2015. Available: <https://www.gaf.com/en-us/blog/3-types-of-moisture-in-low-slope-roofing-systems-281474980065135>.
 20. ASHRAE Handbook 1977 Fundamentals, American Society of Heating, Refrigerating and Air-Conditioning Engineers, Inc., 180 Technology Parkway NW, Peachtree Corners, GA 30092. p. 19.6.
 21. "A Guide to Vapor Retarder Design in Low-Sloped Roofs." GAF Technical Services. June 2020. p. 7.
 22. G.O. Handegord, "CBD-73. Moisture Considerations in Roof Design." National Research Council Canada. January 1966. p. 2.
 23. Karim Allana, PE, RRC, RWC, "Avoiding Condensation in Low Slope Roofing Assemblies." 2018 33rd RCI International Convention and Trade Show. p. 9.
 24. "A Guide to Vapor Retarder Design in Low-slope Roof Systems." loc. cit. pp.13-18.